Contouritic depositional systems influenced by complex seafloor topography
–
Late Cenozoic seismoacoustic reconstructions from the Galicia and Angola Continental Margins

Dissertation

Zur Erlangung des Doktorgrades der Naturwissenschaften

am Fachbereich Geowissenschaften

der Universität Bremen

vorgelegt von

Julia Haberkern

Bremen, Oktober 2017

Universität Bremen

Gutachter:

Prof. Dr. Volkhard Spieß

Prof. Dr. David Van Rooij

Datum des Kolloquiums: 12.12.2017

Contents

Abbreviations

AABW – Antarctic Bottom Water

AAIW – Antarctic Intermediate Water

CAS – Central American Seaway

CDS – Contouritic Depositional System

CMP – Common Midpoint

CWC – Cold Water Coral

ENACW – East North Atlantic Central Water

LSW – Labrador Sea Water

LDW – Lower Deep Water

MCS – Multichannel Seismic

MOW – Mediterranean Outflow Water

NADW – North Atlantic Deep Water

NCW – Northern Component Water

NMO – Normal Moveout

SACW – South Atlantic Central Water

SASSW – South Atlantic Subtropical Surface Water

Abstract

Contourites are sediment drift bodies that form under the persistent influence of bottom currents. As their morphology and composition records changes in the ambient current regime, they form excellent paleoceanographic archives. The shape and size of a contourite is determined by strength and variability of the bottom current as well as sediment supply, but also by the topographic framework with which the current interacts. Especially smaller scale topographic features such as seamounts are known to interact with and thereby amplify bottom currents, leading to the evolution of distinct contourite drifts. The interplay between topography and bottom current and the resulting depositional pattern are complex and not entirely understood. However, due to the associated amplification of currents the resulting deposits are often more sensitive to variations in the background hydrodynamic regime. This makes them especially valuable for paleoceanographic reconstruction. However, before that information can be utilized, the interaction mechanisms which ultimately shape the drift have to be understood in their entirety. Moreover, changes in topography, be it through burial by sediments, tectonic activity or even biogenic construction of topographic features, may cause similar changes in the interaction process as a variation in the current forcing.

This project addresses interaction between currents and topography in two representative yet diverse study areas. At the Galicia Margin, a strongly dissected topography formed during the opening of the North Atlantic Ocean and was furthermore shaped by the Pyrenean and Betic orogenies. Various seafloor features, such as topographic obstacles and ridges have interacted with ocean density fronts passing through the transition zone between Mediterranean Outflow Water and Labrador Seawater, which was lowered during glacials and shoaling in deglacial periods. The second study area is located at the shallow Angola Margin, where the seafloor is actively deforming through gravity-driven salt tectonic processes. Extensional grabens open up in the process of salt rafting and are rapidly filled by sediments depositing under the influence of bottom currents. Furthermore Cold Water Corals grow in marked mound and ridge structures in the area, adding more variability to the already dynamic topography.

Both areas were investigated by means of high-resolution multichannel seismic data as well as bathymetric data and, in case of the Galicia Margin, Parasound sediment echosounder data. At the Galicia Margin, a paleoceanographic reconstruction spanning the last 40 Myrs was performed. The findings show the evolution of the depositional pattern at the Galicia Margin in six phases. From the first to the fifth phase, increases in current strength, which reflect changes in the large scale North Atlantic circulation were identified. The first change is related to the onset of Northern Component water in the early Oligocene. A second increase of current influence, associated with distinct interactions with the adjacent topographic features, is caused by the outflow from the Tethys, which started after the seaway between Tethys and Indian Ocean was closed 14 Ma ago. Further current intensification happened after the reopening of the Strait of Gibraltar at 5.33 Ma when Mediterranean Outflow Water started to flow. In the Lower and Middle Pleistocene the intensity of this outflow increased and imprinted on the sediments. Only the last of the captured periods the Upper Pleistocene is not related to an increase in bottom water flow, it recorded a weakening of the Mediterranean Outflow instead. Throughout all phases, mass-transport processes have also influenced sediment distribution at the Galicia Margin. They are most dominant from Eocene to the start of the Pliocene and eventually regain influence in the Late Pleistocene. The established

reconstruction resolves variations of Atlantic Ocean circulation in the interval between Eocene and Plicoene for the first time, thereby confirming a strong influence of outflow from the Tethys on the Galicia Margin. Moreover, the findings reflect a sustained domination of Mediterranean Outflow Water since it first influenced the Galicia Margin. Hence, this study underlines the significant control of nearby oceanic gateways on the regional current regime.

The second case study at the Galicia Margin is based on high-resolution mapping and classification of diverse topographic features and adjacent drift deposits. Several existing concepts for the interaction of topography and bottom currents were applied and adjusted to cover the interaction processes and explain the observed sedimentary deposits. As a result the following processes were identified to shape the area: The dissected topography on top of one obstacle was recognized to split the bottom current and focus it into several current cores, leading to the deposition of a multi-crested drift. Further attention was paid to flow focussing depending on the slope angle of topographic obstacles, which mainly leads to the deposition of separated mounded drifts. Furthermore, the height of topographic features seems to control the width and depth of the moat, whilst their shape and size control moat orientation and length. At the largest of the topographic obstacles, the effects of flow detachment and eddy shedding were identified in the sedimentary record. Additionally, sediment waves were found to have built up on one of the ridges under a current which closely follows the contours of the ridge. Eddy shedding and flow detachment had been captured by site specific and conceptual models before, hence the findings of this study can confirm their imprint on the sedimentary record. The examples for the multi-crested drift and the sediment waves on the ridge exhibit an extraordinarily strong control of the topography on the deposit. Moreover, due their high sensitivity to bottom-current variations, the high potential of small-scale contouritic depositional systems for paleoceanographic studies was underlined.

The third case study of this thesis is based on data from the Angola Margin. Here, the influence of bottom currents at the border between a salt raft and the adjacent extensional graben was discovered for the first time. The occurrence of a moat and a separated mounded drift along a pronounced fault (termed Anna Fault) conclusively shows, that the fault offset at the seafloor is capable of focussing the bottom current regime. A stacked record of ten phases of separated mounded drifts reports that the subsidence of the graben infill deposit, which is related to the ongoing extension creates accommodation space, which is successively filled up under the influence of bottom currents. The variation recorded in this newly discovered setting of a fault-controlled contouritic depositional system presumably reflects both changes in fault activity and the modifications in the paleo-current regime. At a later stage, a Cold Water Coral ridge built up on the salt raft directly next to the fault, as the focussed bottom current provides a suitable habitat for the corals. Their structure reaches 100 m in height, thereby also focussing the bottom current, as evident from the growth of an additional separated mounded drift on top of the salt raft after Cold Water Coral growth. Consequently, in this setting the control of a fault on the orientation and position of a Cold Water Coral ridge is exerted via bottom current focussing.

Overall, the present thesis provides new insight into the interaction of bottom currents and small-scale topographic features and their role in shaping contourite depositional systems through numerous examples. Conceptual models of the influence of these interaction processes on sedimentary deposits were advanced and the influence of bottom current topography interaction in previously undisclosed settings was discovered. The detailed

investigation of these processes is an important step to more holistic understanding to the role of bottom currents in shaping complex continental margins and also a step towards the deciphering of valuable paleoceanographic information archived in these systems.

Kurzfassung

Sediment Driftkörper die sich unter dem beständigen Einfluss von Bodenwasserströmungen aufbauen, auch Konturite genannt, stellen wertvolle paläoozeanographische Archive dar, da sie auf Änderungen im sie umgebenden Strömungsregime mit Änderungen ihrer Morphologie und Zusammensetzung reagieren. Generell werden Größe und Form eines Konturiten von der Stärke und Variabilität der Bodenwasserströmungen, Sedimentverfügbarkeit, aber auch von topographischen Rahmenbedingungen gesteuert. Besonders lokale Erhebungen sind dafür bekannt mit Strömungen zu interagieren und sie dadurch zu verstärken. Dadurch entstehen besonders prägnante konturitische Driftkörper. Der genaue Ablauf von Strömungsinteraktion mit topographischen Elementen und insbesondere deren Einfluss auf sedimentäre Ablagerungsmuster ist überaus komplex und noch nicht vollständig erforscht. Ungeachtet dessen, reagieren diese Ablagerungen deutlich empfindlicher auf Änderungen der überregionalen Strömungsgeschwindigkeit, da diese im Laufe der Interaktion mit der Topographie verstärkt werden. Das macht sie besonders wertvoll für paläoozeanographische Rekonstruktionen. Bevor diese Informationen allerdings nutzbar sind, muss der Einfluss der Interaktionsprozesse auf die Drift Morphologie insgesamt verstanden werden. Außerdem müssen mögliche Änderungen der Topographie selbst in Betracht gezogen werden, da sie genau wie eine Änderung der Hintergrundströmung die Interaktionsprozesse beeinflussen können. Änderungen der Topographie können im einfachsten Fall durch das Verschütten mit Sedimenten aber auch durch Tektonische Aktivität oder sogar durch biogene Konstruktion von Topographie hervorgerufen werden.

Im Zuge dieser Arbeit wurden Interaktionsprozesse in zwei repräsentativen und voneinander sehr verschiedenen Arbeitsgebieten untersucht. Am galizischen Kontintalhang hat sich eine stark gegliederte Topgraphie als Folge der Nordatlantiköffnung und späteren plattentektonischen Vorgängen, namentlich der Pyrenäischen und Betischen Orogenesen entwickelt. Die verschiedenen Strukturen am Meeresboden interagieren mit horizontalen ozeanographischen Dichtegradienten, welche durch die Mischungszone zwischen Labradorseewasser und Mittelmeerwasser wandern. Diese Mischungszone verlagerte sich während Glazial und Deglazial, sodass sie in der passenden Tiefe war um mit der Meeresbodentopographie zu interagieren. Das zweite Arbeitsgebiet ist am Angolanischen Kontinentalhang, welcher durch aktive Deformation durch Salztektonik charakterisiert ist. Durch sogenanntes *salt-rafting* öffnen sich Extensionsgräben, welche schnell durch konturitische Sedimentation verfüllt werden. Des Weiteren bauen Kaltwasserkorallen markante Strukturen in Hügel oder Rückenform, wodurch die Variabilität der Topographie noch erhöht wird.

Beide Arbeitsgebiete wurden anhand von hochauflösender Mehrkanalseismik sowie bathymetrischen Daten und im Falle des galizischen Kontinentalhanges auch Sedimentecholot Daten untersucht. Am galizischen Kontinentalhang wurde eine paläoozeanographische Rekonstruktion über die letzten 40 Millionen Jahre durchgeführt. Die Ergebnisse zeigen eine Verstärkung des Strömungseinflusses über fünf Stadien und eine leicht Abnahme im sechsten Stadium. Diese Stadien entsprechen Änderungen in der großskaligen Nordatlantik Zirkulation. Die erste Änderung wird durch den Einsatz von Nordatlantischer Tiefenwasserbildung im

frühen Oligozän induziert. Eine weitere Verstärkung und der Beginn von Interaktion zwischen Strömung und Topographie ist mit dem Ausfluss von Tethyswasser in den Atlantik verbunden, welcher begann als sich der Seeweg zwischen Tethys und Indischem Ozean vor 14 Mio. Jahren geschlossen hat. Die nächste Intensivierung der Strömungsregimes wurde durch den Beginn von Ausfluss aus dem Mittelmeer nach der Öffnung der Straße von Gibraltar vor 5.33 Mio. Jahren hervorgerufen. Im Unteren und Mittleren Pleistozän hat sich dieser Ausfluss verstärkt, um dann im Oberen Pleistozän wieder abzunehmen. Während des gesamten Zeitraumes hatten auch hangabwärts gerichtete Sedimentationsprozesse einen Einfluss auf die Sedimentmächtigkeit am galizischen Kontinentalhang. Sie dominierten vom Eozän bis ins frühe Pliozän und gewannen im Oberen Pleistozän wieder verstärkten Einfluss. In dieser Rekonstruktion werden zum ersten Mal Strömungsvariationen im Zeitraum vom Eozän bis zum Pliozän erfasst. Des Weiteren wird der Einfluss von Tethyswasser auf den galizischen Kontinentalhang bestätigt. Die Dominanz des Mittelmeerwassers in späteren Phasen zeigt auf wie stark die Kontrolle von Wassermassenausfluss aus benachbarten Ozeanbecken ist.

Die zweite Fallstudie am galizischen Kontinentalhang basiert auf einer hochauflösenden Kartierung der diversen topographischen Strukturen, welche weiterhin verwendet wurde um die Strukturen in Kombination mit den angrenzenden Driftkörpern zu klassifizieren. Verschiedene bekannte konzeptuelle Modelle wurden angewendet und angepasst um die aus der Interaktion zwischen Topographie und Strömung entstehenden Driftkörper zu erklären. Daraus wurden die folgenden Prozesse identifiziert, die auf die Morphologie im Arbeitsgebiet Einfluss nehmen. Es wurde erkannt, dass die stark gegliederte Oberfläche einer Erhöhung die Bodenwasserströmung in verschiedene Kerne zerlegt, unter denen sich ein sogenannter *multi-crested* Driftkörper ablagert. Weiterer Betrachtungsgegenstand war die Fokussierung von Bodenströmung in Relation zum angrenzenden Hangneigungswinkel, welche zur Entstehung von sogenannten *separated mounded drifts* führt. Hierbei scheint die Höhe der angrenzenden Erhebung Einfluss auf die Tiefe und Breite des sogenannten *moats* zu nehmen, während Größe und Form der Erhebung die Orientierung und Länge kontrollieren. An der größten Erhebung wurden Indikatoren gefunden die anzeigen, dass sich der fokussierte Strömungskern von der Erhebung löst. Außerdem entstehen Eddies auf der Leeseite der Erhebung. Auf einem der Rücken wurden Sedimentwellen gefunden. Diese entstehen unter einer Bodenströmung die Richtung gegenüber der allgemeinen Strömung ändert und den Konturen des Rückens folgt. Die Entstehung von Eddies und das Ablösen des Strömungskernes waren bereits in konzeptuellen und einem lokalen Modell abgebildet, mit den Ergebnissen dieser Studie kann nun ihr Einfluss auf die Ablagerungsmuster bestätigt werden. Die Beispiele der *multi-crested drift* und der Sedimentwellen auf dem Rücken zeigen eine außerordentlich starke Kontrolle von Topographie auf die Sedimentverteilung auf. Des Weiteren zeigt die Studie auf wie empfindlich kleinskalige konturitische Ablagerungsystem auf Änderungen des Strömungsregimes reagieren und untermauert damit ihren Wert für paläoozeanographische Studien.

Die dritte Fallstudie in dieser Arbeit basiert auf Daten vom angolanischen Kontinentalhang. Dort wurde zum ersten Mal der Einfluss von Bodenwasserströmungen an der Grenze zwischen einem Salzraft und dem angrenzenden Extensionsgraben entdeckt. Das Vorhandensein von einem *moat* und einer *separated mounded drift* zeigt, dass der Störungsversatz am Meeresboden ausreicht, um die Bodenwasserströmung zu fokussieren. Zehn Phasen von Konturitablagerungen zeigen, dass Subsidenz im Graben, bedingt durch Extension, Ablagerungsraum kreiert, welcher fortlaufend unter Strömungseinfluss verfüllt

wurde. Die Variation in den Ablagerungsgeometrien wird durch ein Gemisch von Änderungen in der Störungsaktivität, sowie Variationen im Paläoströmungsregime hervorgerufen. In einem späteren Entwicklungsstadium beginnt das Wachstum von Kaltwasserkorallen welche einen Rücken auf dem Salzraft direkt neben der Störung aufbauen. Die Fokussierung der Strömungen am Störungsversatz ist ein entscheidender Faktor um ein passendes Habitat für Kaltwasserkorallen bereit zu stellen. Der Rücken erreicht eine Höhe von 100 m und ist damit selbst in der Lage Bodenwasserströmungen zu fokussieren, was in weiterem Driftwachstum auf der Störungsabgewandten Seite der Korallen geschieht. Zusammengefasst lässt sich sagen, dass die Störung am Salzraft die Ausrichtung und Position der Kaltwasserkorallen indirekt durch das Fokussieren der Strömung lenkt.

Die gesammelten Ergebnisse dieser Doktorarbeit geben neue Einblicke in die Interaktion zwischen Bodenwasserströmung und kleinskaliger Topographie sowie deren Signifikanz auf die Ausformung von konturitischen Depositionsystemen. Konzeptuelle Modell wurden angepasst und erweitert. Außerdem wurde der Einfluss von Interaktion zwischen Strömung und Topographie in bis dato unbekannten Konfigurationen gezeigt. Die hochauflösende Betrachtung dieser Prozesse ist ein wichtiger Schritt zu einem gesamtheitlichen Verständnis des Einflusses von Bodenwasserströmungen auf die Morphologie von komplexen Kontinentalhängen, sowie ein weiterer Schritt die wertvollen paläoozeanographischen Informationen zu entziffern welche in diesen Systemen verschlüsselt sind.

1 Introduction

1.1 Motivation and Objective

Knowing the past climate is the key to understand the present, as well as to reliably predict forthcoming changes. Hence, sedimentary climate archives such as contourite deposits have received significant attention among scientific communities during the past decades. Since they form under the prevalent influence of currents, contourites provide essential information on modifications in the ocean circulation. This in return can then be linked to climatic changes, tectonic processes, and sea-level variations (Knutz, 2008). Therefore, contourites represent an ideal natural laboratory to conduct paleoceanographic research and develop paleoceanographic reconstructions. In addition to their scientific significance, contourites are of economic value as they are associated with potential hydrocarbon reservoirs or source rocks (Rebesco, 2005). Furthermore they received attention related to slope stability implications, as water saturated contouritic deposits might serve as gliding planes (Rebesco, 2005).

The size, shape and composition of contourites are a product of the current strength, position and variability and also the time it prevailed, but the nature of the deposit is as well influenced by sediment supply and most interestingly in this thesis, the topographic framework (Faugères et al., 1999). Contourite deposits located in the vicinity of topographic obstacles, including seamounts, outliers, ridges, mud volcanoes, or even Cold Water Coral mounds (e.g. Van Rooij et al., 2003; Hernández-Molina et al., 2006; Vandorpe et al., 2014; Hanebuth et al., 2015;) represent particularly interesting sites for paleoceanographic studies. The reason for that, is that such topographic features strongly interact with the present current regime and, thus, even subtle changes in the prevailing currents are amplified and recorded in the adjacent contourite. While the interaction of the hydrodynamic regime with topography is already quite well understood, the question how it influences the resulting sediment deposits cannot be fully answered yet (Turnewitsch et al., 2013). In conclusion, the interaction processes need to be understood before the paleoceanographic information can be extracted from contourite deposits associated to multifaceted topography.

Further complexity arises from topography changes which occur on the same time scale as contouritic sedimentation. This might happen through (a) burial of the topography by sediments (e.g. the Le Danois system Van Rooij et al., 2010), (b) tectonic activity, (c) active mud volcanism (Vandorpe et al., 2014) or (d) the growth of biogenic seafloor topography for instance by Cold Water Corals (e.g. Van Rooij et al., 2003). These processes might induce changes of the current topography interaction, resulting in variation of the depositional pattern without a change of the primary oceanographic forcing.

In this thesis, the interaction between distinct topographic features and the bottom current regime shall be investigated in two different working areas. The first area, the sediment-starved Galicia Margin, inherited its seafloor topography from its tectonic formation and, thus, the strongly dissected topography is only slowly buried. Since furthermore no indicators for an impact of Cenozoic tectonic activity on the shape of the topography were found, it is considered a prime location to study the interaction of the bottom current regime with a static, unchanging topography. Hence temporal changes in the interaction processes can be mostly attributed to the hydrodynamic forcing. Furthermore the large variety of topographic structures within a rather small area guarantees that the background current regime is not changing by itself throughout the area, thus the interaction mechanisms and resulting deposits may be attributed to the different topographies. The second working area, the Angola continental margin,

provides a contrast in the fashion, that active salt tectonics and high sedimentation rates result in a dynamic change of seafloor topography and therefore the interaction with the bottom currents resulting in temporal variation in the depositional pattern. Furthermore, the occurrence of Cold water corals at the seafloor and in the shallow subseafloor areas provide more examples of dynamically changing topography interacting with a current and imprinting on sedimentary structures.

The first objective of this thesis is an area-wide mapping and analysis of sedimentary structures to establish a stratigraphic framework for the area at the Galicia Margin. Analysis of the area-wide sediment distribution allows to identify the processes which dominantly influence the sediment distribution, and allows to extract the impact of bottom currents on sediment deposition, with the ultimate goal to reconstruct the paleo-current activity in the area and fit it into a paleoceanographic reconstruction of the Atlantic circulation.

The second objective is the development of conceptual models for the interaction of specific topographic features with the ambient hydrodynamic regime at the Galicia Margin. This is approached with a detailed mapping of sedimentary deposits associated to distinct topographic structures in the working area to reconstruct current pathways and areas of current focusing. Comparison to conceptual models from other studies allows to identify the interaction processes and if necessary the models may be expanded or refined. With the ultimate goal to provide a classification of topographic features and corresponding contourite deposits as well as the formation mechanisms in question, which should be applicable to other areas with dissected topography.

The third objective is a specific case study based on the data collected at the Angola Margin. A detailed structural analysis of a newly identified type of fault-controlled contouritic depositional system at the border between a salt raft and adjacent extensional graben will be presented in this thesis. Special attention lies on the structural framework and evolution of the system, including contourite activity as well as the impact of Cold Water Coral growth within the system.

1.2 Contourites

The term contourites embraces sedimentation under the influence of bottom-water circulation. The contourite paradigm roots on the photographic discovery of ripples and furrows on the seafloor in the deep sea by Heezen and Hollister (1964). Naturally, the definition of contourite deposits and the understanding of associated processes has undergone changes as research advanced throughout the last 51 years (Rebesco et al., 2014).

In fact, contourites as objects of investigation have received significant attention during the last decades due to (1) their great potential as continuous climatic archive, (2) their relevance for slope stability (i.e., geohazard assessment), and (3) their potential economic value. First of all, their mere existence provides evidence for current activity in ambient bottom water masses. Drift onset or cessation implicates appearance or vanishing of a current which can help to pinpoint the timing of gateway openings and closures related to plate tectonic and/or volcanic processes (Knutz, 2008). Moreover, their temporal evolution records changes in the position and strength of the current, thus, contourite deposits represent valuable paleoceanographic archives. Furthermore, a contourite drift which is active on the continental slope over several million years, associated with high sedimentation rates or a combination of both, large amounts

of sediment are emplaced on the slope which is provides the initial potential of hazardous slope failures. Additionally, contourites which consist of low-permeable, fine grained material with a high pore–water content might form over-pressurised gliding planes, thereby increasing the risk of large mass wasting events (Rebesco, 2005). Economically, contourite are of significant relevance as the deposition of sediment under the influence of fast-flowing currents is always associated with winnowing and leaves behind a well-sorted, coarse-grained drift body, representing potential storage for hydrocarbons. On the other hand, accumulation under lower current speed might lead to the deposition of source rocks (Rebesco 2005).

The identification of contourite drifts can be done based on sedimentological evidence or by seismic and acoustic imaging of seafloor and subseafloor structures. The classification of contourites based on sedimentological evidence is not an easy task and facies models are continuously refined and debated (Stow and Faugères, 2008, Rebesco et al., 2014). The most recent integrated classification contains work of many authors and results in a distinction of

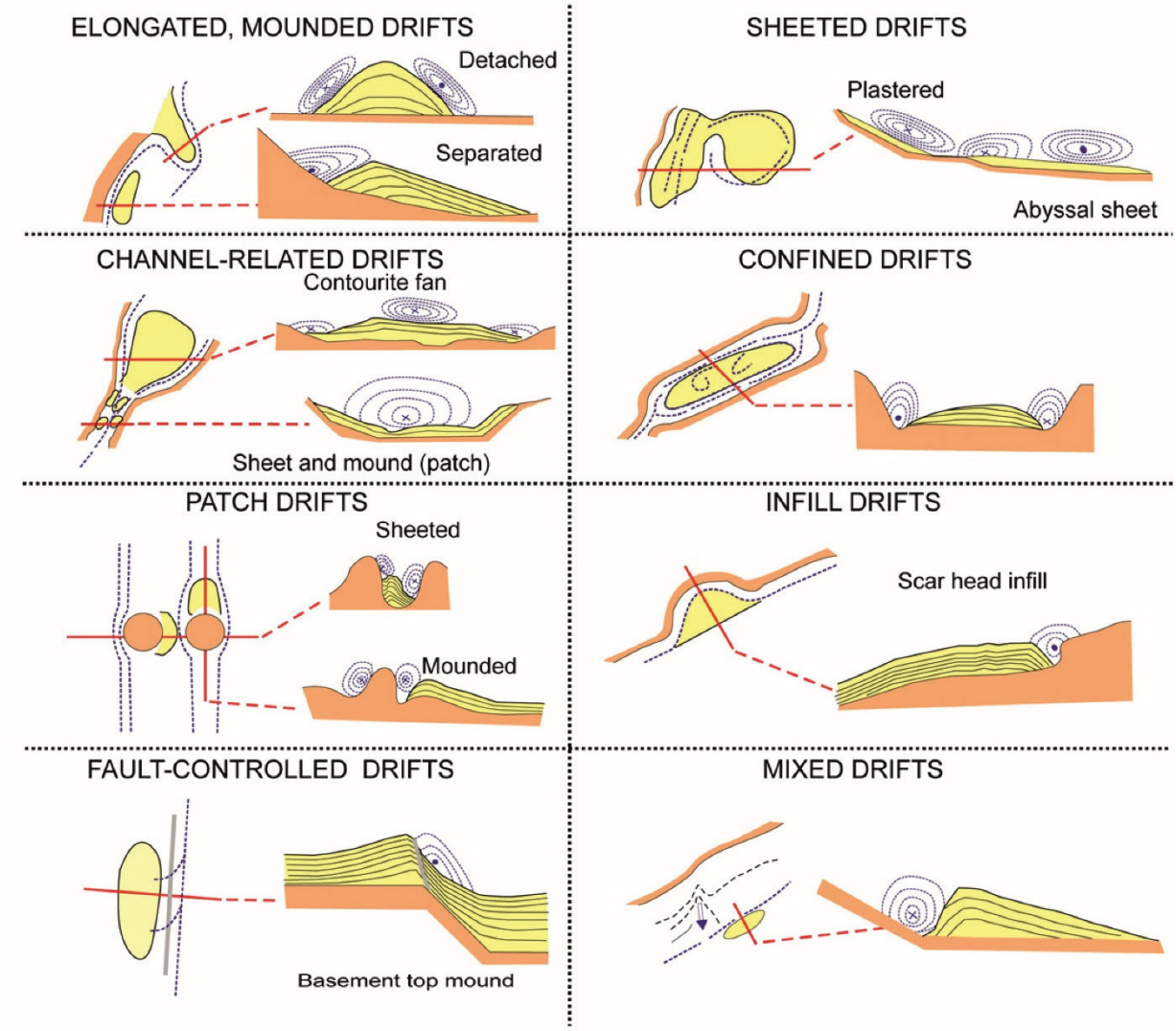

Figure 1.1 – Most recent compilation of different contourite drift types and inferred bottom-current paths composed by Rebesco et al. (2014), based on the original classification by Faugères et al. (1999), Rebesco and Stow (2001) and Stow et al. (2002) and modified by Rebesco (2005) as well as Hernández-Molina et al. (2008a).

clastic, volcanoclastic, shale clasts, calcareous and siliceous bioclastic as well as chemogenic contourites (Stow and Faugères, 2008; Rebesco et al., 2014).

To classify contourites based on seismic and acoustic data, the large-scale morphology as well as internal seismic facies are used. Internal variation such as progradation or aggradation as well as discontinuities provide insight into the spatial and temporal evolution of the drift (Faugères et al., 1999). Drift dimensions range from small channel-related drift patches with extent of 10 km² up to large abyssal plain sheet drifts covering areas of 10^6 km². Sedimentation rates vary according to the current velocity and sediment supply. In areas with fast-flowing bottom waters they may be very low due to erosion and non-deposition, while under calmer conditions accumulation rates may exceed 60cm/kyr (Stow, 2001). The shape of contourite drifts is influenced by the bottom-current velocity, variability and time duration, as well as the topographic framework and sediment supply (Faugères et al., 1999). However, not only depositional drift bodies record the imprint of bottom currents on the depositional regime, also the presence of erosional features is a strong indicator of enhanced current conditions. Therefore the term of contouritic depositional system (CDS) embracing both erosional and depositional features which develop under the influence of the same water mass was coined (Hernández-Molina et al., 2008b).

In the following paragraph the state-of-the-art classification of drift morphologies (Figure 1.1) is presented, it follows the most recent compilation by Rebesco et al. (2014) but is based on the original classifications by Faugères et al. (1999), Rebesco and Stow (2001) and Stow et al. (2002), which were updated by Rebesco (2005) as well as Hernández-Molina et al. (2008). This definition primarily relies on drift morphology as the distinguishing factor, yet drift morphology or the orientation of drifts is often dependent on the margin morphology in combination with formation mechanisms, thus the morphology of the drift cannot be an exclusive criterion. As a result, overlaps of the different drift types are common so “that they are actually within a continuous spectrum of deposits“ (Rebesco et al., 2014) (Figure 1.1).

All drifts are mounded to a certain extent and usually elongated in along-slope direction. The largest examples – being **giant elongated mounded drifts** – are found mostly on the lower slope and can be divided into separated and detached drifts (Figure 1.1). **Separated drifts** are usually associated with steeper slopes and feature a distinct moat characterised by erosion and, or non-deposition under a focused current. The focusing of the current is a consequence of first the Coriolis force deflecting it to the right on the northern, and the left on the southern hemisphere, and secondly the presence of the slope restricting the current in that direction. Therefore, the current impact is enhanced at the slope and deposition occurs further downslope (Faugères and Stow, 2008). In general, separated drifts are expected to migrate upslope; however, examples of separated drifts which simply aggrade or migrate downslope are also known (e.g. Hanebuth et al., 2015). As separated drifts often occur in combination with topographic obstacles, such as seamounts and ridges, they are of special interest in this thesis. **Detached drifts** usually originate from a change in margin trend and are elongated not along the margin but deviating from it, where they began to form at first (Faugères et al., 1999). Sheeted and plastered drifts do not have much relief as they are rather faintly mounded**. Sheeted drifts**, mostly occurring on abbysal plains, are prevalently aggrading and have an almost uniform thickness which thins towards the margins. **Plastered drifts** might be a little more mounded than sheeted drifts but they still have considerably less relief than giant elongated mounded drifts, also they occur in shallower water than sheeted drifts and on gentle

slopes (Faugères et al., 1999). **Channel related drifts** can be found in gateways under high flow velocities. **Confined drifts** are characterized by moats at both flanks of the drift as they form along the axis of a small basin. **Infill drifts** are basically semi-confined drifts forming in slope incisions, such as scars from slope failures. The last three are strongly controlled by margin morphology on a regional scale (Rebesco et al., 2014). The architecture of **patch drifts** is mainly influenced by smaller scale seafloor irregularities and are likewise irregular on a small scale, still they might be elongated (Hernández-Molina et al., 2006; Rebesco et al., 2014). **Fault-controlled drifts** develop as a response to current perturbations at either the top or the base of fault generated relief at the seafloor (Rebesco 2005). **Mixed drifts** is the term chosen to represent all systems, which are significantly influenced by other depositional processes (Rebesco et al., 2014).

For large-scale erosional features Rebesco et al. (2014) proposed a differentiation between linear and areal features. According to their definition, terraces and abraded surfaces may be regarded as areal features. **Terraces** are found along the slope relative to the position of the interfaces between different water masses. They are created by erosional as well as depositional processes and are characterized by low, seaward-dipping gradients. **Abraded surfaces**, on the other hand, are created only by erosion by strong tabular currents in a localized fashion. Linear large-scale erosional features are further subdivided into contouritic channels, moats and marginal valleys (Hernández-Molina et al., 2008a; Garcia et al., 2009). **Contouritic channels** are erosional features, which occur parallel to a margin. **Moats** also trend parallel to a margin, however, they are not necessarily erosive but have a genetic

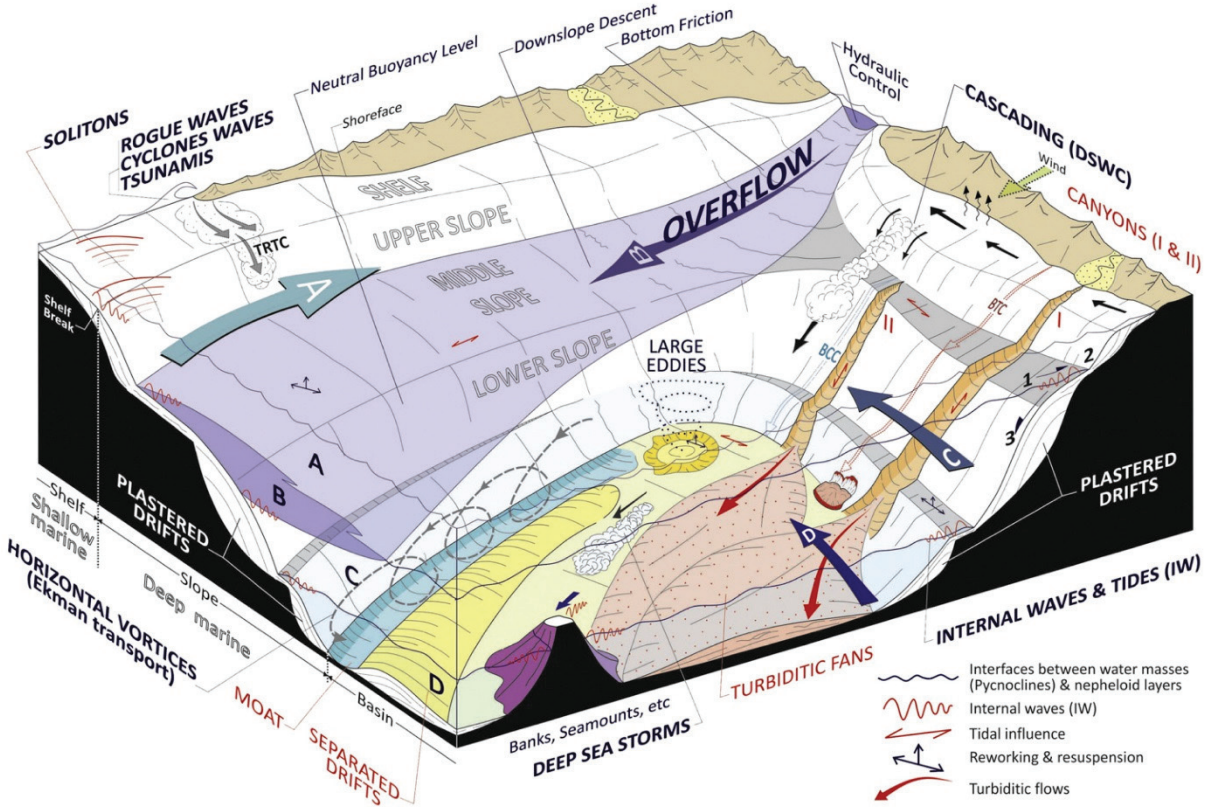

Figure 1.2 - Schematic synthesis of possible oceanographic processes, which might influence bottom current velocity at the seafloor. Including density and barotropic currents, density overflows, internal waves and tides, density cascading, large eddies, deep sea storms, vortices, tsunamis, cyclone waves and rogue waves.

relationship to a separated mounded drift. **Marginal valleys** or troughs are erosional channels related to the presence of an obstacle.

Frequently, contourite drifts or areas of large-scale erosion feature additional bedforms such as dunes, sediment waves, furrows, scours, and lineations just to name a few examples, ranging in size from a few decimetres up to kilometres. According to the bedform-velocity matrix developed by Stow et al. (2009), such bedforms may be utilized to extract additional information on velocity and flow direction of the bottom current responsible for their formation. For instance, for longitudinal bedforms, which are elongated parallel to the flow, it is known that depositional types, such as comet marks or sand ribbons, form under the influence of low current velocities, whilst erosional types, such as furrows and scours, indicate higher current velocities. Transverse bedforms including ripples, dunes, and sediment waves, on the other hand, are oriented perpendicular to the flow and feature mainly undulating bedforms (Stow et al., 2009). Sediment waves which are often sorted into the category of transverse bedforms actually fall somewhere between bedforms and contourite drifts (Rebesco et al., 2014). Wavelength of sediment waves (or mud waves) range from 500 m to 10 km and their height varies between 15 and 50 m but also higher (Wynn and Stow, 2002). However special care has to be taken when linking the occurrence of sediment waves to their formation process as there are also sediment waves forming under turbidity currents (Wynn and Stow, 2002).

As formation processes for contouritic deposition initially only thermohaline density currents flowing over abyssal plains were recognized (Heezen et al., 1966). Nowadays contourite deposits have been found in water depths from the abyssal plains up to shallow water settings and even in lake environments (Rebesco et al., 2014). Furthermore, a multitude of oceanographic driving mechanisms are known today (Figure 1.2). Along-slope flowing thermohaline density currents, driven by cooling and evaporation, are still the most famous example. One of the best known thermohaline water mass might be the North Atlantic Deepwater (NADW), which forms through cooling of highly saline surface water in the Nordic seas. The Mediterranean Outflow Water (MOW) provides a contrasting example of a water mass that gains density only through evaporation (Baringer and Price, 1997). Thus, even though it does not represent a thermohaline current sensu stricto, it is still a density current. Water masses which form in basins exit those through a narrow or shallow strait (e.g. the Strait of Gibraltar). After they passed the constraining topography of the straits, they are steered to the right on the Northern Hemisphere and to the left on the Southern Hemisphere by the Earth's rotation. In the course of this process, the current spreads while its speed is driven by its relative density to the overlying water mass and the slope of the seafloor. The bottom current is further modified by bottom friction and the entrainment of ambient water (Rebesco et al., 2014 and references within). Along continental slopes, the main current cores flow generally parallel to the isobaths or contour lines, hence they are termed contour current. In cases in which these current cores are strong enough to erode sediments along the slope, they are frequently associated with deposition on the downslope side of the current core and thus create a separated drift. This observation has been linked to the development of a horizontal eddy, a so-called helicoidal flow path, which creates a clockwise secondary circulation in addition to the flow of the general bottom current. This secondary circulation is a result from the interplay of bottom friction and Coriolis force (Faugères et al., 1999; Rebesco et al., 2014). Not only the current core of a water mass is associated to highly energetic currents, also water mass boundaries are known to be highly dynamic zones. There, energetic current patterns are created through turbulent mixing between water masses as well as the displacement of the

water mass interface by internal waves, barotropic and baroclinic tides, solitons and eddies (Figure 1.2). All these processes have the potential to resuspend sediment and thus to shape the seafloor (e.g. Pomar et al., 2012; Preu et al., 2013, Hanebuth et al., 2015; Zhang et al., 2016a). Further driving mechanisms for contouritic sedimentation are dense shelf water cascades, wind driven currents as well as tsunami-related traction currents, rogue and cyclonic waves (Figure 1.2) (Rebesco et al., 2014). Of course all these processes do not occur solitarily but often overlap and interact. Thus, an along-slope flowing density current might for example be modulated by internal tides. To add to the complexity topographic features such as seamounts or canyons are known to amplify and modulate the hydrodynamic regime further. For instance, the interaction of a density current with a small-scale topographic obstacle like a seamount, may lead to an acceleration of the flow, thereby causing local erosion and long-term suspension of particles in the water column (Rebesco et al., 2014). This has been observed around ridges, seamounts, outliers, mud volcanoes, and even structures build by organisms such as Cold Water Coral mounds (e.g. De Mol et al., 2002; Van Rooij et al., 2003; Van Rooij et al., 2010; Hanebuth et al., 2015; Hebbeln et al., 2016; Vandorpe et al., 2016). The interaction with these topographies furthermore modulates the current regime, which potentially results in vastly complex hydrodynamic pattern (Turnewitsch et al., 2013) with phenomena such as attached eddies or eddy shedding (Boyer and Zhang, 1990). These phenomena in turn influence local bottom current velocities and thus the sediment distribution around the topography. Whilst the understanding of the hydrodynamic pattern around seamounts improved through modelling over past times, the impact on the sediment distribution around the topographic features is not yet fully understood (Turnewitsch et al., 2013, Zhang et al., 2016).

1.3 Regional setting of the working areas

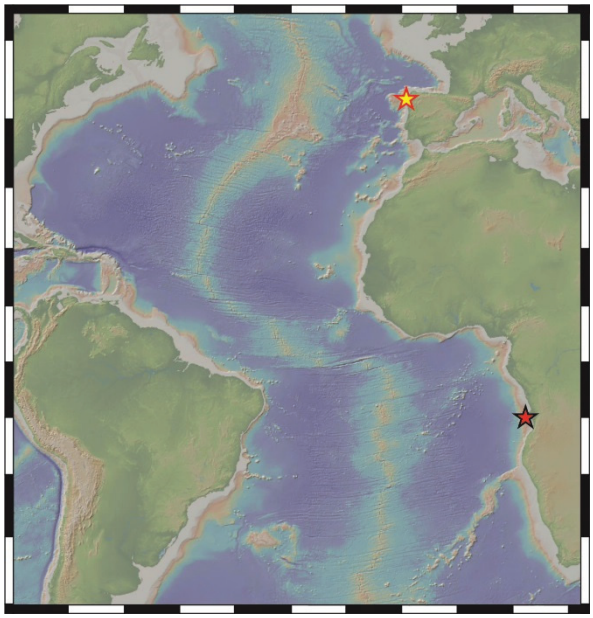

Figure 1.3 - Overview map of the Atlantic Ocean. The yellow and red star indicates the location of the Galicia working area and the red and black star indicates the working area at the Angola continental margin.

Within the framework of this thesis, two working areas (Figure 1.3), representing remarkably different bottom-current influenced settings along the east Atlantic continental margin, were examined. The first working area is located on the Galicia continental margin offshore northwest Spain. There, bottom currents interact with the strongly dissected seafloor topography of a slope internal basin. The topography is inherited from an underlying horst and graben system, which developed during the rifting phase of the margin, and is only slowly buried by sediments. Based on data from this region, two case studies discussed in Chapter 3 and 4 were developed. The second working area focuses on the salt rafted Angola continental margin. There active faulting leads to deformation at the seafloor, which is balanced by high sedimentation rates under the influence of bottom currents. Moreover mound and ridge structures, built by Cold Water Corals interact with the hydrodynamic regime. Data from this area lay the foundation for the third study discussed in Chapter 5. The following chapters will introduce both areas with their respective geological and oceanographic background.

1.3.1 Regional geology of the Galicia Margin

The N-S striking part of the Galicia continental margin is structured by several physiographic provinces. The continental shelf is relatively narrow with only 30 to 50 km width and reaches down to a water depth of 160 to 180 m (Dias et al., 2002b). The continental slope is interrupted by a slope-interior basin, the Galicia Interior Basin (GIB). The GIB reaches down to almost 3000 m and is bordered to the west by the Galicia Bank, a structural high over which water depth shallows to 700 m (Ercilla et al., 2008). West of the Galicia Bank, the deep Galicia Margin slopes down to the Iberia Abyssal Plain (Figure 1.4).

In the scope of this study, the water depth range between 100 and 2800 m along the eastern flank of the GIB was investigated (Figure 1.4). The morphology of this margin is to a large extent controlled by the margin genesis and general tectonic history. It started with the opening of the GIB which was associated to an early rifting phase in the very late Jurassic and early Cretaceous, prior to the opening of the Atlantic Ocean basin in the Lower Cretaceous (Murillas et al., 1990). The rifting of the GIB was associated to hyperextension and sequential faulting and today the area is underlain by a horst and graben system with tilted blocks (Pérez-Gussinyé et al., 2003; Brune et al., 2017) (Figure 1.4).

Sediments, which deposited before the rifting of the GIB, originate from a shallow marine environment and subsided during the rifting process (Murillas et al., 1990; Sutra and Manatschal, 2012). In the syn-rift deposits from the Lower Cretaceous, mass-wasting deposits were recognized (Murillas et al., 1990). In the late Cretaceous the subsidence was concluded

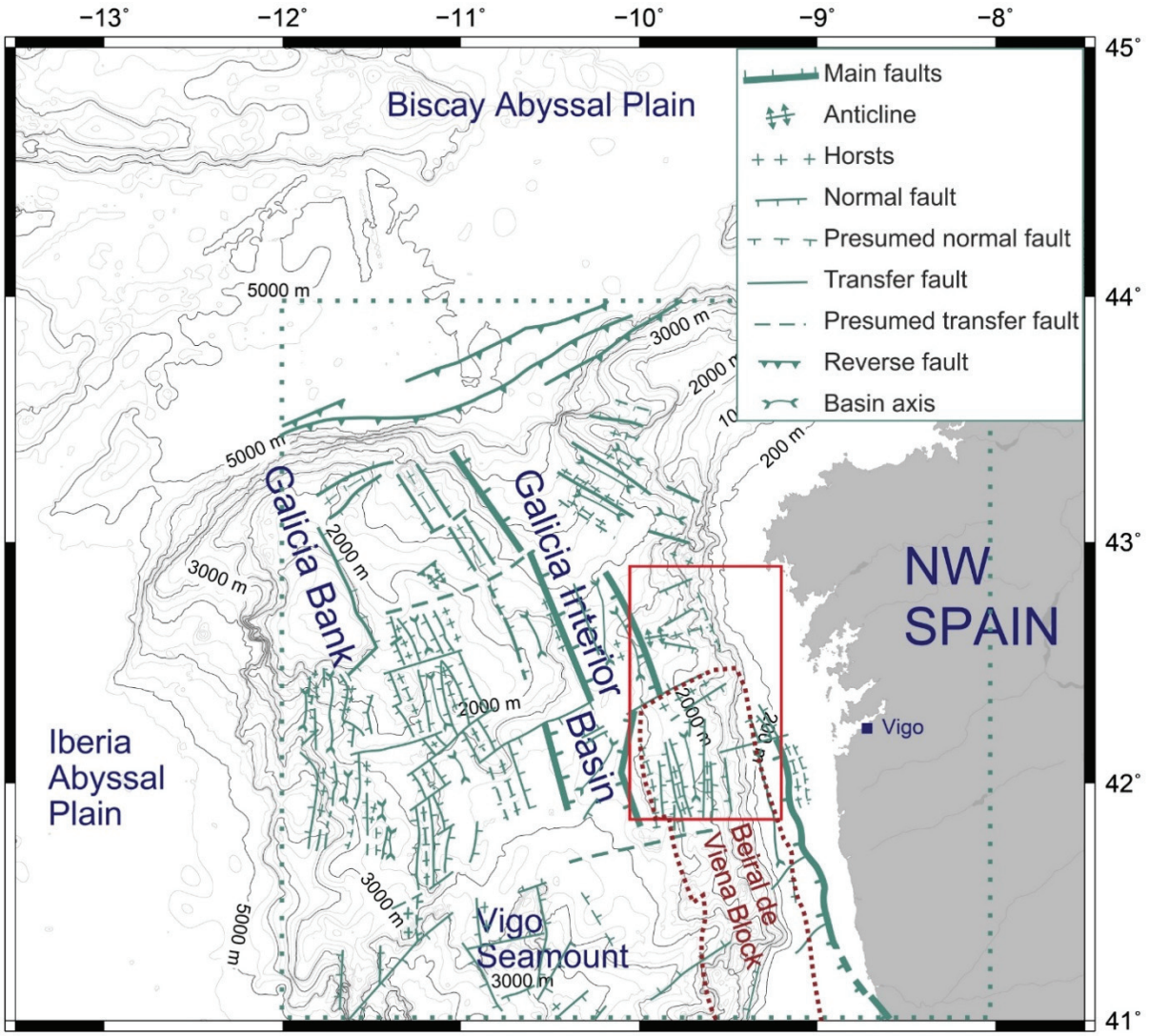

Figure 1.4 - Overview map of the Galicia continental margin overlain by tectonic features (redrawn from Murillas et al., 1990). The red rectangle indicates the working area of the first two studies in this thesis.

(Groupe Galice, 1979) and in the post rift sequence of the GIB no indications of tectonic influence have been found. The opening of the Atlantic during late Aptian times and the onset of seafloor spreading at the deep Galicia Margin only imprinted on the GIB when ocean circulation established in the Upper Cretaceous and caused a hiatus in the GIB (Murillas et al., 1990). During Paleogene and Neogene times the GIB and the surrounding domains were repeatedly subjected to tectonic stress leading to fault reactivations.

During the Pyrenean Orogeny in the Mid-Eocene the Iberian and Eurasian continents collided and subduction of oceanic crust took place in the Bay of Biscay (Boillot et al., 1979) (Figure 1.5A). It mainly affected northern Iberia but led to a north-south directed compressional regime, which offshore NW Iberia affected large topographic structures and caused small-scale faulting leading to uplift of local structural heights and anticlines (Muñoz et al., 2003; Murillas et al., 1990). The Pyrenean Orogeny was followed by the Betic Orogeny, which is associated to the convergence of Africa and Iberia from the early Miocene onward, and subjected large parts on and offshore of western Iberia to compressional stress (Groupe Galice, 1979; Muñoz et al., 2003) (Figure 1.5B). It again caused the reactivation of faults but furthermore caused the uplift at the eastern flank of the GIB where the entire Beiral de Viena Block uplifted and reduced the

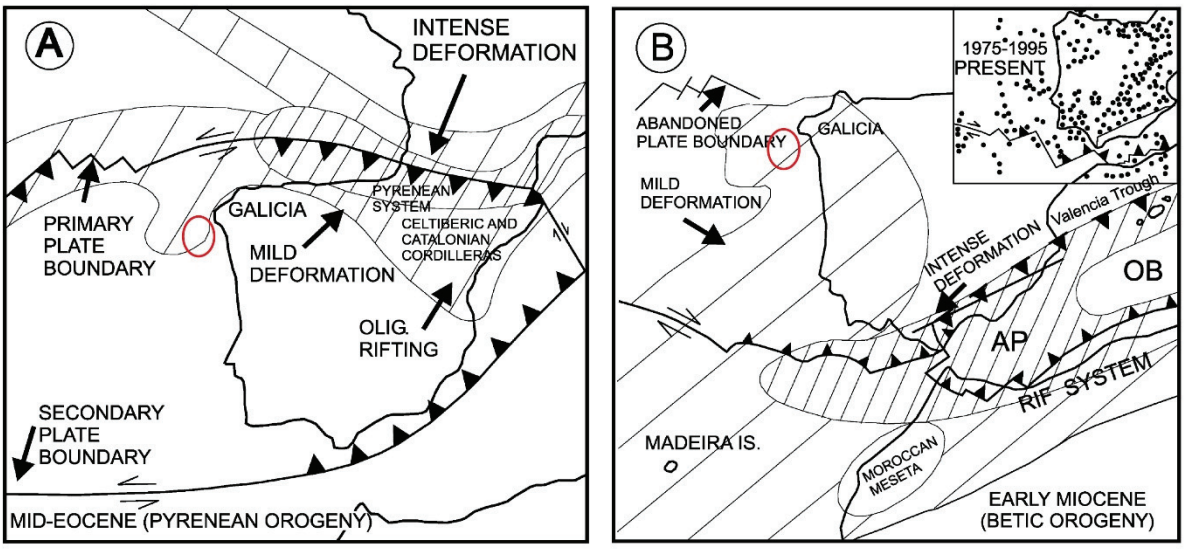

Figure 1.5 - Extent and direction of deformation around Iberia during A: the Pyrenean Orogeny in from Mid-Eocene times onward and B: the Betic Orogeny from the Early Miocene times onward. Hachured areas indicate deformation whilst the spacing of the hachures reflect the intensity of deformation. The inlay in B shows the location of present-day seismic activity. The red ellipses indicate the location of the Galicia working area (modified from Muñoz et al., 2003).

water depth in the interior Basin (Muñoz et al., 2003). Occasional seismic activity reports that some faults are active until recent times (Murillas et al., 1990; Muñoz et al., 2003).

Paleo and Neogene sedimentation appears mostly pelagic to hemipelagic in seismic sections (Boillot et al., 1979) but also mass-transport deposits and evidence of contourites have been found in the GIB and especially around the Galicia Bank (Ercilla et al., 2008; Murillas et al., 1990).

The Quaternary and particularly the Holocene sedimentary system has received significant scientific attention during the last decades. For instance, studies on the continental shelf revealed, that sediment is supplied by Portuguese rivers especially the Duoro river in recent times. It is then transported northward on the shelf, settling in a Mid-shelf mudbelt (Dias et al., 2002a, 2002b; Lantzsch et al., 2009, 2010; Oberle et al., 2014a; Zhang et al., 2016a). Off-shelf transport prevalently occurs in nepheloid layers, forming from resuspension during storm events (Dias et al., 2002b; Oliveira et al., 2002; Vitorino et al., 2002; Oberle et al., 2014b) and providing material for hemipelagic deposition on the continental slope (Bender et al., 2012). Additionally, deposition on the continental slope includes downslope-transported material as well as phases of contouritic activity (Bender et al., 2012; Hanebuth et al., 2015; Zhang et al., 2016b).

Several of these mechanisms are highly susceptible to glacial- interglacial changes. On the one hand, the reduced shelf area during glacials leads to a heightened supply of coarser material as river mouths are closer to the shelf break (Bender et al. 2012). Furthermore, the Mediterranean Outflow Water (MOW) was denser and, therefore, circulated in greater depth around Iberia compared to its modern mode (Schönfeld and Zahn, 2000). It assumedly did not flow through the GIB during glacials. During deglacial transition, on the other hand, it shoaled and when it appears in the GIB it interacts with local topography leading to the build-up of distinct contouritic depositional systems (Hanebuth et al., 2015; Zhang et al., 2016b).

1.3.2 Regional oceanography at the Galicia Margin

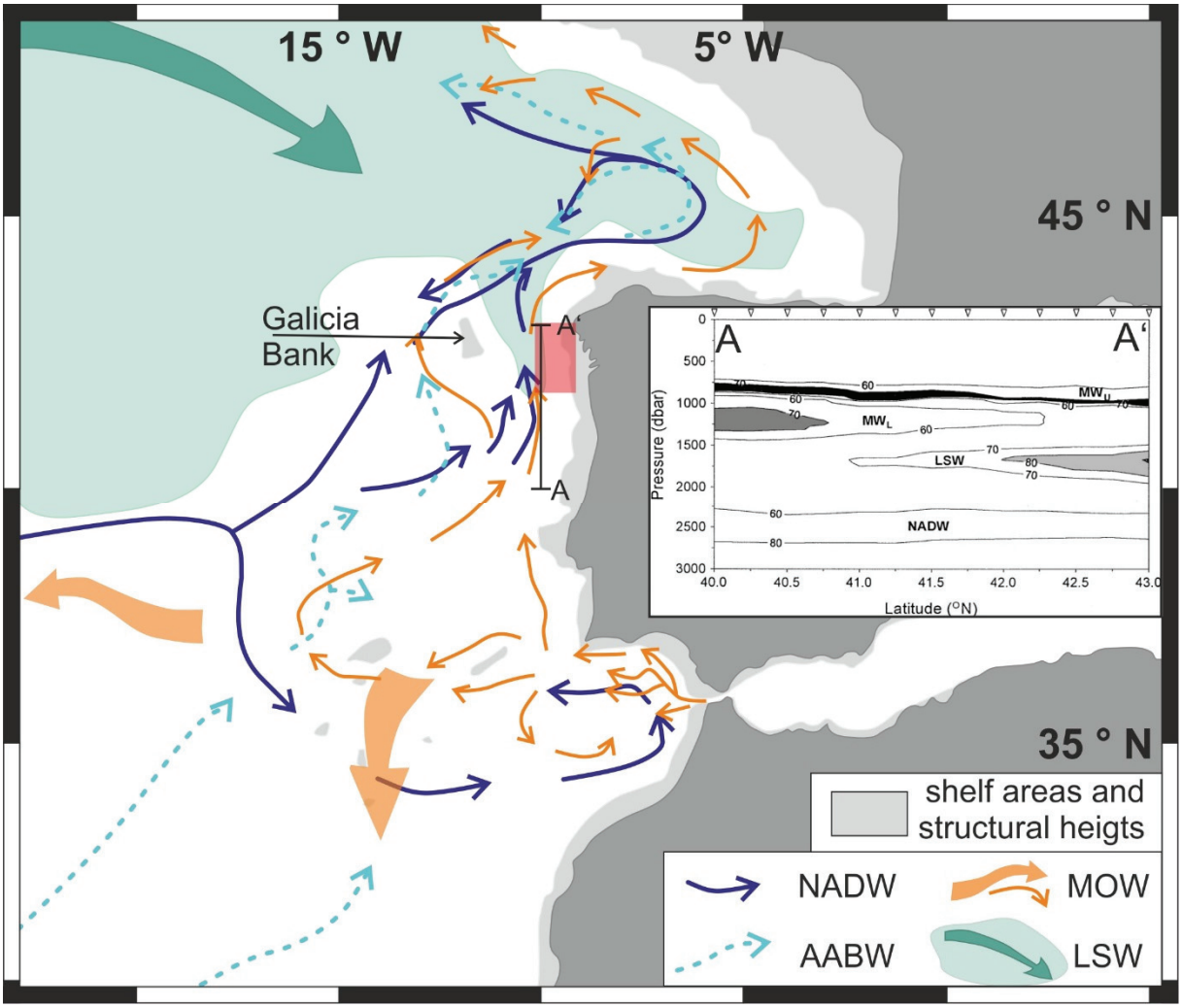

Figure 1.6 - Schematic overview of the circulation pattern of Atlantic water masses around Iberia below a depth of 500 m. Featuring Antarctic Bottom Water (AABW), NADW, LSW and MOW. Broad arrows indicate the general spreading direction of MOW and LSW respectively. The circulation pattern were redrawn and modified from Hernández-Molina et al. (2011). The transect (A-A') originates from the study of Fiúza et al. (1998). The red rectangle indicates the location of the Galicia working area.

Presently, under a mixed layer of up to 100 m vertical extent, the Galicia Margin is bathed by five main water masses being the East North Atlantic Central Water (ENACW), the Mediterranean Outflow Water (MOW), the Labrador Sea Water (LSW), the North Atlantic Deep Water (NADW), and the Lower Deep Water (LDW). The ENACW is usually reported in depth from 100 to 500 m (Hernández-Molina et al., 2001 and references within) but was also found reaching down to 600 m (Fíuza et al., 1998) or even 800 m (McCave and Hall, 2002). It consists of two cores, a warm saline upper core, which is formed in subtropic regions along the Azores front (ENACWst), and a colder and less saline core of subpolar origin (Fiuza et al., 1998; Varela et al., 2005). The MOW represents a relatively warm and saline water mass that exits the Mediterranean through the Strait of Gibraltar (Figure 1.6). Through mixing with Atlantic Water at different depth and along several paths an upper and a lower core develop (Fíuza et al., 1998). Several studies reported different depth ranges for these two cores with values ranging from 500 – 800 m and 780 –1400 m for the upper and lower core, respectively (Fíuza et al., 1998; Varela et al., 2005; Hernández-Molina et al., 2011 and references within). The different paths along which the MOW cores entrain Atlantic Water furthermore lead to different

spreading of the water in the Atlantic basin (Figure 1.6). As a consequence, only the upper MOW core is present in the GIB (Fíuza et al. 1998) (Figure 1.6 A-A'). Below the MOW, the LSW, which originates from the northwestern Atlantic, is present down to a water depth of 2200-2300 m (Hernández-Molina et al., 2011; Fíuza et al., 1998) and in places even down to 3000 m depth (Varela et al., 2005). NADW is reported until a water depth of 4000 m (Fíuza et al., 1998, Hernández-Molina et al., 2011) However, other studies suggest that the entire water column below the LSW is dominated by the LDW, comprising the Antarctic Bottom Water (AABW) and the Labrador Deep Water (Hernández-Molina et al., 2011, Varela et al., 2005).

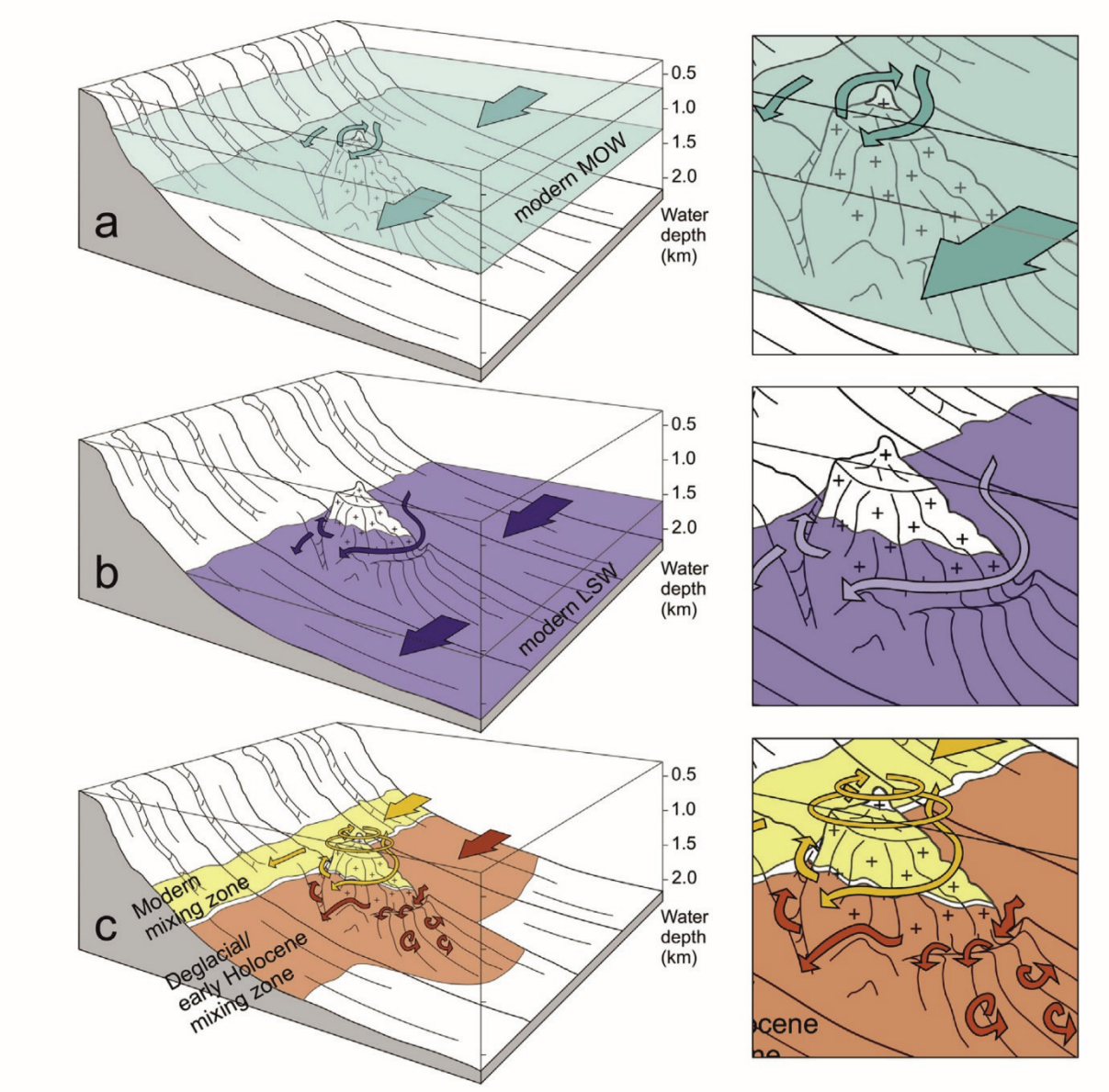

Figure 1.7 - Conceptual scheme of the water mass structure around the Pontevedra Outlier (Hanebuth et al., 2015) a: Depicts the depth of the modern MOW around the obstacle and its interaction with the obstacle.b: Position of modern LSW bathing the foot of the obstacle and the adjacent contourite drift. c: Depth of the mixing zone. The yellow color represents the modern mixing zone which interacts with the top of the obstacle and the slope. The deglacial/early Holocene mixing zone is depicted in brown, it is associated to oceanic density fronts and eddies which have an impact on the contouritic sedimentation on the drift and erosion in the moat.

The circulation pattern of these water masses is quite complex as they occasionally bifurcate and recirculate, especially in the Gulf of Cadiz and the Bay of Biscay (Figure 1.6). The situation within the GIB is less complicated as all water masses flow northward (Fíuza et al., 1998).

The circulation of MOW changed significantly under glacial and deglacial conditions. Due to reduced freshwater input to the Mediterranean, the glacial MOW was denser and thus flowed deeper in the Atlantic compared to interglacial conditions. Along the Iberian Margin, indicators for glacial MOW influence have been found 300 to 700 m deeper to its modern position (Schönfeld and Zahn, 2000; Rogerson et al., 2005; Hanebuth el al., 2015; Zhang et al., 2016b). Furthermore the deglaical periods were identified as periods of contouritic activity. Modelling at the *Pontevedra outlier* in the GIB showed that oceanic density fronts travelling through a 300 m lowered transition zone between LSW and MOW would create sufficiently enhanced bottom currents when they interact with the topography to build up contouritic drifts (Figure 1.7) (Hanebuth et al. 2015; Zhang et al., 2016b).

1.3.3 Regional geology of the Angola Margin

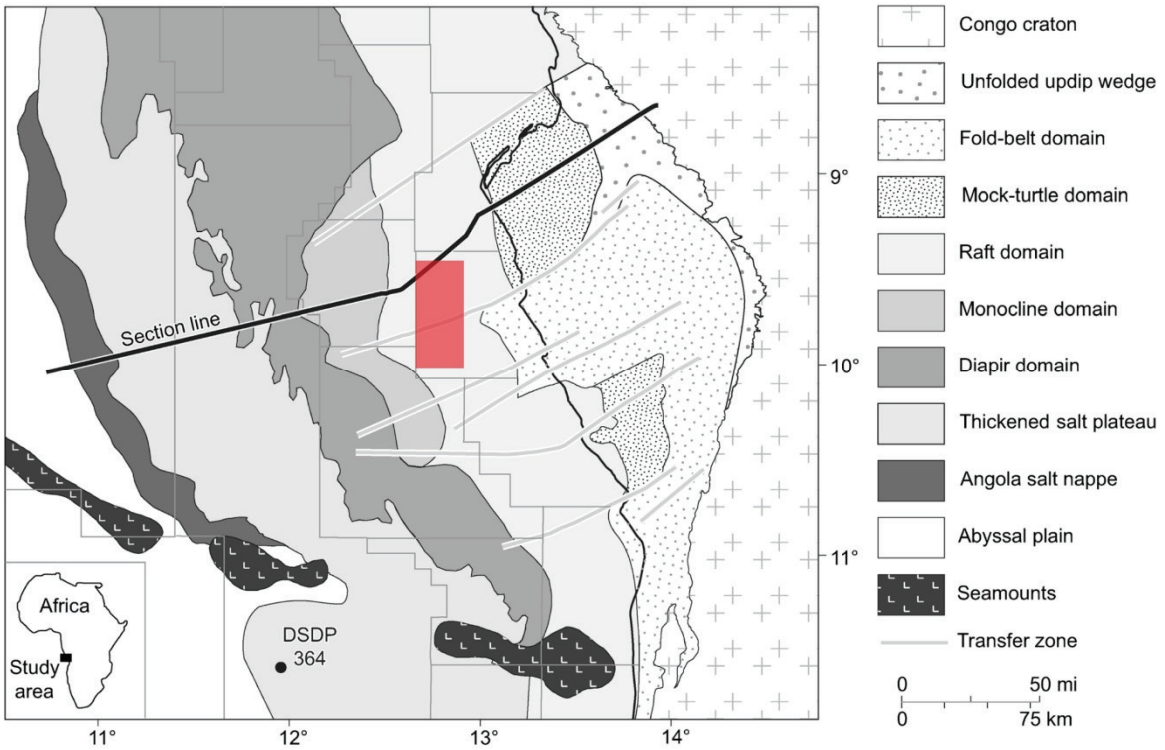

Figure 1.8 - Overview map showing different structural domains in the Kwanza Basin at the Angola Margin (modified from Hudec and Jackson, 2004). The red rectangle indicates the location of the working area presented in Chapter 5 of this thesis. The section line is shown in Figure 1.9.

The working area along the Angola continental margin (Figure 1.3) is situated in the outer Kwanza Basin in water depth between 200 and 800 m (Figure 1.8). The entire Kwanza Basin covers an area of 120000 km² of which about 25% are presently located onshore, forming the inner Kwanza Basin (Kukla et al., 2017). Like other West African basins (e.g. Gabon and Congo Basin), the Kwanza Basin has been shaped by the occurrence of salt and the associated deformational processes and was extensively explored for hydrocarbons (Ala and Selley, 1997).

Rifting at the Angola Margin in the context of the opening of the South Atlantic in the Lower Cretaceous started around 144-140 Ma and ended around 127-117 Ma (Guiraud and Maurin, 1992; Fort et al., 2004). Sediment deposition in the newly formed West African basins can be subdivided into pre-salt deposition, salt deposition and post-salt deposition (Lundin, 1992). In the Kwanza Basin the pre-salt sequence comprises clastic deposits from lacustrine environments but also deposits of volcanic origin including basaltic lava and tuff (Ala and Selley, 1997). Massive salt deposition of possibly up to 1 km thickness resulted from marine transgression in the Aptian (Lavier et al., 2001). Albian to Eocene sedimentation featured carbonate platforms, marls as well as shales and are bounded by a widespread hiatus related to the onset of deep sea circulation at the Eocene Oligocene Boundary (McGinnis et al., 1993; Lavier et al., 2001). Cenozoic sedimentation is characterized by prograding clastic deposits

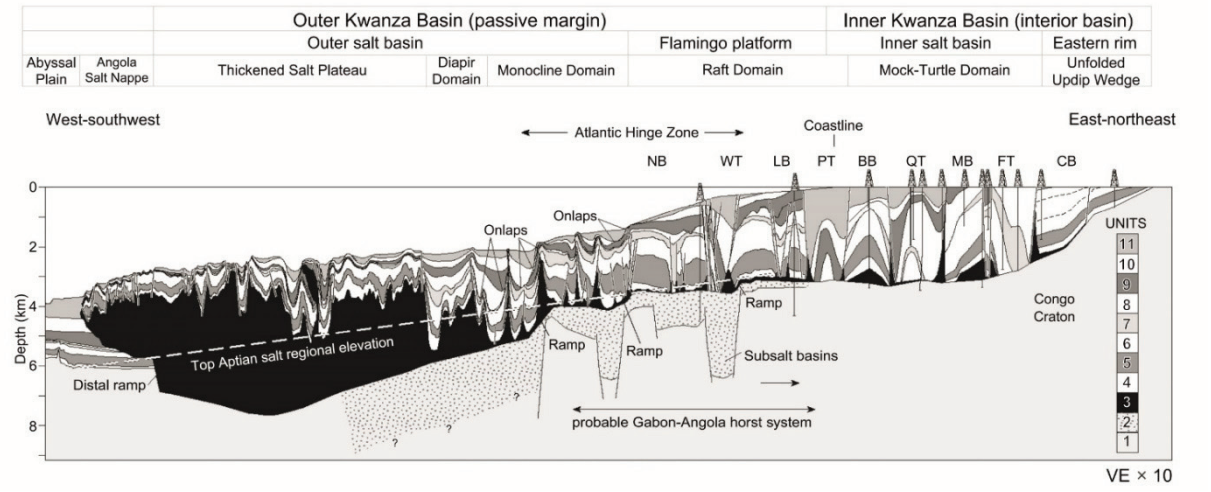

Figure 1.9 - Transect across the Angola Margin from Hudec and Jackson (2004). The origin of the transect is indicated in Figure 1.8 as section line.

with clinoform morphology. Coastal uplift in Miocene times led to further erosional events as well as high sedimentation rates due to enhanced coastal erosion (Lavier et al., 2001).

Gravity deformation of post-salt deposits in the Kwanza Basin started when the overburden was only a few hundred meters thick around 110 Ma (Duval et al., 1992). In terms of tectonic stress, salt deformed margins can always be divided into an upslope extensional domain, where the salt is thinning, and a downslope compressional domain (Cramez and Jackson, 2000; Marton et al., 2000). Deformation resulting from these stresses lead to the formation of different features characterizing specific domains along the margin (Figure 1.8, Figure 1.9) (Hudec and Jackson, 2004). In Angola, the deep margin east of the abyssal plain represents a salt nappe, consisting of allochthonous salt, that is overthrusted on abyssal-plain sediments (Cramez and Jackson, 2000; Marton et al., 2000; Hudec and Jackson, 2004). East of it a thickened salt plateau reaches thicknesses of up to 4.5 km. Subsiding minibasins which shape the bathymetry above the plateau, indicate that, although the salt is considered to be authochthonous, deformation is ongoing (Hudec and Jackson, 2004). The diapir domain is quite complex as it is characterized by a multitude of structures, such as salt-cored anticlines, salt rollers, salt stocks, salt walls and salt sheets. In most parts of the margin it is wider than it appears in the transect in Figure 1.9 (compare Figure 1.8) (Hudec and Jackson, 2004). Further upslope, the downslope movement of sediment over ramps in the base salt resulted in the formation of the monocline domain. East of it, the raft domain is the last offshore domain. The process of salt rafting will be reviewed in greater detail in the following paragraph, as it is of particular interest in this thesis. Onshore, in the inner Kwanza Basin, the mock-turtle domain can be found, which was named after its characteristic depositional pattern in troughs, and the unfolded updip wedge (Figure 1.9). In some onshore areas a fold-belt domain, containing different contractional structures, is present (Figure 1.8) (Hudec and Jackson, 2004).

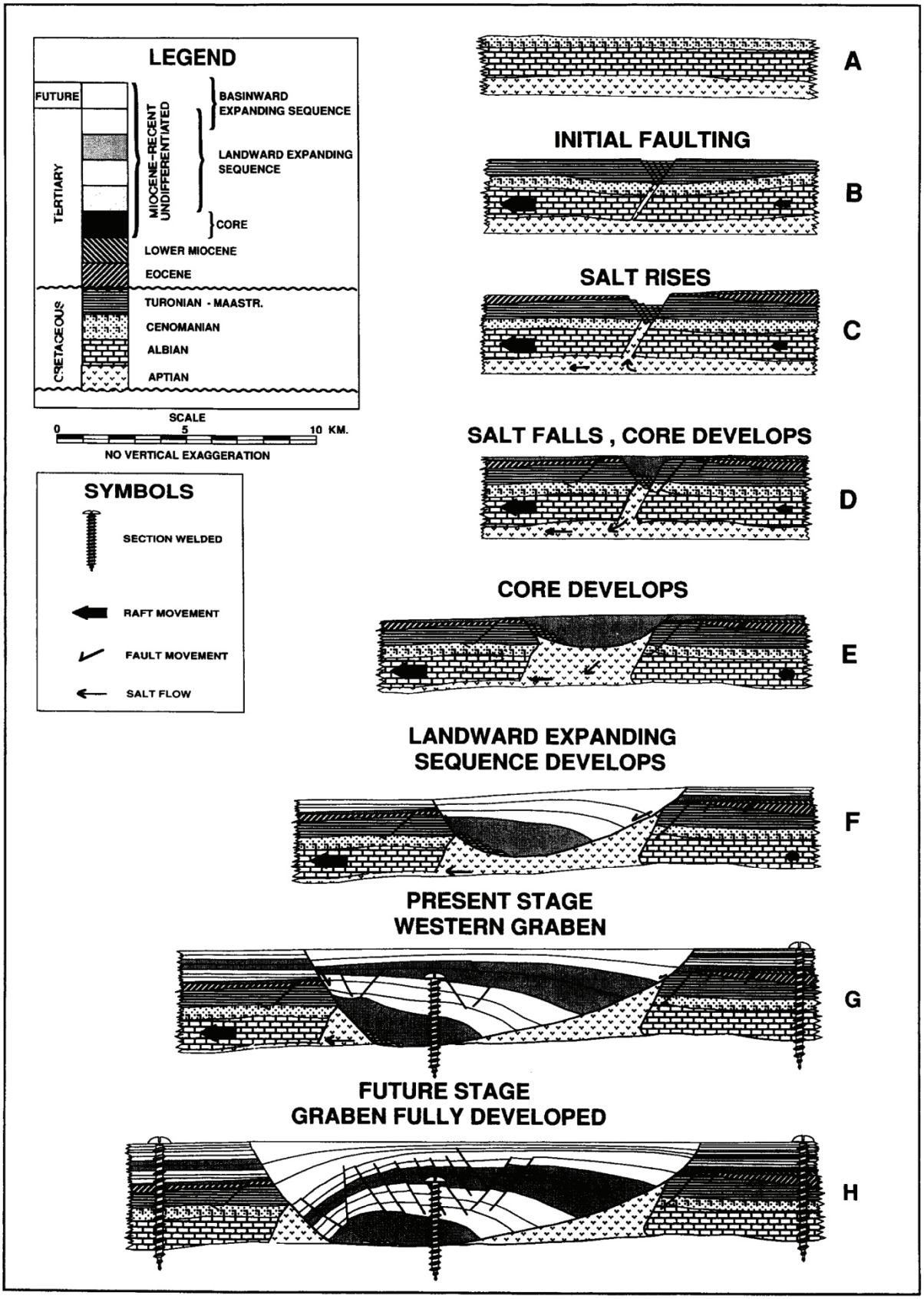

Figure 1.10 - Conceptual model of salt rafting in the Kwanza Basin, developed by Lundin (1992). The model comprises eight stages, from an undisturbed sediment column to a fully developed and sediment filled extensional graben.

The study area of the Angola Margin is located in the Salt raft domain (Figure 1.8). Salt Rafting is an extensional process during which overburden sediment fully separates in rafts, which are blocks of sediment, moving over a décollement of thin evaporates without being in contact with each other (Duval et al., 1992). In between the rafts, grabens open, which are filled by syndeformational sediments (Lundin, 1992). In the Kwanza Basin, a type location for salt rafting, two phases of salt rafting occurred. Phase 1 or pre-raft blocks already ruptured and tilted in the Middle to Upper Cretaceous. They extended for a few kilometers in across slope direction. Upper Cretaceous sedimentation subsequently conjoined the phase 1 rafts (Duval et al., 1992). The blocks which ruptured during the second phase of rafting are much larger and not tilted (Duval et al., 1992; Lundin, 1992). Duval et al. (1992) time the phase 2 rafting to 55 to 10 Ma whilst the model by Lundin (1992) indicates that the most seaward raft block and associated depocenter is not fully developed yet.

The model of Lundin (1992) partitions the evolution of salt rafts and grabens into the following eight stages (Figure 1.10A-H):

It starts with a seemingly undisturbed coherent sediment package, which just as well could be constructed from conjoined phase 1 rafts (Figure 1.10A) (Lundin, 1992). These sediments are faulted under extensional stress during downslope movement (Figure 1.10B) (Lundin, 1992). Then salt rises in the fault, while the initial graben develops over the diapir due to the seaward raft moving faster than the landward raft (Figure 1.10C) (Lundin, 1992). Sediment deposition in the graben leads to the development of a so-called core, whilst the salt level in the fault is falling again. The graben and the core widen, while the movement of the landward block diminishes (Figure 1.10D, E) (Lundin, 1992). In the next step a marked asymmetry is established in the graben filling in the form of a landward expanding growth sequence. Presumably, this is related to fact that material is mostly delivered from land in a prograding fashion (Figure 1.10F) (Lundin, 1992). Growing and rotation of this landward expanding growth sequence in combination with continuously falling salt levels eventually result in the grounding of the graben fill on pre-salt strata. Without the salt acting as a decollement the position of the landward raft block and the sedimentary core in the graben are fixed. The seaward block and the remaining salt keep on moving downslope, which causes the seaward part of the graben filling to subside. During that process, faults may develop in the graben sediments (Figure 1.10G) (Lundin, 1992). In the last evolutionary step, the subsidence at the seaward flank of the graben leads to the formation of a basinward expanding sequence (Figure 1.10H) (Lundin, 1992). The pattern which is observed in a cross section in the graben now resembles the shell of a turtle hence the term mockturtle.

This formation of sedimentary depocenters yields important stratigraphic implications. First, the sedimentary fills in the grabens might be underlain by stratigraphic gaps of 60 to 90 Ma (Duval et al. 1992). Secondly, and of great importance for the study presented in Chapter 5 of this thesis, it creates lateral age discontinuities and a strong lateral variation of sedimentation rates unrelated to the amount of sediment supplied but solely controlled by accommodation space created through subsidence in the graben.

1.3.4 Regional oceanography at the Angola Margin

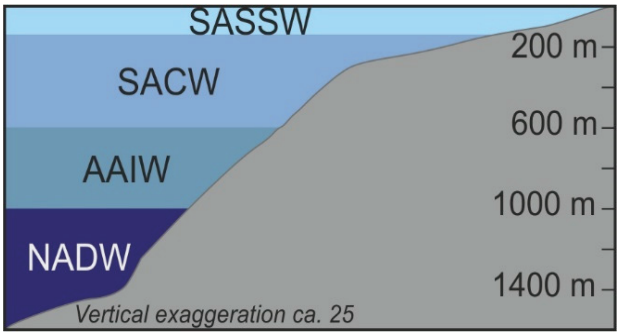

Figure 1.11 - Sketch of the water mass structure off Anglola below 40 m, based on the findings of M122 (Hebbeln et al 2017). The slope morphology was redrawn following the transect of Hudec and Jackson (2004) see Figure 1.9.

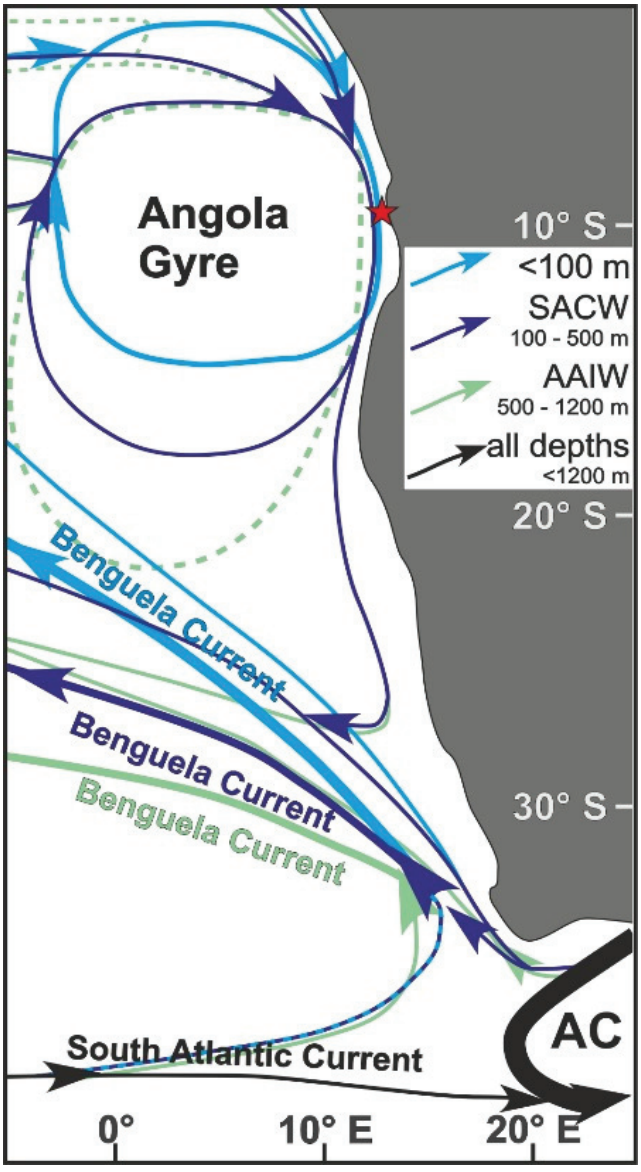

Figure 1.12 - Schematic circulation in water depth down to 1200 m in the South East Atlantic (redrawn from Stramma and England, 1999).

During the cruise M122 the following water mass structure was encountered offshore Angola (Figure 1.11) (Hebbeln et al. 2017). The surface waters down to 10 m are very warm and fresh due to insolation and river discharge, between 10 and 40 m water depth more saline surface waters are derived from the water masses of the South Equatorial Counter current. From 40 to 70 m water depth South Atlantic Subtropical Surface Water (SASSW) occurs. It is underlain by South Atlantic Central Water (SACW), which extends down to 600 m. The two lowermost encountered water-masses are the Antarctic Intermediate Water (AAIW) in depths greater than 600 m and the North Atlantic Deep Water (NADW) of which first traces appear in 1000 m depth (Hebbeln et al 2017).

The main circulation in the eastern South Atlantic off West Africa, is dominated throughout the upper 1200 m by the cyclonic Angola Gyre and the Benguela Current (Figure 1.12) (Stramma and England, 1999). Their position moves southward with greater water depth but the general circulation pattern is similar in all depth above 1200 m. Additionally, a frontal zone, the Angola Benguela Front, is situated in the upper 50 – 200 m around 20° to 18° S (Gordon and Bosley, 1991; Stramma and Schott, 1999). Figure 1.12 however shows clearly, that in the study area of Chapter 5 all water masses flow southward in the Angola Gyre.

Cold Water Corals

One of the main objectives of the *RV Meteor Cruise M122* to the Angola Margin, was to sample and map previously mostly unexplored Cold Water Coral (CWC) mounds. Cold Water Corals as framework building corals are sessile suspension

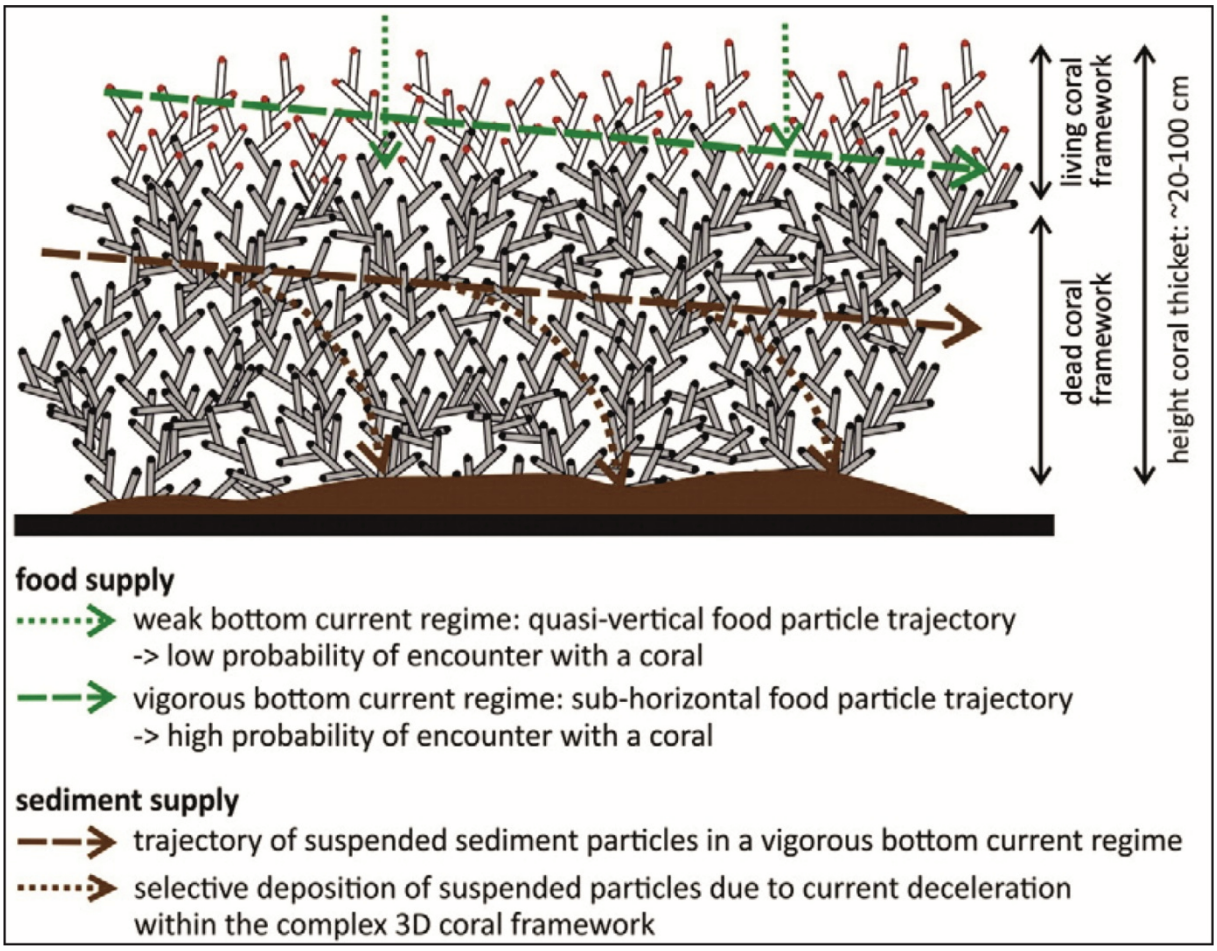

Figure 1.13 - Schematic illustration on how Cold Water Corals benefit from an active hydrodynamic regime considering food and sediment supply (Hebbeln et al., 2016).

feeders which are able to build up seafloor structures of up to 200 m in height (eg. De Mol et al. 2002). Up until now CWC studies mostly concentrated on the North Atlantic however CWC have been discovered in most oceans by now (Hebbeln and Samankassou, 2015). They are frequently encountered alongside contouritic depositional systems, as they prefer highly energetic bottom current conditions for the advection of food and sediment. The beneficial role of advected sediment is to settle within the coral framework and thus stabilize the structure (Hebbeln et al., 2016).

The evolutionary sequence of initial erosion, followed by initial CWC growth and contouritic deposition, often changes after the mounds have reached a certain height. From then on, bottom currents interact with the mound structure (e.g. De Mol et al., 2002; Van Rooij et al., 2003) causing further changes in the distribution of sediments (Hebbeln et al., 2016).

1.4 Thesis outline and contribution declaration

Chapter 1 provides a general introduction into the scientific background of contourite research, the geologic and oceanographic background of each study area as well as the motivation and aims in this thesis. Chapter 2 introduces the material and methods with a special focus on multichannel seismic data acquisition and processing. Chapters 3 to 5 each consist of a standalone manuscript. The manuscripts were developed in cooperation with co-authors and shall be published as peer-reviewed articles. More details on each manuscript are given below. Chapter 6 concludes the thesis with a short summary and outlook for future research.

Chapter 3 describes a paleoceanographic reconstruction based on the current influence on sediment distribution at the Galicia Margin. It consists of the manuscript below and is ready for submission:

Increasing impact of North Atlantic Ocean circulation on sedimentary processes along the passive Galicia Margin (NW Spain) over the past 40 million years

Authors: Julia Haberkern, Tilmann Schwenk, Till J.J. Hanebuth, Volkhard Spieß

To be submitted to *Marine Geology*

Author contributions: The seismic datasets (GeoB06, GeoB11) used in this study were acquired during two research cruises to the Galicia Margin. The GeoB06 data was acquired during *RV Poseidon* cruise PO 342, during which the co-author Till Hanebuth was chief scientist. The GeoB11 data and the bathymetric data were acquired during *RV Meteor* cruise M84-4 during which the co-author Till Hanebuth was chief scientist, co-author Tilmann Schwenk was responsible for the multichannel seismic and hydroacoustic data acquisition. I participated in this cruise as a student assistant for hydroacoustic and multichannel seismic data acquisition. The bathymetric data was processesd by Tilmann Schwenk. I confirm, that I processed all utilized multichannel seismic data, developed the scientific concept in communication with the co-authors, created all figures/tables and wrote all sections of the manuscript. Draft versions were reviewed by Tilmann Schwenk and Till Hanebuth. *(Personal contribution 85%)*

Chapter 4 classifies the distribution of topographic structures and contouritic features at the Galicia Margin and furthermore identifies the interaction processes responsible for the shape of the contouritic depositional system. It consists of the manuscript below and is ready for submission:

Morphology and evolution of contouritic depositional systems steered by the interaction of bottom currents with distinct seafloor topography at the Galicia Margin (NW Spain)

Authors: Julia Haberkern, Tilmann Schwenk, F. Javier Hernández-Molina, Till J.J. Hanebuth, Volkhard Spieß

To be submitted to *Marine Geology*

Author contributions: The seismic dataset (GeoB11) the bathymetric data and the Parasound echosounder data were acquired during *RV Meteor* cruise M84-4 to the Galicia Margin, during which the co-author Till Hanebuth was chief scientist, co-author Tilmann Schwenk was responsible for the multichannel seismic and hydroacoustic data acquisition. I participated in this cruise as a student assistant for hydroacoustic and multichannel seismic data acquisition. The bathymetric data was processesd by Tilmann Schwenk. I confirm, that I processed all utilized multichannel seismic data, developed the scientific concept in communication with the co-authors, created all figures/tables and wrote all sections of the manuscript. The morphosedimentary map presented in the Chapter was derived together with co-author Javier Hernández-Molina. Draft versions were reviewed by Tilmann Schwenk. *(Personal contribution 85%)*

Chapter 5 presents the evolution of a fault-controlled contouritic depositional system related to salt-rafting at the Angola Margin. Additionally the position and influence of Cold Water Corals within the system is shown. It consists of the manuscript below and is ready for submission:

Fault controlled contouritic depositional systems beneath and around Cold Water Corals – an example from the salt rafted Angola Margin

Authors: Julia Haberkern, Tilmann Schwenk, Paul Wintersteller, Stefan Wenau, Claudia Wienberg, Dierk Hebbeln, Volkhard Spieß

To be submitted to *Marine Geology*

Author contributions: The Seismic dataset (GeoB16) and the bathymetric data utilized in this study were acquired during *RV Meteor* cruise M122 to the Angola and Namibia Margin. During this cruise co-author Dierk Hebbeln was chief scientist, co-author Paul Wintersteller was responsible for the acquisition of bathymetric data and I was responsible for the acquisition of multichannel seismic data. Paul Wintersteller furthermore processed the bathymetric data. I confirm that I processed the multichannel seismic data with the help of a student assistant and developed the scientific concept in communication with the co-authors, created all figures/tables and wrote all sections of the manuscript. Draft versions were reviewed by Stefan Wenau and Tilmann Schwenk. *(Personal contribution 90%)*

2 Data and Methods

In this thesis multichannel seismic (MCS) data, Parasound echosounder data and Multibeam data from both the Galicia and the Angola working area were used for joint data interpretation. In the Galicia working area, 41 MCS profiles were acquired during *RV Meteor Cruise Galiomar III (M84-4)* in 2011. This dataset was completed by three additional seismic profiles collected during the *RV Poseidon cruise POS 342* in 2006. In the Angola working area 27 profiles were acquired during *RV Meteor Cruise M122* in 2016.

2.1 Multichannel seismic data acquisition

The general setup of the Multichannel Seismic acquisition system consisted of a seismic source, a streamer, the acquisition unit and the GPS/Navigation system from the ship for each of the cruises (Figure 2.1).

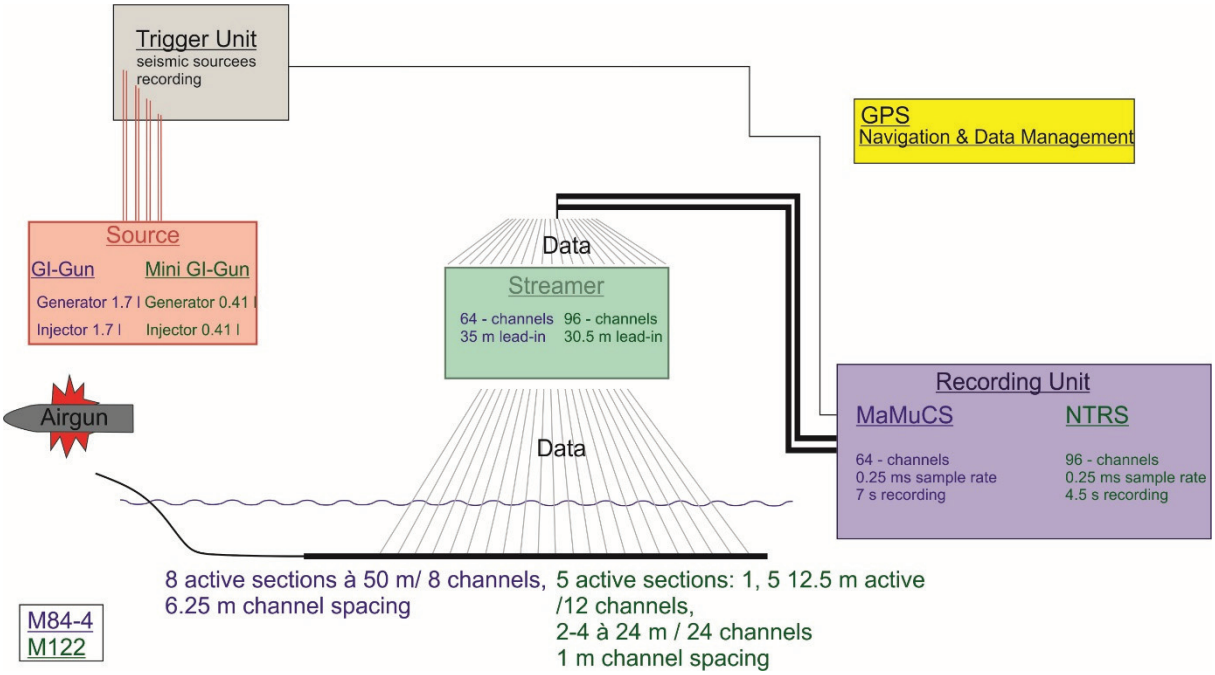

Figure 2.1 - Schematic diagram of the main components of the MCS acquisition system, blue writing gives the specifications used during M84-4 and green writing the ones of M122

2.1.1 M84-4

During the *RV Meteor cruise Galiomar III (M84-4)* to the Galicia Margin in 2011, a GI-Gun (generator volume 1.7 l, injector Volume 1.7 l) served as seismic source. It was shot in harmonic mode with an injector delay of 0.25 s to prevent a bubble signal. Highly pressurized air was supplied by a compressor container manufactured by the Sauer Company. The gun was shot at an air pressure between 145 and 155 bar. It was towed 16 m behind the ship at the port side. With an average survey speed of 5 kn and a shot rate of 7 s the average shot spacing amounted to 10 m.

For recording a 400-m long 64-channel analogue streamer from the company SYNTRON was used. It had 8 active sections of 50 m length each, which contained hydrophone groups of 6.25 m length with up to 13 hydrophones per group. The streamer was towed with 35 m lead in and a stretch of 48 m length. For depth control of the streamer five Digi Birds were used. They were set to the surveying depth before each survey by a Digi Bird Controller PC. Online surveying of their depth was switched off due to connection and trigger problems.

Data recording was performed with the custom made MaMucCS-System (Marine Multichannel Seismic System) developed at University of Bremen. The main components were a Pentium IV based PC (3 GHz, 1GB RAM, Windows XP) and three NI6052E 16-bit AD-converters. Each of the AD-converters was connected to 32-channel multiplexer (NI-SCXI1102-C) with onboard pre-amplification and anti-alias filter. The acquisition software recorded nearly continuously and stored the data in demultiplexed SEG-Y format on hard-disk. The MaMuCS PC was also used for logging of the ships GPS data and distributed the data to other PCs via the network.

To trigger the different components of the acquisition setup a separate IBM compatible PC with a Windows NT 4.0 operating system was used. A real-time controller interface card (SORCUS) with16I/O channels synchronized by an internal clock is included in the unit. It was connected to an amplifier unit, which converted the controller output to positive TTL levels, and a gun amplifier unit, which generated a 60V/8A trigger level, strong enough to control the magnetic valve of the gun. Custom made software running on the PC allowed for the definition of arbitrary combinations of trigger signals, which could be changed at any time during recording. This was used to optimize the trigger time for minimum shot distance but recording long enough to cover the entire penetration depth of the seismic source, furthermore recording delays were adapted to water depth during recording.

2.1.2 POS 342

During *RV Poseidon Cruise Galiomar (POS 342)* to the Galicia Margin in 2006 a Mini-GI-Gun (generator volume 0.25 l, injector Volume 0.25 l) was shot in harmonic mode with an injector delay of 0.2 s. Highly pressurized air was provided by two portable KAP14 Bauer compressors. The gun was operated at an air pressure of 140 to 150 bar. It was towed 12.5 m behind the ship at the port side. The shooting rate was adjusted to water depth between 8 and 9 s which in combination with an average survey speed of 4 n resulted in a shot-point distance of 17 m.

The signal was recorded with a 101-m long 16-channel analogue streamer form the company Teledyne Exploration Co. The active section contains 16 hydrophone groups of 6.25 m length each consisting of 8 hydrophones. It was towed with a 12.5 m lead in and a 25 m stretch.

For recording and triggering the same units as during M84-4 were used. With the only difference that only one of the AD-converters was needed to record the 16 channels.

2.1.3 M122

During the *RV Meteor cruise M122* at the Angola Margin in 2016 a mini-GI gun (generator volume 0.49 l, injector volume 0.49 l) was shot with an injector delay of 0.15 s. Highly pressurized air was supplied by a compressor container manufactured by the Sauer Company. The gun was operated at an air pressure of 150 bar. The towing position of the gun varied between surveys from 15.4 to 17.5 m behind the ship on the port side. The shooting rate was adapted to water depth and signal penetration. Most of the time it was set to 4.5 s. Average survey speed was 4.5 kn thus shot spacing varied between 7 and 10 m.

The signal was recorded with a Hydroscience Technologies Inc. (HTI) 96-channel digital streamer of 120 m length. It consisted of 5 active sections, of which the first and the last accommodated 12 channels and 12.5 m of stretch, whilst the middle three sections accommodated 24 channels. Within the section the channels were spaced 1 m apart of each other and at section boundaries the spacing went up to 1.95 m since between any two sections a HTI SeaMUX A/D converter was built in to digitize data previous to transmission. Furthermore the streamer was towed with a lead in of 30.5 m length, which combined with the 12.5 m stretch

in the first section amounts to a total distance of 53 m distance between the ships stern and the first active channel. For streamer depth control four Digi Birds were attached to the first four sections of the streamer and the tail was trimmed with lead. The Digi Birds were set to depth form a PC running ION System 3 bird control software. The PC and the Digi Birds were interfaced during surveying through a magnetic communication coils and a Data Management Unit (DMU) as well Line Interface Unit (LIU), which both are a physical interface between the PC and the sensors and cables. The power supply for the streamer was a Glassman High Voltage power source which provided a constant current of approximately 750 mA using 8-10 V per section. For security the power was controlled by a Ground Interrupt Unit (GFI).

To record the data a HTI NTRS (New Technology Acquisition System), a PC running the acquisition software was used. The interface between the NTRS and the streamer was a Quad-Array Interface panel (QA) connected to the 50 m decks-cable and a decks Junction Box. The acquisition software facilitated nearly continuous recording in an HTI internal SEG-D format to hard disk with a maximum sampling rate of 250 microseconds. The data were converted to SEG-Y format (IBM) using the custom-made software PS32SEGY of the University of Bremen. Navigation data was logged on a separate PC.

For triggering all components of the system, the same unit and amplifiers used during M84-4 were used.

2.2 Multichannel seismic data processing

The advantage of marine multichannel reflection seismic data over data recorded by single-channel devices is based on sampling a single point on the seafloor multiple times, while the equipment is moving over it. These multiple samples always contain the same geological signal as well as different random noise. Stacking of the signal will enhance the geologic part as it will stack constructively, whilst randomly occurring noise will be supressed. Thus the main objective of data processing lies on enhancing the signal to noise (S/N) ratio to achieve the best possible structural image of the subseafloor. A standard processing sequence contains pre-processing steps such as geo-referencing of traces and delay corrections as well as the removal of bad traces. Generally, the processing routine can be divided into pre- and post-stack measures. Before stacking, normal move-out and residual statics were corrected as well as some noise reduction measures like despike and frequency filters were applied. After CMP stacking, further signal enhancing methods as well as post-stack migration were carried out (Figure 2.2).

Single processing steps are quite sensitive to recording parameters such as offsets, receiver spacing, water depth and noise content, as well as the frequency content of the data. Therefore the entire processing sequence should be adjusted to the specifications of the data.

For the data presented this thesis the program *VISTA 2013 2D/3D Seismic Data Processing Software processing* was used. The following chapter will explain the applied processing routine, as well as the differences in the treatment of the two large datasets. An overview of all steps and the specifications for either dataset is found in Figure 2.2.

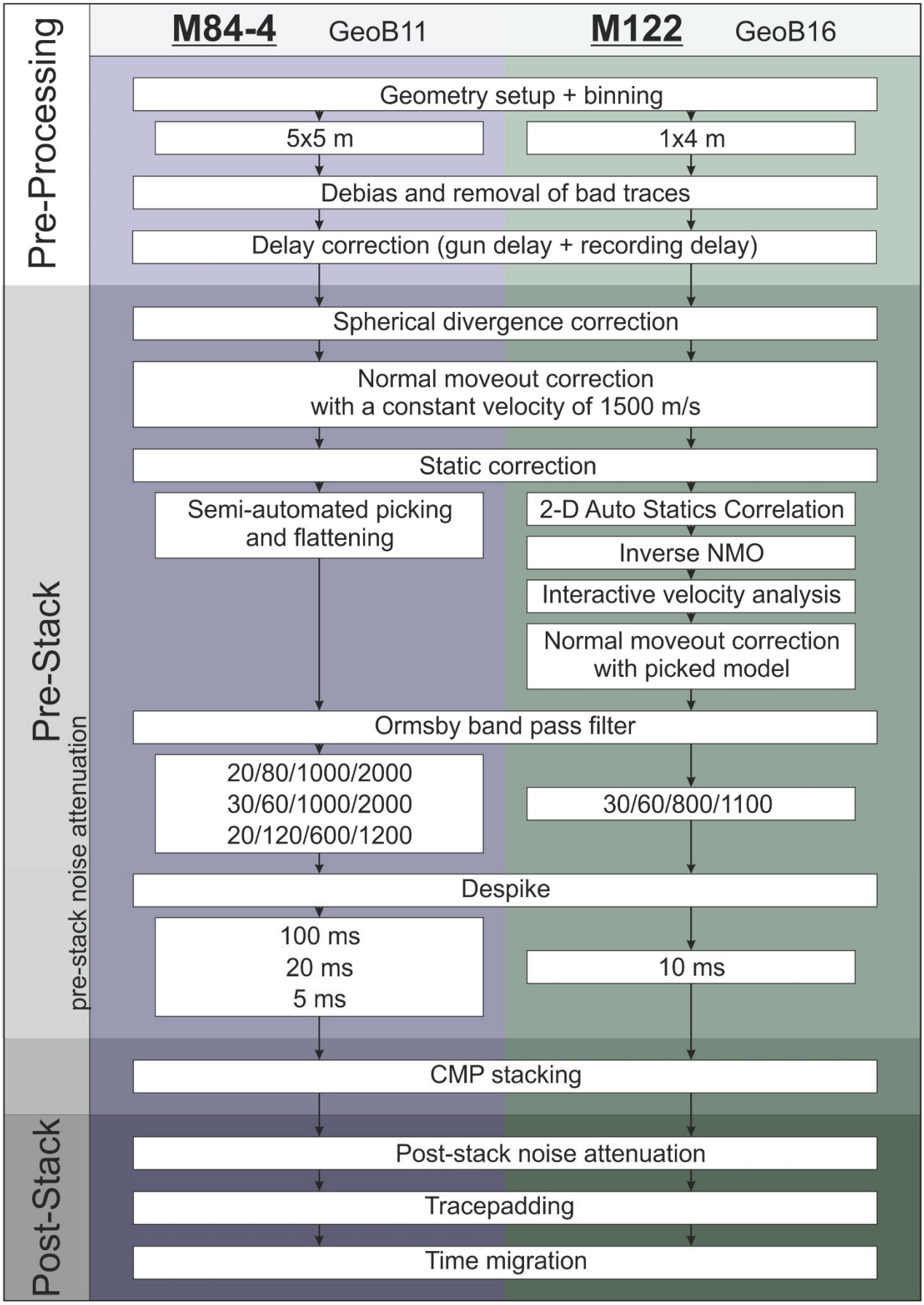

Figure 2.2 - Flowchart showing the processing workflow for the M84-4 dataset on the left and the M122 dataset on the right.

2.2.1 Pre-processing

Since the true value of any geological information is closely tied to the knowledge of its location, geo-referencing is one of the most crucial steps in pre-processing of MCS data. The header of the data recorded only contained crude or no navigation information. To obtain the exact location of the reflection of the seismic signal on the seafloor for each receiver in every shot, each seismic trace was combined with navigation data depending on the time-stamps of both datasets. Furthermore, the relative positions of the source and each receiver to the GPS-antenna were used to calculate their absolute position for each shot. These steps were carried out in the custom made software WinGeoApp, which furthermore allows to smooth navigation data and remove bad data points. Under the assumption of a horizontal seafloor topography the mid-point between source and receiver represents the point where the seismic signal is reflected and thus the origin of the seismic trace. After calculation of their position, all mid-points within a certain area on the seafloor were assigned to a common midpoint (CMP). This processing step is called binning, with one bin being the area on the seafloor in which all traces may be assumed to image the same point and therefore will be stacked during processing. Thus the along-track bin size defines the final horizontal data resolution which becomes higher with decreasing bin sizes. At the same time and in a reverse fashion, it controls the fold, the amount of traces contributing to one stacked trace. A larger bin sizes results in a larger fold which results in a higher S/N after stacking and furthermore may contribute to the efficiency of certain methods which rely on statistic stability such as the estimation of static corrections. The fold naturally also depends on the overall coverage of data which in turn depends on shot rates and receiver spacing. In older equipment receivers often deteriorate resulting in lower signal to noise ratio or even no signal content in the recorded trace. These traces have to be omitted, which then compromises the data coverage. For example of the 64 channels of the syntron streamer deployed during M84-4a, less than 17 worked reliably. Therefore binning to an along-track resolution of 5 m in this data resulted in a fold between 4 and 6. The M122 dataset in contrast was recorded with a new digital streamer with 96 working channels in shallow to intermediate water which allowed for higher shooting rates. On this data binning to an along-track size of 1 m still provided an average fold between 8 and 12.

After binning, bad traces were omitted, and the two way traveltimes of the data were adjusted for the mechanical delay of the gun as well as possible recording delays by bulkshifting all affected traces. Furthermore a debias filter was used to centre the amplitudes in each trace around zero.

Figure 2.3 illustrates the differences between the datasets after pre-processing, which mostly stem from their acquisition geometry and the equipment used. It shows the traces of one shot gather sorted by offset (distance between source and receiver) both have been additionally treated with a low cut filter of 10 to 20 Hz to supress the swell noise. The most striking difference is amount of traces and also the range of the offsets. The M122 data is distributed evenly over the entire offset of around 140 m whilst the M84-4 data cover an offset of almost 400 m with much fewer traces, which on top of that are very irregularly distributed. Also in terms of scaling and penetration as far as it is shown, the M122 appears very uniform and regular and poses a strong contrast to the M84-4 example where traces are differently scaled and therefore show different penetration. Furthermore different kinds of noise add to the observed irregularities. These differences are credited to the use of different streamers, while

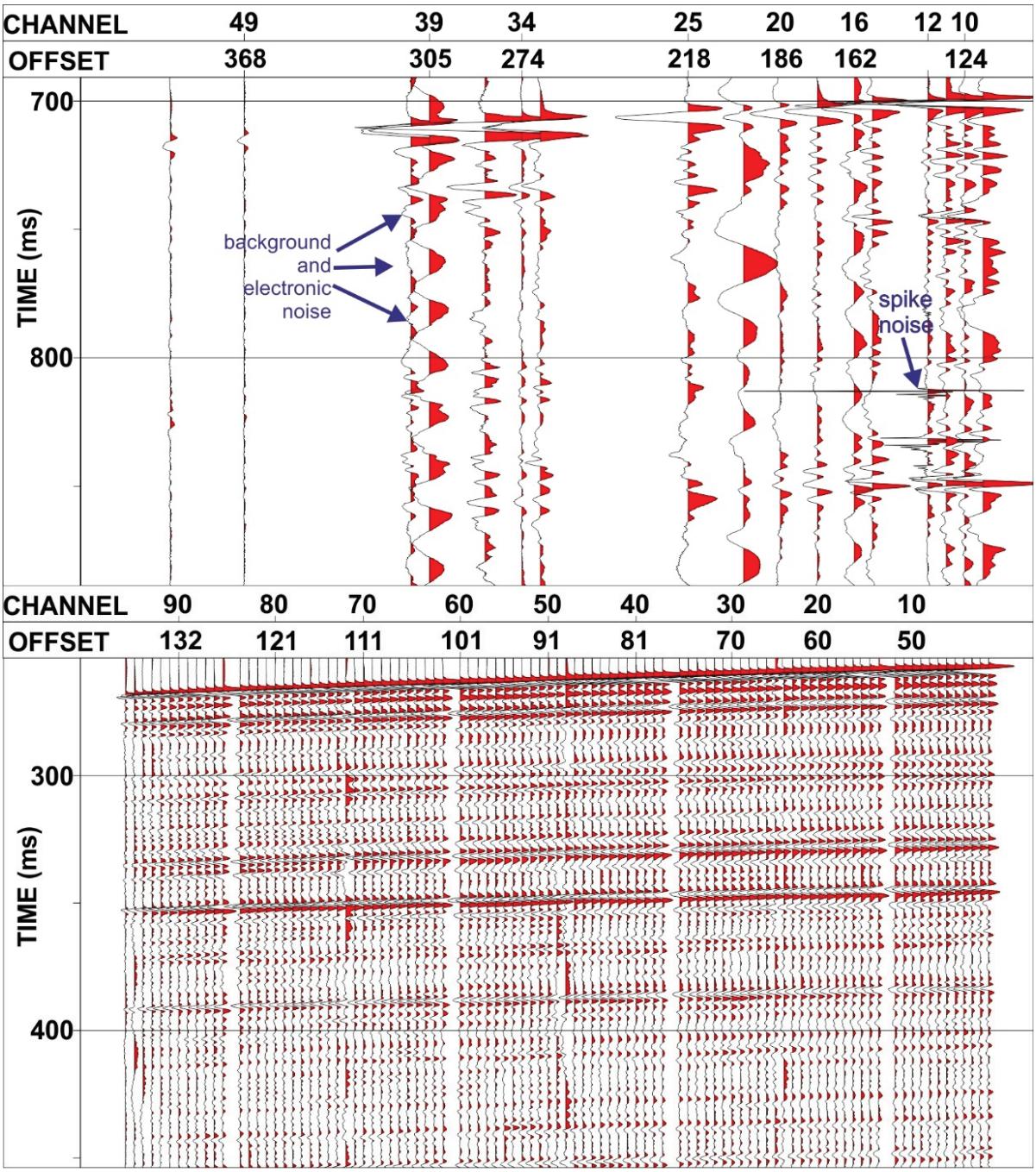

Figure 2.3 - Exemplary shot of each dataset after pre-processing in similar vertical scaling, furthermore treated with a low cut filter of 10 to 20 Hz.

the wavelength of the signal reveals the use of different sources. This comparison already shows that both datasets require different treatment while processing.

2.2.2 Normal-moveout correction

Normal-moveout (NMO) describes the time difference of a signal at a given offset compared to a zero-offset trace due to the longer pathway of the signal. Therefore in an offset sorted display a reflection from any horizontal layer occurs as a hyperbola. The exact shape of the hyperbola is dependent on the depth of the layer and the medium seismic velocity above the layer. Prior to stacking seismic traces have to be NMO corrected, which transforms them to a zero-offset trace. The velocities which are therefore required are called NMO-velocity (Yilmaz, 2001). The Vista Processing Software offers the option of an interactive velocity analysis in

which a velocity model may be manually picked at selected CMPs along the profile and into depth, via the comparison of the NMO velocity along hyperbolic events, the quality of stacks produced with the application of different velocities and the semblance which represents the normalized energy of said stacks. For a good outcome of this analysis seafloor and underlying strata should be close to horizontal. Additionally it is helpful if offsets are relatively large compared to the water depth since in that case the shape of the hyperbola appears more pronounced and variations of the shape are easier to determine. For the M122 dataset the interactive velocity analysis was carried out for all profiles. On M84-4 data in contrast it proved not to be feasible as the diminished far offset channels in combination with steep topography complicated picking. Additionally the M84-4 are situated in water depth up to 2700 m thus the velocity of the water column dominates the mean velocity. Thus a correction with a constant NMO velocity of 1500 m/s turned out, to produce the best results.

Right before the application of the NMO correction the data are corrected for spherical divergence which amounts for the loss of energy (factor: $1/r^2$) resulting from the fact that acoustic waves distribute their energy on a spherical surface, which increases with traveltime. Due to this relationship to traveltime, the correction needs to be applied prior to NMO correction. It generally enhances amplitudes in the deeper parts of the data.

2.2.3 Residual static correction

During acquisition, the equipment in the water is subjected to wave movement. This causes a relative movement in all three dimensions between source and receivers, which is reflected in vertical displacements of traces remaining after NMO correction within a CMP gather, but also between neighbouring CMPs. Hence, correcting these movements by shifting traces to their proper vertical position has two benefits, first a better stacking result within a CMP and secondly an increase in reflector coherency along the stacked profile. The necessary shifts can be estimated statistically by cross-correlating traces while applying different shifts and thus identify the shift with the best correlation coefficient. This requires a good data coverage and only can properly treat static shifts up to half a wavelength. To provide coherency across CMPs the auto statics 2D algorithm implemented in the Vista Processing Software considers a stacked profile as reference model.

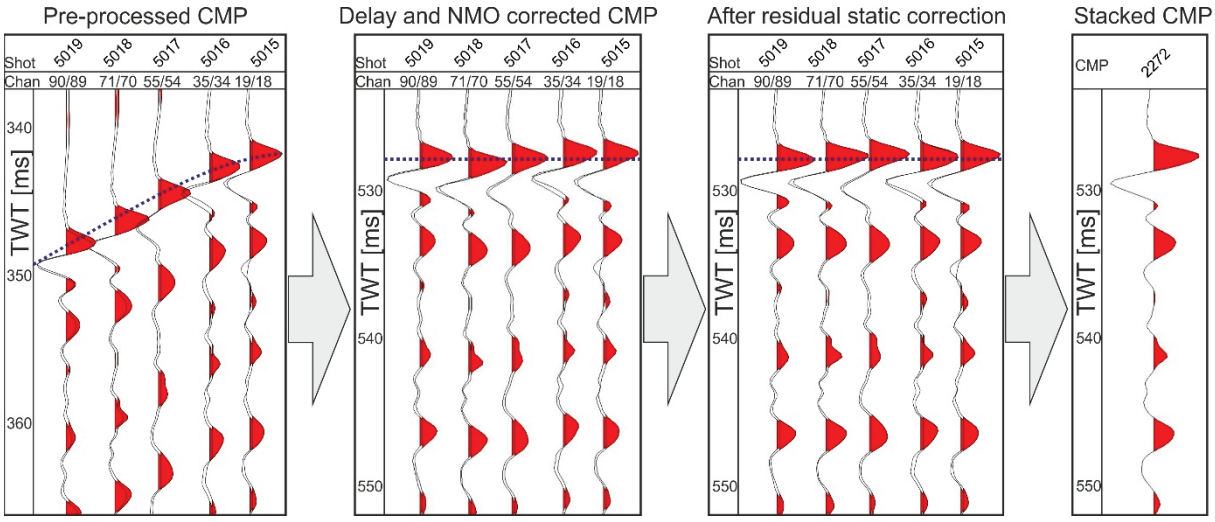

Figure 2.4 - Illustration showing the results of delay and NMO correction, static correction and stacking at one exemplary CMP gather.

Static shifts in the M122 data were sufficiently removed by this method. In the M84-4 dataset however the low data coverage did not provide enough statistical stability, since occasionally CMPs only contain one or two traces. Thus another method, allowing for more manual control, had to be chosen.

The general idea of this method is to semi manually identify the first-break which in marine seismic represents the seafloor reflection and assign all first-breaks within one CMP to the same previously specified seafloor depth. Coherency along the stacked profile is then generated through smoothing. Technically the first-breaks are initially identified within a stacked section of the data. The depth of the first-break in each CMP is then used to identify the first-breaks within the respective unstacked CMP-gathers. In a second step the first-breaks picked along the stacked profile are smoothed by employing a running mean and each trace in the unstacked CMP gathers is shifted to the depth of the CMP after smoothing. This method is quite time intensive, since the semi manual first break picking requires thorough revising, in exchange it very reliably improves stacking results. Special care and considerations have to be taken when it comes to the seafloor smoothing as it also averages the horizontal resolution of the data. Therefore only 5 traces were used in the running mean. Nonetheless diffraction hyperbolas at the seafloor due to the highly variable and steep topography of the Galicia Margin proved to be a pitfall for this method: in the last processing step the energy of the hyperbolas should migrated to their point of origin, however at some locations the smoothing altered the shape of hyperbolas and thus would compromised the success of the migration. To prevent that, after smoothing, in areas where a lot of hyperbolas occurred first-breaks were manually restored to their original position.

Naturally, strong residual statics complicate an interactive velocity analysis, as they lower the stacking result and also obscure the normal-moveout hyperbola. Therefore the M122 data were first subjected to a NMO correction with a constant velocity model of 1500 m/s, then residual statics were corrected and afterwards and inverse NMO correction was used to undo the initial NMO correction. These data were then used for the velocity analysis and finally again NMO corrected with the picked model.

2.2.4 Noise attenuation (Pre-stack)

During the acquisition of seismic data different noise sources may contribute to the recorded signal, in the water there might be background noise originating from the ships engine or waves. Electrical noise might be induced into the electric cables as an example *RV Meteor* is

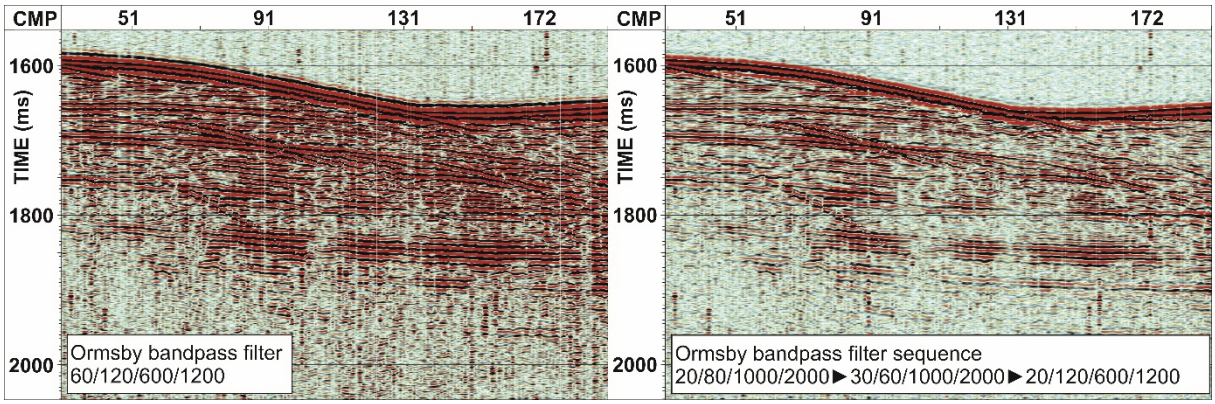

Figure 2.5 - Comparison of the bandpass filter sequence (right) to the same data filtered in only one pass (left). On the left strong ringing can be observed at the seafloor and at reflectors in greater depth.

known to emanate a distinct electrical noise with a frequency of 50 Hz, which also produces several harmonic peaks. Here the advantage of the digital streamer comes into play as no electronic noise is visible in the data. Frequency dependent noise was tackled for both datasets with an Ormsby Bandpass filter. For the M122 dataset a single filter with the flanks 30/60/800/1100 provided excellent results. The electric noise of 50 and 100 Hz showed to be quite disturbing in the M84-4 data so it was aimed to cut low frequencies at 120 Hz. One single bandpass filter however turned out to produce a tremendous amount of ringing since the low cut had to be placed in the low frequency peak of the amplitude spectrum. Therefore a sequence of three different bandpass filters was determined to gradually remove the energy from the low frequencies. The flanks 20/80/1000/2000, 30/60/1000/2000 and 20/120/600/1200 were employed in that order to minimize the ringing (Figure 2.5).

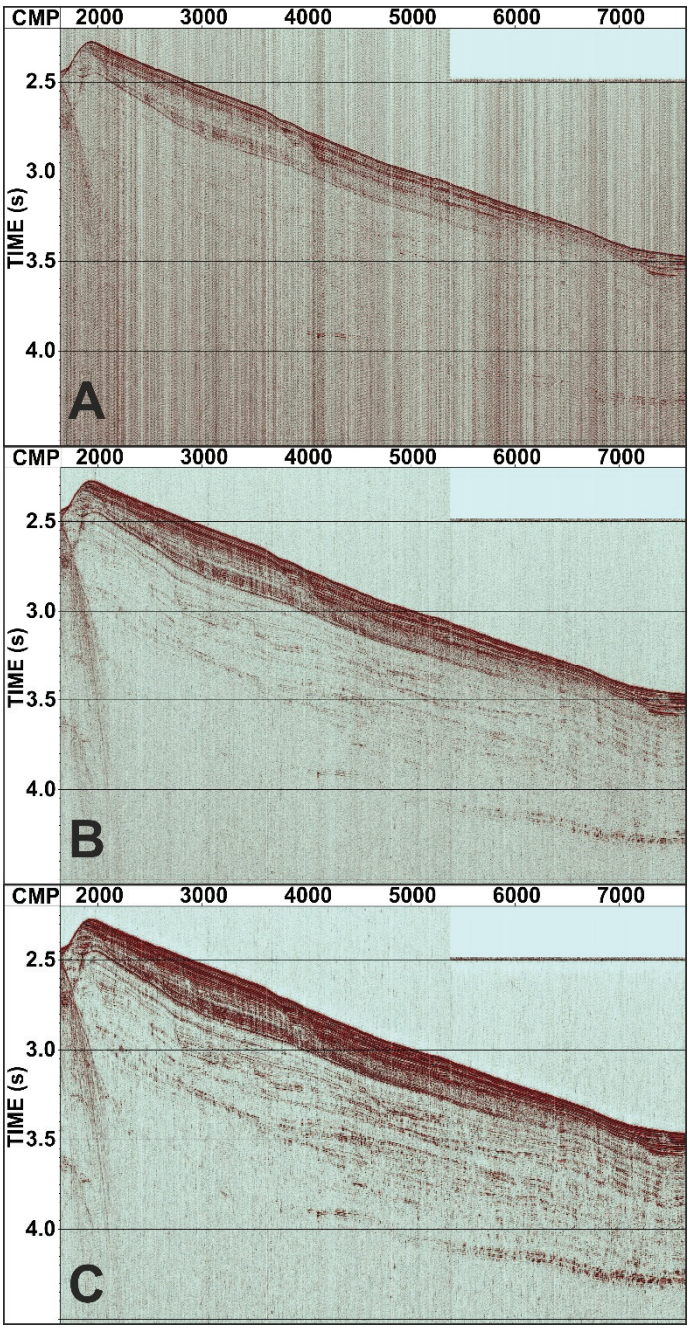

Figure 2.6 - Data enhancement and noise supression after A: filtering, B: filtering and despike, C: white noise suppression. After each step, background noise is reduced and reflectors are enhanced.

In a second step of noise removal, spike noises, sudden events of high amplitudes, have been removed with a despike algorithm. This algorithm relies on the spatial similarity of the geologic signal to construct a background amplitude around one trace, by averaging several adjacent traces in its CMP. Then, in a distinct traveltime interval, a so-called time window, the amplitude of each single trace is compared to its ambient background amplitude, if it exceeds it by more than a certain threshold, it is scaled down. This comparison is repeated along the whole trace and performed for each trace. Thereby the length of the time window determines the length of the spike noises which may be attenuated by the algorithm. In the M122 data only short spikes fitting into a time window of 10 ms occurred and were omitted in that fashion, whilst in the M84-4 data three consecutive runs of 100, 20 and 5 ms proved to create the most excellent results (Figure 2.6).

2.2.5 CMP-stacking

Although data are stacked for quality control at different steps of the workflow a final stack is produced after frequency filtering and despiking. Mathematically a stacked CMP trace is calculated by summing up all

unstacked traces in the CMP and dividing the result by their number plus one, to normalize the amplitudes.

2.2.6 Noise attenuation (Post-stack)

The Vista Processing software furthermore provides another useful tool for signal enhancement, which improves the data quality most, when applied post-stack. The method is called White Noise Suppression or 4D-DEC Algorithm and basically extracts energy from the data, which cannot be assigned to any continuous reflection throughout multiple traces. The identification of the energy as noise relies on spatial coherency of the geologic signal and thereby considers that reflectors might be dipping. This method proved to be very useful in enhancing the overall imaging quality in both datasets through removal of noise even in the source frequency (Figure 2.6).

2.2.7 Migration

To prepare the data for migration, the final step in the processing sequence, empty CMPs were filled by trace padding as for the migration an equidistant spacing of traces is important. After that, a Finite Difference (FD) Time Migration was performed. It requires the input of a velocity model thus for the M122 dataset the picked models were used, whilst for M84-4 profiles a constant velocity model of 1500 m/s was employed. The major aim of migration is to move energy, which is distributed by diffraction to its point of origin. Diffraction leads to dips of surfaces being underestimated and hyperbolas at edges.

The FD Time Migration algorithm was chosen as it is robust to faulty velocity models. It proved to be effective in collapsing most of the diffraction hyperbolas and correcting dipping reflectors to their true gradient. However since in 2D profiles the energy can only be shifted along the profile during migration, diffracted energy from topography next to the profile, cannot be properly relocated and therefore side echoes cannot be removed during 2D migration. Thus special care was taken during data interpretation not to interpret these artefacts (e.g. Figure 2.7).

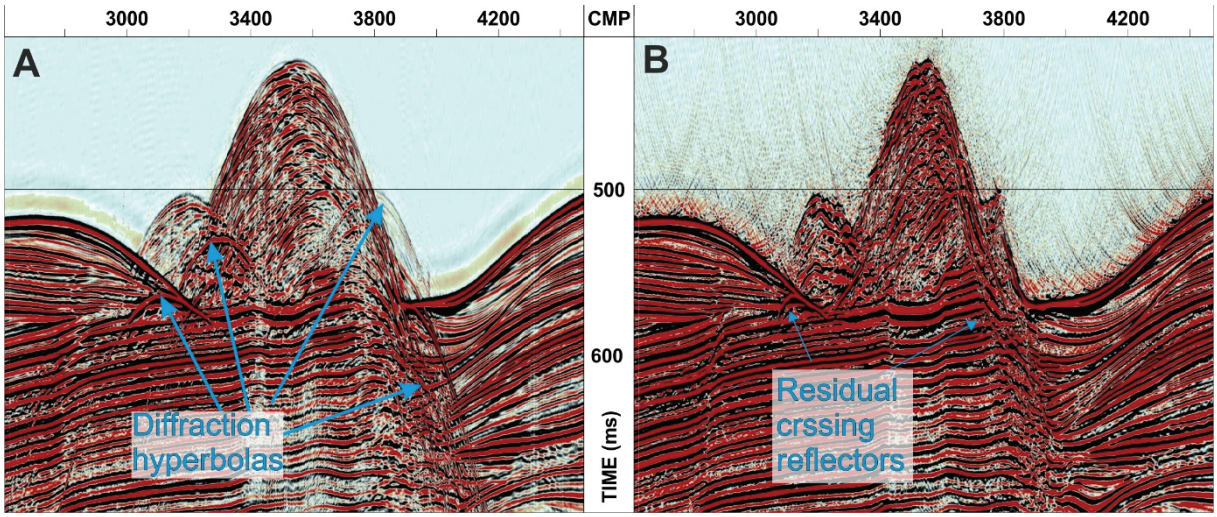

Figure 2.7 - Cutout of Profile GeoB16-034 A: prior to migration and B: after migration. It is clearly visible that most of the diffraction hyperbolas collapsed. Only a few reflector crossings remain which are attributed to side echoes.

2.3 Hull mounted echosounder systems

Since the RV Meteor is equipped with a hull mounted Parasound sediment echosounder and two Simrad Kongsberg Multibeam echosounders these devices were used during cruise M84-4 as well as M122 in similar fashion.

2.3.1 Parasound Sediment Echosounder

The Parasound Sediment Echosounder P70, which is installed on *RV Meteor,* utilizes the parametric effect to create a high intensity signal suitable for sediment profiling in a narrow cone. Therefore two waves of similar frequencies are emitted simultaneously, one of these primary frequencies is fixed to 18 kHz the second primary frequency can be varied between 18.5 and 24 kHz. The parametric effect leads to the development of so-called secondary frequencies, which are equal to the sum and the difference of the two primary frequencies. Usually the second primary frequency is chosen to create a secondary low frequency (SLF) around 4 kHz, which then travels in the narrow cone (4.5°) of the high primary frequencies. This significantly improves the footprint compared to the wide opening angles (30°) of conventional sediment echosounders. Combined with a sub-meter scale vertical resolution the SLF is able to image sedimentary structures in a high resolution with penetration depth of 20 - 200 mbsf depending on the sediments encountered.

Since Parasound Data were acquired nearly continuously during both *RV Meteor* cruises and were available readily processed for this thesis, large datasets are available both in the Galicia and the Angola working area. Exploiting all information held in that data is well beyond the scope of this thesis, nonetheless the availability of high resolution data helped to identify small-scale surficial features such as sedimentary waves and or resolve whether erosional areas have been draped in the Holocene. It was only used systematically in the Galicia working area.

2.3.2 Multibeam Swath Bathymetric Data

Two hull-mounted Kongsberg Simrad multibeam echosounders are available on *RV Meteor*, the EM 710 for bathymetric mapping in shallow water depth and the EM 122 for middle and deep water depth. The EM 122 uses a frequency of 12 kHz with 288 beams having each a footprint of 1° by 2°.

The EM 710 operates with frequencies between 70 and 100 kHz it can be used with 256 or 400 beams of an along-track beam width of 1°. In across track direction the beams can be distributed over up to 150 ° either in equiangular or equidistant fashion.

On both cruises processing and imaging of the data were carried out mostly on board. The bathymetric map of the Galicia working area is a blend of datasets from both EM 122 and 710, gridded to a resolution of 100 m. For the Angola working area, a bathymetric map of a resolution of 15 m was produced from the EM 710 data.

2.4 Data interpretation

For an integrated Data interpretation the MCS profiles were loaded to the Kingdom Software together with bathymetric and Parasound Data from the respective working area. Therefore SEG-Y files and ascii tables containing the navigation information were created as a last step in the Vista Processing Software. Interpretation steps in the Kingdom Software included horizon and fault picking in both datasets. In the Galicia working area the horizons were furthermore gridded and maps of sedimentary thickness for each seismic unit, were created

by subtracting the depth values of lower boundary from the ones of the upper boundary. Mean thickness from these thickness maps was then utilized to calculate mean sedimentation rates for each seismic unit. In the Angola Dataset fault picking was another important part of the seismic interpretation.

3 Increasing impact of North Atlantic Ocean circulation on sedimentary processes along the passive Galicia Margin (NW Spain) over the past 40 million years

Haberkern, J.[a, *], Schwenk, T.[a] Hanebuth, T.J.J.[b, a], Spiess, V.[a]

[a] MARUM – Center for Marine Environmental Sciences and Faculty of Geosciences, University of Bremen, Germany

[b] Department of Costal and Marine Systems Sciences, Coastal Carolina University, SC, U.S.A.

Abstract

Along the modern continental margin of Galicia (NW Spain) a vigorous current regime, dominated by Mediterranean Outflow Water (MOW), interacts with the complex basement topography. MOW exists since 5 Myrs, while the Galicia Interior Basin (GIB), a slope interior basin, developed during the rifting phase of the North Atlantic accumulating sediment since the Early Cretaceous. The evolving North Atlantic Ocean circulation left current-related imprints in the depositional pattern of the basin fill, which can in turn be utilized as paleoceanographic archive. Additionally Neogene phases of tectonic activity (Pyrenean and Betic orogenies) imprinted on the depositional pattern at the Galician margin in the form of small-scale faulting and mass wasting. This study reconstructs the evolution of the sedimentary system in the GIB since the Mid-Eocene, namely as the result of the interplay between downslope and along-slope processes, using high-resolution multichannel seismic data. Six major stages of the depositional history are identified and linked to the evolution of the North Atlantic Ocean circulation. The influence of contour currents on the depositional pattern steadily increased since Mid-Eocene. The strengthening of Northern Component Water, associated with the opening of the Faeroe Shetland basin, is documented at the southwestern European margin for the first time by the onset of a plastered contourite drift. The data also provide evidence that the closure of the Tethys-Indian seaway in the Miocene led to outflow of Tethys water into the Atlantic Ocean at intermediate water depths. Until the Mid-Miocene, the tectonic stress regime initially associated with the Pyrenean and later with the Betic orogeny led to mass wasting in the study area, which is documented in the form of deposits and scars. The onset of modern-style MOW after the Messinian Salinity Crisis (5.33 Ma) caused a distinct change in the depositional system from combined along- and down-slope transport processes towards predominant contouritic sedimentation, which is evident from the construction of separated mounded drifts during Pliocene and Early Pleistocene. Drift construction continued during Middle and Late Pleistocene, but with gaining influence of down-slope processes.

3.1 Introduction

The paleo-circulation of the North Atlantic water masses, particularly the formation of deep waters at northern high latitudes, as key element of Atlantic Meridional Overturning Circulation (AMOC) as well as the influence of Mediterranean Outflow Water (MOW), are important pieces in the big paleoceanographic puzzle. A wealth of paleoceanographic proxies has been used to unravel the evolution of North Atlantic Ocean circulation. $\delta^{13}C$ isotopes may, for instance, determine the age of bottom water masses and their flow direction (Woodruff and Savin, 1989). Neodymium (Nd) isotope signatures help to identify water masses and determine flow paths and water mixing (Stille et al., 1996). Divergence of Nd-signatures can ultimately indicate the closure of oceanic gateways. $\delta^{18}O$ isotopes, which reflect water temperatures and ice volume, give insight into ocean-atmosphere interactions (Wright et al., 1992). Contourite drifts, as bottom-current induced sediment deposits, proved to be useful in reconstructing the opening and closure of gateways (Knutz, 2008, and references within). In this fashion, the onset of drift formation in the northern North Atlantic (e.g. Feni, Eirik and Gloria drifts) accurately captures the opening of gateways to the Nordic Sea basins, in the Paleogene and Neogene, which from that time on supplied dense water to the AMOC. The Gulf of Cadiz contourite system is a younger example where contourites have been drilled recently to exactly date contourite drifts related to the Gibraltar Strait opening and the onset of Mediterranean Outflow (Stow et al., 2013). To complete the puzzle of basin-wide circulation, information from as many as possible locations around the North Atlantic basin are needed.

Since ocean gateways are natural bottlenecks for bottom water flow, they are usually associated to higher bottom current speeds, which might slow down further away from the gateway. Thus the observation of contourite drift construction close to a gateway, although a viable indicator for flow through the gateway, does not hold evidence for the impact of the water mass on overall basin circulation. It also does not hold much information on the pathway along which the water mass is flowing after it left the restricted gateway morphology. In return, the mere record of the presence of a water mass, does not automatically hold information on the general bottom-current velocity and its associated capability to influence local sedimentation pattern. The onset of North Atlantic Deep Water (NADW) production, close to its geographic origin referred to as Northern Component Water (NCW), is, for instance, considered to have initiated the south-eastern Faeroe Drift after the opening of the Faeroe-Shetland Basin around 35 Ma (Davies et al., 2001). Via and Thomas (2006) detected NCW at the Walvis Ridge over the past 33 Ma, which suggests that this water was transported to the South Atlantic shortly after the opening of this basin. Preu et al. (2012), in contrast, observed a significant NCW influence on sedimentation pattern at the Argentine continental margin only after the closure of the Central American Seaway in the late Pliocene (Duque-Caro, 1990; Haug and Tiedemann, 1998). This shows, how the pathway of a water mass and its influence on sedimentation pattern far away from its source can be altered without a change at its origin. Consequently the contribution of individual water masses to the overall North Atlantic Ocean circulation is best studied further away from any gateway.

This study focuses on the passive continental margin off Galicia (NW Spain), where contourites deposited under the influence of deep water, coming from the Nordic seas, and of MOW (Hanebuth et al., 2015) which are present since the Pliocene (Nisancioglu et al., 2003; Hernández-Molina et al., 2014). Marine deposition in this region is documented since the Upper Jurassic (Murillas et al., 1990). Previous studies have either focused on very deep

structures to understand the opening dynamics of the North Atlantic Basin (Boillot et al., 1979; Groupe Galice, 1979; Murillas et al., 1990; Muñoz et al., 2003; Pérez-Gussinyé et al., 2003), or on the Late Quaternary sediment dynamics (Bender et al., 2012; Hanebuth et al., 2015). The sedimentation system between middle Eocene and Pleistocene have, in contrast, not been studied in great detail, although significant changes in the Atlantic Ocean circulation took place in this time interval (Woodruff and Savin, 1989; Davies et al., 2001). This study utilizes a new high-resolution multichannel seismic (MCS) dataset, which resolves the late Paleogene and Neogene deposits well enough to differentiate the imprint of major gateway events, such as the opening of the Faeroe-Shetland Channel in late Eocene, the closure of the Tethys-Indian Seaway in early Miocene, and the intermittent closure of the Strait of Gibraltar in early Pliocene times. The dense lateral coverage with seismic data allows for distinguishing between the effect of successive tectonically active phases in the Neogene, which induced submarine down-slope sediment transport at the continental slope, and the interaction of the bottom-current regime with local topographic elements. Although both slope-related processes occur simultaneously, this study documents the transition from a domination of down-slope to predominantly slope-parallel sediment transport after the onset of Mediterranean Outflow.

3.2 Geology of the Galicia Margin

The Galician continental margin is characterized by the presence of an intraslope basin, the Galicia Interior Basin (GIB). It is almost 3000 m deep and separated from the Iberian Abyssal Plain by the Galicia Bank, a structural high peaking up to less than 700 m water depth (Ercilla et al., 2008). The study area is located at the eastern flank of the GIB (Figure 3.1A) and covers water depths from 100 until 2800 m. The evolution of the morphology in the whole area was initially controlled by several phases of tectonic activity. The GIB opened during an early rifting phase, in the very late Jurassic and early Cretaceous, preceding the ultimate opening of the Atlantic Ocean basin (Murillas et al., 1990). It poses an example of rifting of thin and cold crust, which led to hyperextension and sequential faulting, subsequently resulting in a horst and graben system with tilted blocks (Pérez-Gussinyé et al., 2003; Brune et al., 2017). Sediments that deposited prior to the opening of the GIB indicate shallow-marine conditions prior to and during rifting (Murillas et al., 1990; Sutra and Manatschal, 2012). Thus the recent depth of the GIB of 3000 m must have resulted from major subsidence after basin widening (Sutra and Manatschal, 2012). The subsidence was concluded in the late Cretaceous (Groupe Galice, 1979). Syn-rift sedimentation in the Lower Cretaceous was, to a certain degree, associated with mass wasting (Murillas et al., 1990). The mode of syn-rift sedimentation lasted until the late Aptian when a distinct stratigraphic unconformity at the deep Galicia Margin west of the Galicia Bank indicates the eventual breakup of the Atlantic Ocean basin. The post-rift sequence in the GIB, does not show any indicators of tectonic influence and is followed by a stratigraphic hiatus attributed to an early deep ocean circulation in the early Upper Cretaceous (Murillas et al., 1990).

The GIB and surrounding domains have repeatedly been subjected to tectonic stresses in Paleogene and Neogene times. During the Mid-Eocene, the Pyrenean orogeny exerted an N-S compressional regime, which affected large topographic structures and caused small-scale faulting, folding and inverted-graben formation mainly offshore NW Iberia (Muñoz et al., 2003) as the Iberian and Eurasian continents collided and oceanic crust was subducted in the Bay of Biscay (Boillot et al., 1979). Local structural features, such as an isolated topographic height and an anticline (TO 1 and Ridge 1 in Figure 3.2B) experienced uplift in the GIB during this

period (Murillas et al., 1990). Further compressional stress resulted from the convergence of Iberia and Africa during the Betic orogeny in the early Miocene, which affected large parts of western Iberia tectonically (Groupe Galice, 1979; Muñoz et al., 2003). The uplift of the Beiral de Viena Block at the eastern flank of the GIB reduced the overall size of the basin (Muñoz et al., 2003), when also faults and folds were reactivated and remained active till recent times (Murillas et al., 1990; Muñoz et al., 2003). Information on the history of post-rift sediment dynamics inside the GIB is sparse. Boillot et al. (1979) suggested pelagic or hemipelagic conditions during Paleogene and Neogene, whereas Murillas et al. (1990) additionally reported slides and contourites. A similar variety of sedimentation processes was described at the adjacent Galicia Bank (Ercilla et al., 2008).

Quaternary and recent sediment dynamics are, in contrast, comparably well understood. The continental sediment is mainly supplied from Portuguese rivers and is intermittently stored in a mid-shelf mudbelt (Dias et al., 2002a, 2002b; Lantzsch et al., 2009, 2010; Oberle et al., 2014a; Zhang et al., 2016a). Resuspension during storm events allows for efficient off-shelf transport of fine material in bottom nepheloid layers (Dias et al., 2002b; Oliveira et al., 2002;

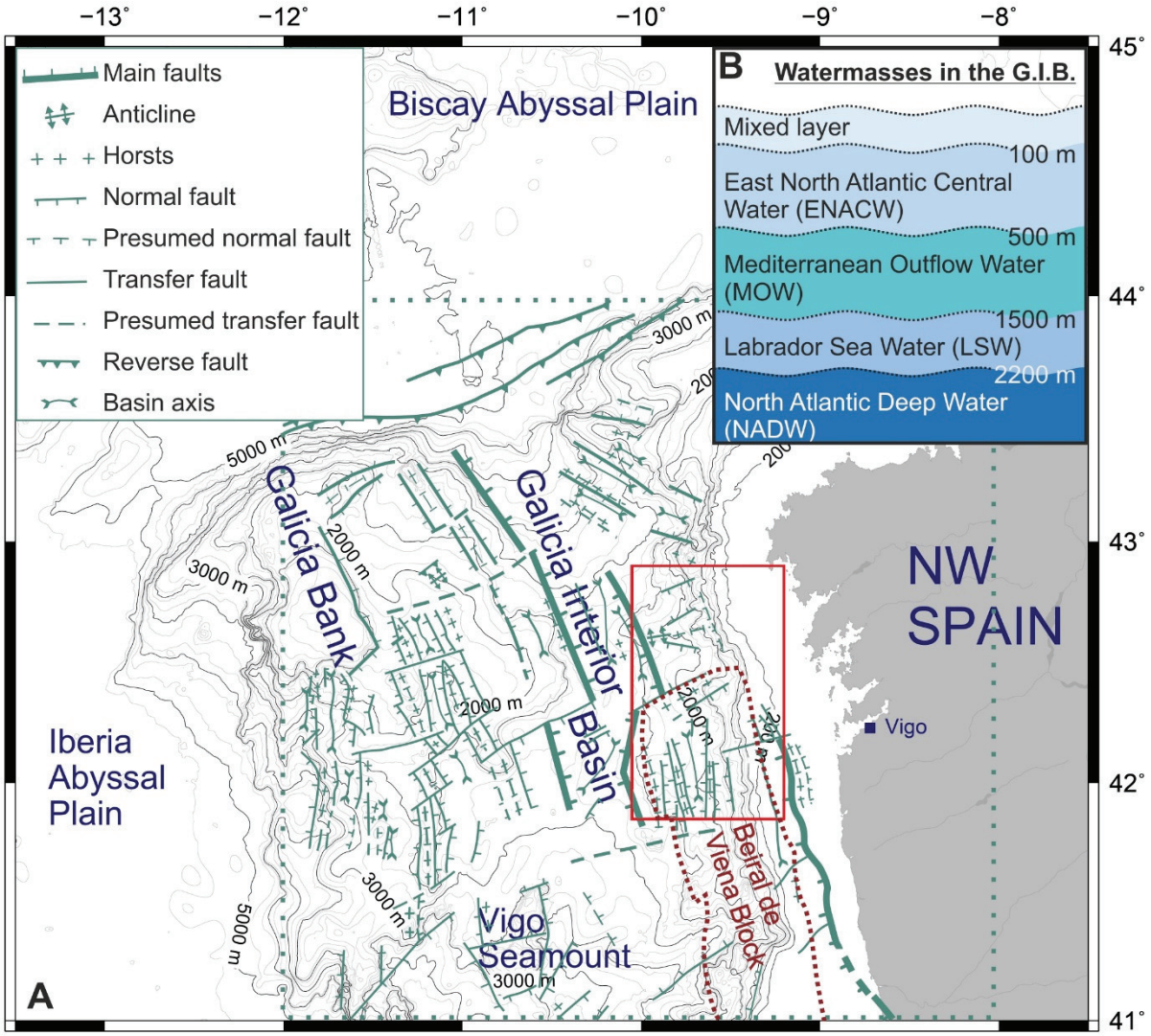

Figure 3.1 - A: Overview of the Galicia continental margin including the coastline, GIB, Galicia Bank and Iberia Abyssal plain. The overlay of tectonic faults was redrawn from Murillas et al. (1990). B: Generalized water mass stratification in the GIB compiled from: Fiúza et al. (1998), Hernández-Molina et al. (2011) and references within, McCave and Hall (2002) and Varela et al. (2005).

Vitorino et al., 2002; Oberle et al., 2014b). Sediment deposition at the continental slope is governed by hemipelagic deposition, downslope processes and phases of contouritic activity (Bender et al., 2012; Hanebuth et al., 2015; Zhang et al., 2016b). Sedimentation was particularly sensitive to major changes from glacial and interglacial stages, as the river mouths were assumedly located near the shelf break (Bender et al., 2012) and MOW, which in the Gulf of Cadiz and at the Portuguese Margin flowed deeper, did not reach the Galician margin during glacial times. MOW shoaling during the deglacial transition and a strong interaction with local topography led to the build-up of distinct contourite deposits (Schönfeld and Zahn, 2000; Hanebuth et al., 2015; Zhang et al., 2016b).

3.3 Oceanography of the Galicia Margin and the evolution of the North Atlantic circulation

Today five main water masses flow northward along the continental slope in the GIB (Figure 3.1B) (Fiúza et al., 1998; McCave and Hall, 2002; Varela et al., 2005; Hernández-Molina et al., 2011, and references within). The mixed surface layer extends down to 100 m (Fiúza et al., 1998; McCave and Hall, 2002; Varela et al., 2005). Underlying East North Atlantic Central Water (ENACW) shows two current cores between 300 and 500 m (Fiúza et al., 1998; McCave and Hall, 2002). MOW is split in two cores as well. Reports of their depth vary between 500 – 700 m (upper core) and 800 – 1400 m (lower core) (Hernández-Molina et al., 2011, and references within) or around 800 m and 1100 m, respectively (Fiúza et al., 1998; Varela et al., 2005). While Labrador Sea Water (LSW) is present in depths from 1500 down to 2200 – 2300 m. The deepest water mass is North Atlantic Deep Water (NADW) (Fiúza et al., 1998; Hernández-Molina et al., 2011, and references within) extending down to 4000 m in the abyssal plains and underlain by Lower Deep Water (LDW) (Hernández-Molina et al., 2011, and references within). Bottom currents led to contouritic sedimentation at the eastern flank of the GIB during the last deglacial episode, driven by oceanic density fronts that travelled along the at that time 300 m lowered interface between MOW and LSW (Hanebuth et al., 2015; Zhang et al., 2016b).

As MOW and LSW exist only since the Pliocene (Hernández-Molina et al., 2014), this configuration prevailed for less than 4 % of the 140 Myr long evolution of North Atlantic Ocean circulation.

Initial North Atlantic Circulation, in the Early and Middle Cretaceous, was characterized by formation of warm and saline bottom waters in low latitudes forced by warmer climate. (Roth, 1986). Surface and intermediate water masses exchanged through circum-equatorial pathways and with the South Atlantic. Deep and bottom water masses were limited to the North Atlantic and Tethys Oceans, therefore they were poorly ventilated (Roth, 1986). Bottom water ventilation improved with the deepening of the South Atlantic basin. From late Cretaceous on, bottom water mainly formed at southern high latitudes (Robinson and Vance, 2012). The onset of deep water production at northern high latitudes did not start before 35 Ma as indicated by onset of the Southeast Faeroes Drift in the Faeroe-Shetland Basin (Davies et al., 2001). NCW influence has been detected at the Walvis Ridge, dating back to 33 Ma (Via and Thomas, 2006), which shows that it was distributed across the whole Atlantic Ocean basin by then. Still the dominant bottom water mass transport was directed from south to north until 15 Ma (Woodruff and Savin, 1989) suggesting a dominance of a southern sourced deep water mass. The opening of the Drake Passage induced a major reorganization of the global current system from 25 to 20 Ma as the circum-Antarctic current system established (Stille et al., 1996), an

evolution which timewise overlapped with the closure of the Tethys-Indian Seaway 20 Ma ago (Stille et al., 1996; Rögl, 1999).

The exchange pattern between the then semi-enclosed Tethys Ocean and the Atlantic Ocean is still under debate. A possible scenario would be an analogue to the recent mode with an inflow of Atlantic surface water and an intermediate, warm and salty outflow from the Mediterranean Sea (Kouwenhoven and van der Zwaan, 2006). The NCW significantly strengthened 16 Ma ago, when the subsidence of the Iceland-Faeroe Ridge opened an additional pathway for bottom water masses forming in the Norwegian and Greenland Sea (Stille et al., 1996). Consequently, the prevalent transport of bottom water in the Atlantic Ocean was directed southward over the past 14 Ma (Woodruff and Savin, 1989). NCW circulation strengthened in the later Mid-Miocene by shoaling of the Central American Seaway (CAS) (Nisancioglu et al., 2003; Bell et al., 2015). 12 – 10.2 Ma ago, this passage shallowed to 1000 m water depth and ultimately closed between 4.2 and 2.4 Ma (Duque-Caro, 1990; Haug and Tiedemann, 1998). The eventual CAS closure temporally followed the onset of MOW outflow 5.33 Ma ago (Hernández-Molina et al., 2014). The initial MOW in the Gulf of Cadiz was, however, too weak for a built-up of contourite drifts prior to 4.5 Ma (Hernández-Molina et al., 2014). Also, LSW initially appeared in the north-east Atlantic Ocean 4.5 Ma ago (Nisancioglu et al., 2003). In the Plio-Quarternary, NCW production decreased along with the onset of northern hemisphere glaciation. NCW formation, nevertheless, intensified during two subsequent intervals, one coinciding with the Mid-Pleistocene Transition (MPT) 1 to 0.7 Ma ago, and a second from 0.3 Ma to present (Poore et al., 2006), whereas MOW strengthened prior to the MPT, and weakened afterwards (Hernández-Molina et al., 2014).

3.4 Material and Methods

This study is based on the interpretation of multichannel seismic (MCS) profiles and multibeam bathymetry. The main part of the data was acquired during RV METEOR cruise GALIOMAR III (M84-4; Hanebuth et al., 2012). The bathymetric map is the product of merging data from the two hull mounted Kongsberg Simrad swath-sounding systems EM122 and EM710 into a grid of 100 m resolution. Necessary processing steps to remove bad data were carried out in advance, using the open-source software MB system and FLEDERMAUS (QPS).

Multichannel seismic data was acquired during M84-4 by shooting a GI Gun with a volume of 2 x 1.7 l every seven seconds. The emitted frequencies lay in a range of 100 – 300 Hz. The signal was recorded with a 400-m long Syntron Streamer with 64 channels. The M84-4 MCS data set was completed with three lines collected during the preceding RV POSEIDON cruise GALIOMAR I (Pos342; Hanebuth et al., 2007). Those lines were acquired using a Mini GI-Gun with reduced chamber volumes (2x0.25 l) and a frequency range of 100 – 500 Hz. A 101-m long Teledyne streamer with 16 channels was used for recording. MCS data processing was performed using the Vista seismic processing suite (Schlumberger). The standard processing sequence includes binning to an along-track resolution of 5 m, debias, trace editing, normal-moveout correction with a constant velocity of 1500 m/s, static correction, filtering, and despike prior to common-midpoint stacking. After stacking, white noise reduction and FD-migration were carried out.

For an integrated data interpretation the software Kingdom (IHS Global Inc.) was used. Interpretation includes picking and gridding of horizons, as well as contour line calculations. Thickness maps of seismic units between picked horizons were created by subtracting the two

way traveltimes (TWT) of unit boundaries, resulting in true vertical thickness maps. In contrast to true stratigraphic thickness, which is measured perpendicular to the bedding, true vertical thickness may display large thickness values at very steep slopes. This effect was considered during the interpretation of thickness maps in this study. Sedimentation rates for each seismic unit, were estimated using the median thickness over the entire lower slope in the study area. These values were converted from TWT in seconds to meters using a constant velocity of 1500 m/s. The calculated sedimentation rates were additionally corrected for compaction increasing with depth by using the equation for depth-dependent pore volume reduction after Sclater and Christie (1980). To avoid overcompensation the material constants for sand have been chosen over shale and limestone.

3.5 Results

3.5.1 Bathymetry

The seafloor at the eastern flank of the GIB shows two types of structuring, one in E-W and another in N-S direction (Figure 3.2A). From east to west, the continental slope is divided into three physiographic zones (Figure 3.2B). The upper continental slope is associated with gradients generally lower than 3°. It extends from the shelf break at 160 – 180 m water depth down to 300 m. The middle slope extends into water depths of 1300 – 1800 m. This zone is

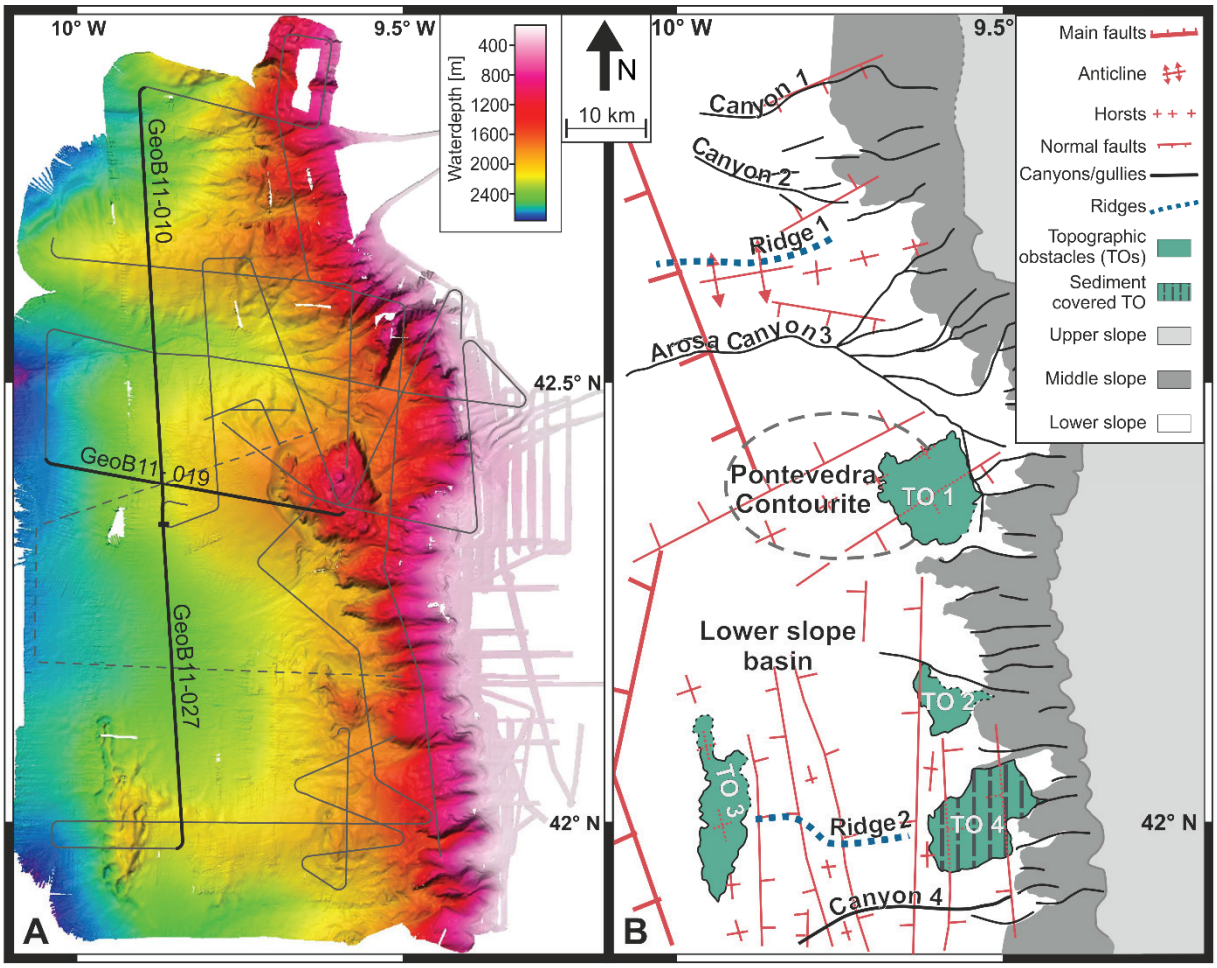

Figure 3.2 - A: Bathymetric map of the working area (modified from Hanebuth et al., 2015) showing the location of seismic lines, hachured lines originate from the RV Poseidon 342 dataset, thick lines are depicted in Figures 3 and 4. B: Interpreted bathymetry, highlighting the outline of upper, middle and lower slope as well as major morphological features. The Overlay of tectonic faults was redrawn from Murillas et al. (1990).

characterized by gradients of 8 – 15° and is dissected by numerous gullies (Hanebuth et al., 2015). The lower slope goes down to 2800 m in the study area with gentler gradients not exceeding 4°.

The lower slope is structured in north south direction by a variety of geomorphological features. It is cut by four larger canyons, which are each connected to at least one of the mid-slope gullies and lead westwards, presumably to the deeper GIB. Two canyons are found in the very north of the study area. The third canyon, named Arosa Canyon (Boillot et al., 1979), is situated about 20 km south of them, and the fourth is located in the very south of the study area (Figure 3.2B). Two topographic ridges, which form elongated E-W trending elevations 15 – 20 km wide and up to 500 m high, are located between Canyons 2 and 3 (Ridge 1), as well as directly north of Canyon 4 (Ridge 2), respectively. In addition, four geographically isolated, irregularly shaped elevations, so-called topographic obstacles (TO 1 – 4; Figure 3.2), are characterized by extremely steep flanks and hummocky surfaces. TO 1 is associated to a separated mounded contourite drift to its west (Hanebuth et al., 2015). This obstacle is dubbed 'Pontevedra Outlier', therefore the drift is referred to as 'Pontevedra Contourite' in the following. The embayment in the lower slope, south of the Pontevedra Contourite and north of Ridge 2, is referred to as 'Lower Slope Basin' (Figure 3.2B).

The overlay of the interpreted bathymetry with the tectonic map compiled by Murillas et al. (1990) (Figure 3.2B) reveals correlation of the majority of the topographic elements described above with buried tectonic features. Ridge 1 correlates with a structural combination of horst and anticline. TO 1 is located near another horst structure. The apparent offsets are attributed to deviations in geo-referencing. It is noteworthy that the structural features in the northern part of the study area correlate to E-W trending faults, while the topographic obstacles in the south (TO 2 – 4) are related to S-N striking horsts and grabens. Solely Ridge 2 does not correlate to any of the previously detected tectonic features.

3.5.2 Seismic profiles and thickness maps

The seismic record is vertically separated by seven horizons (H0 – H6), which represent unconformities on local scale and are often associated with stratigraphic changes in seismic facies. Six seismic facies (A1, A2, B, C1, C2, and D) (Table 3.1) have been defined, their classifications follow the definitons by Faugères et al. (1999) and Nielsen et al. (2008). In general, all facies are associated with contouritic drifts, as neither strictly horizontal nor strictly parallel reflectors have been identified, which would represent turbidites or hemipelagites. Thus the subdivison is based on either material composition or geometry of the drifts. Due to their subparallel reflector geometry facies A1 and A2 are associated with sheeted contourite drifts of different composition, hereby the higher amplitudes of facies A1 are interpreted to result from coarser material. In comparison, the more contorted and less continuous facies B represents mainly sheeted drifts, which have been altered post-depositionally by faulting or creeping and additionally might include minor mass-transport deposits (MTDs). These alterations potentially destroyed strictly horizontal or parallel layering, therefore it cannot be excluded that turbidites or hemipelagites initially contributed to this facies. C1 represents MTDs, which are large enough to be individually separated in the seismic record. While C2 is associated to sediments, whose depositional structures underwent severe alteration during tectonically active phases. In wide areas it represents the seismic basement especially at the topographic obstacles and the upper slope. Facies D represents types of contouritic drifts which are associated with reflector divergence, such as plastered and mounded drifts. The

classification of contourite drift geometry follows the drift types summarized by Faugères and Stow (2008) as well as Rebesco et al. (2014). Small offsets between reflectors of up to 0.005 s and columnar low-amplitude features occur throughout all seismic sections, especially at Ridge 1 and in the area of the Pontevedra contourite, and are attributed to small faults with offsets not exceeding 4 m.

Name	Continuity	Amplitudes	Reflector spacing	Reflector geometry	Example	Interpretation
A1	Highly continuous	High	Large	Subparallel	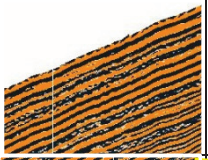	Coarse sheeted contourite drifts
A2	Highly continuous	Medium	Dense	Subparallel	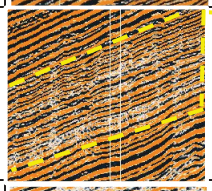	Sheeted contourite drifts
B	Semi continuous	Low to medium	Medium to large	Subparallel to contorted	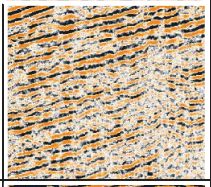	Altered sediments of different origin prevalently sheeted contourite drifts
C1	Discontinuous	Medium to transparent	Medium	Contorted to chaotic	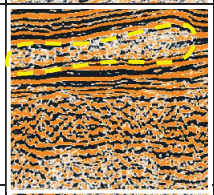	Mass waste deposits with disturbed to no internal structure
C2	Discontinuous	High	Medium	Contorted to chaotic		Tectonically altered sediments, seismic basement
D	Highly to semi continuous	High to low	Dense to large	Divergent and convergent	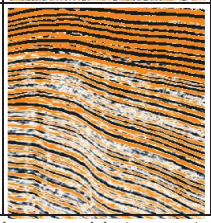	Other contouritic drifts including plastered and mounded drifts

Table 3.1 - Compilation of seismic-facies types, illustrative examples, and interpretation.

Since the deepest Horizon H0 was not continuously imaged in the Lower Slope Basin due to limited penetration of the seismic signal, the upper six horizons are used to define Seismic Units I-VI. As an exception in areas of topographic obstacles and at the upper slope, the deepest horizon is the (seismic) basement, on which the overlying Seismic Units I – IV onlap (Figure 3.3, Figure 3.4). Hence, the base used in the newly developed, regional stratigraphic succession is a blend of H1 and the seismic basement. The resulting map (contour lines in Figure 3.5A) reveals topography in a depth range of 0.5 to 4.1 s. This deep paleo-topography already contains most of the structural elements found at the modern surface (Figure 3.2). TO 1, 2, 3 and 4 are clearly visible as local heights with steep margins, although TO 3 extends further to the northwest in a hook-like shape and TO 4 incorporates an elongated depression.

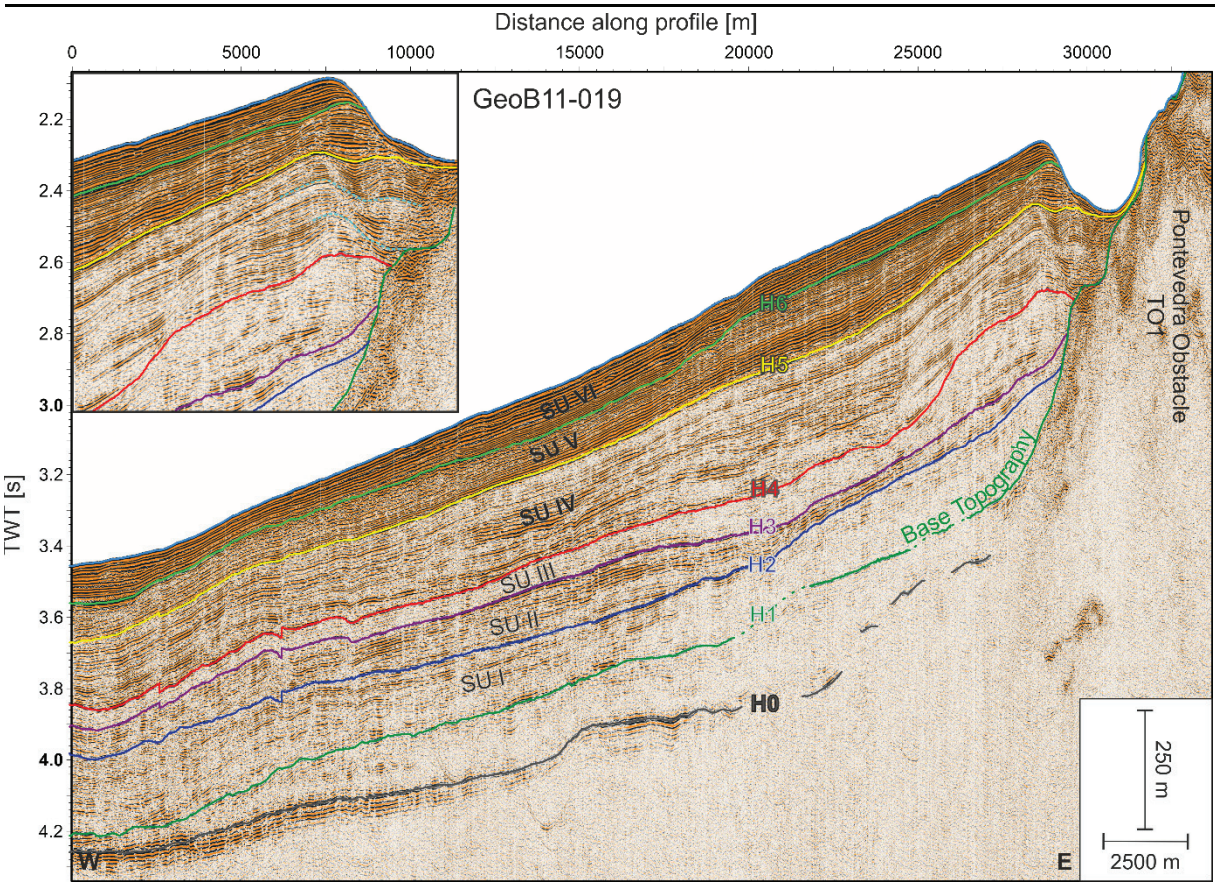

Figure 3.3 - Profile GeoB11-019 cutting the Pontevedra Contourite as well as the Pontevedra Obstacle TO 1. For exact location see Figure 3.2A.

The morphology of Ridge 1 is also visible in the base topography. In contrast, depressions occur at the location of Ridge 2 and underneath the modern Arosa Canyon (Canyon 3). At the location of this canyon, the depression is a product of erosional truncation of H1 into underlying strata, similar truncations occur at the northern flank of Ridge 1 (Figure 3.4).

Seismic Unit I (SU I) is characterized by altered sheeted drifts (facies B) intercalated by MTDs near the TO 1 (Figure 3.3), on the northern flank of Ridge 1 and in the Lower Slope Basin (Figure 3.4). The thickness map of SU I (Figure 3.5A) reveals that the areas of maximum thickness reach up to 0.26 s TWT and are clearly associated to depressions in the underlying topography. The spatially most widespread thickness maximum in the Lower Slope Basin covers at least 30 km and N-S direction. At the Pontevedra Contourite, where the underlying topography is gently rising, thickness is reduced to slightly higher than medium values of around 0.016 s. The local depression underneath Ridge 2, which is about 10 km in diameter, hosts a depocenter of medium thickness (0.013 s). The small-scale depression of 5 km diameter, which is part of the complex base topography of TO 4, is similarly filled by an equally small-scale depocenter. In contrast, the existence of depocenters directly north of Ridge 1 is not steered by confined topographic lows but the extreme thickness values are an artefact of the steep topography. However, the part of up to 0.195 s thickness is associated with a wedge shaped morphology which converges northward (Figure 3.4). SU I does not cover the major canyons, the upper and middle slope and the topographic heights TO 1, 2 and 3, as well as an area northeast of TO 3 and the elevated areas of TO 4. Transition to null thickness values around topographic obstacles and at the middle slope are associated with reflector onlaps (Figure 3.3, Figure 3.4). The lateral transition from null values in the Arosa Canyon (Canyon 3)

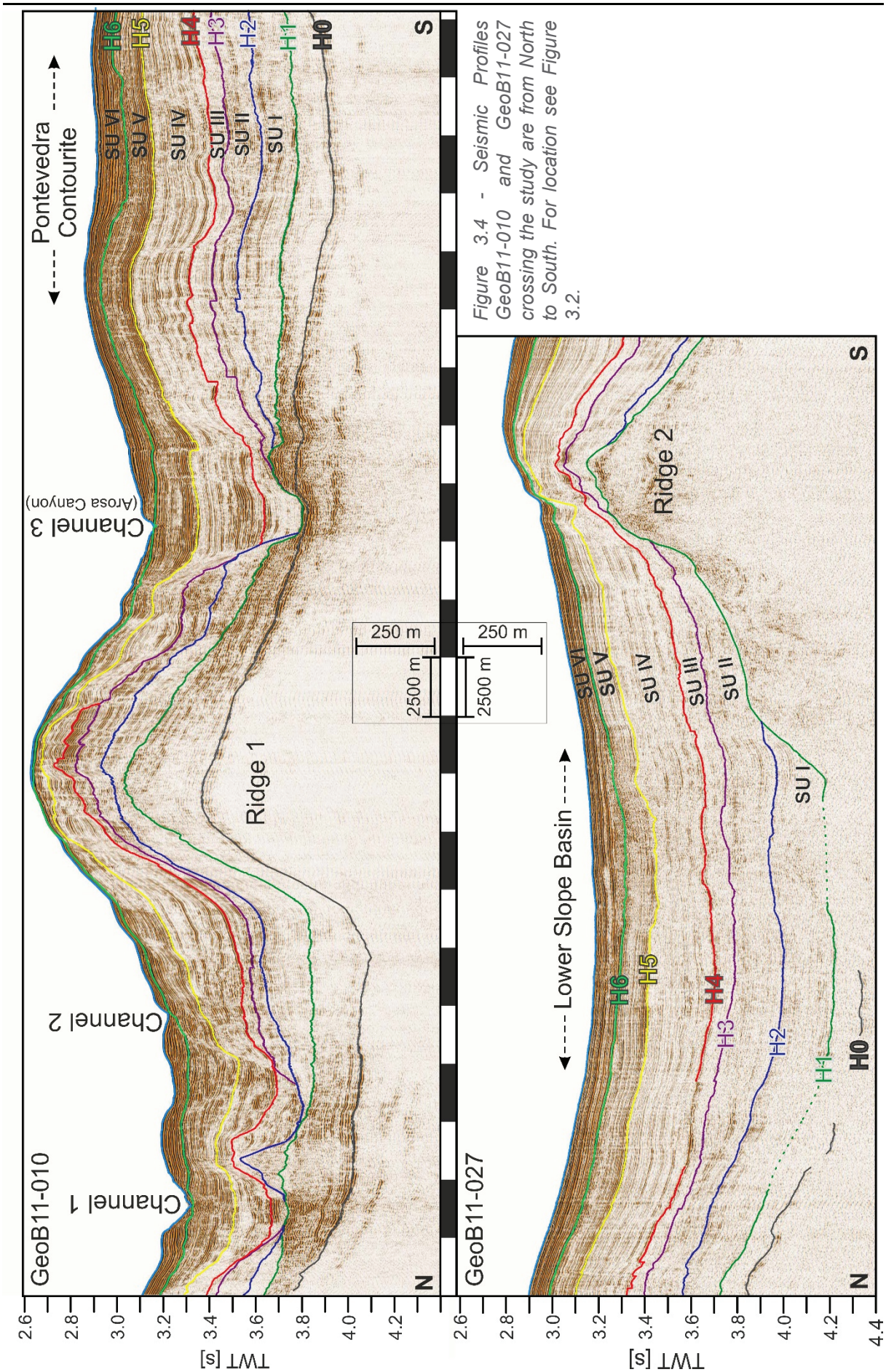

Figure 3.4 - Seismic Profiles GeoB11-010 and GeoB11-027 crossing the study are from North to South. For location see Figure 3.2.

to larger values in the Pontevedra Contourite System, and between Canyon 2 and Ridge 1 (Figure 3.4) are linked to large-scale divergence of internal reflectors. Thickness changes from low (~0.065 s) to medium high (~0.160 s) values occur at the canyon flanks and on top of Ridge 1 due to reflector truncation at H2 (Figure 3.4).

Seismic Unit II (SU II), similar to Unit I, mostly consists of altered sheeted drifts (facies B) with a few patchy MTDs, for example at the Pontevedra Contourite and the Lower Slope Basin (Figure 3.4). Figure 5B shows that maximum sediment thickness (up to 0.28 s) is found in depressions present in H2 between TO 3 and TO 4 (along Ridge 2), and west of TO 3. In the Lower Slope Basin two depocenters of 10 km diameter reach around 0.26 s thickness, they correlate to underlying topography as well. Local thickness variations from medium low (~0.1 s) to medium high (~0.2 s) on a scale of a few kilometres at the Pontevedra Contourite and west of TO 1 are related to a mix of small-scale topographic differentiation of H2, small MTDs (Figure 3.4) and the occurrence of a plastered drift shown in seismic line GeoB11-019 (Figure 3.3). Smaller thickness variations (~0.1 s – 0.15 s) at canyon flanks, and on top of Ridge 1 are related to reflector truncations (Figure 3.4). The canyons, middle and upper slope as well as the topographic heights are not covered by SU II. There transition to null thickness values is associated to reflector onlaps. SU II nevertheless covers a wider area than the underlying SU I.

Seismic Unit III (SU III) consists of altered sheeted contourite drifts (facies B) and MTDs. High amplitudes on the crest of Ridge 1 indicate coarse sediments (Figure 3.4). A mounded drift occurs near TO 1 (Figure 3.3). The thickness distribution in SU III (Figure 3.5C) is significantly different to the two deeper units, because the Lower Slope Basin and the major part of the Pontevedra Contourite are characterized by lower than medium thickness values of 0.09 - 0.1 s. Thickness maxima (up to 0.24 s) are only found in SU III as small localized depocenters around TO 1, on top of Ridge 1, along the Arosa Canyon, and inside Canyon 2 and rarely exceed 5 km in diameter. Additional depocenters, with thicknesses of up to 0.13 s, occur west of TO 2 and TO 4. Pre-existing depressions are only filled inside the canyons. However over most of the study area, it is not possible to link SU III thickness and underlying topography to each other. Seismic data reveals reflector truncation at H4 on top of Ridge 1 next to an area which is not covered by SU III (Figure 3.4). Since the seaward part of the depocenter near TO 1 is obscured by the occurrence of internally chaotic MTDs, the occurrence of reflector truncations in this area can only be inferred. The topographic obstacles and the middle and upper slope are not covered by SU III, though compared to SU II the uncovered areas are smaller. Small areas (diameter < 5 km) without SU III also occur at the southern flank of Ridge 1.

The overall appearance of Seismic Unit IV (SU IV) is determined by a layering of medium amplitude sheeted contourites (facies A2) and sheeted contourites containing MTDs (facies B) (Figs. 3, 4). Thickness of the individual layers vary from 0.01 to 0.1 s. At the Pontevedra Contourite and in the Lower Slope Basin up to nine packages can be distinguished, while on Ridge 1 only six alternations occur. Particularly near topographic obstacles and above irregular topography in H4 on Ridge 1, mounded drifts are present (Figs. 3, 4). Near TO 1, the seismic data reveals a vertical succession of different mounds separated from the obstacle by depressions within SU IV (closeup in Figure 3.3). SU IV is, with a maximum thickness of 0.4 s, considerably thicker than the underlying units (Figure 3.6A). Thickness maxima of up to 0.4 s occur within the depression of the Arosa Canyon. Another thickness maximum in the southern part of the Pontevedra contourite is related to H4 topography as well (Figs. 3, 6A).

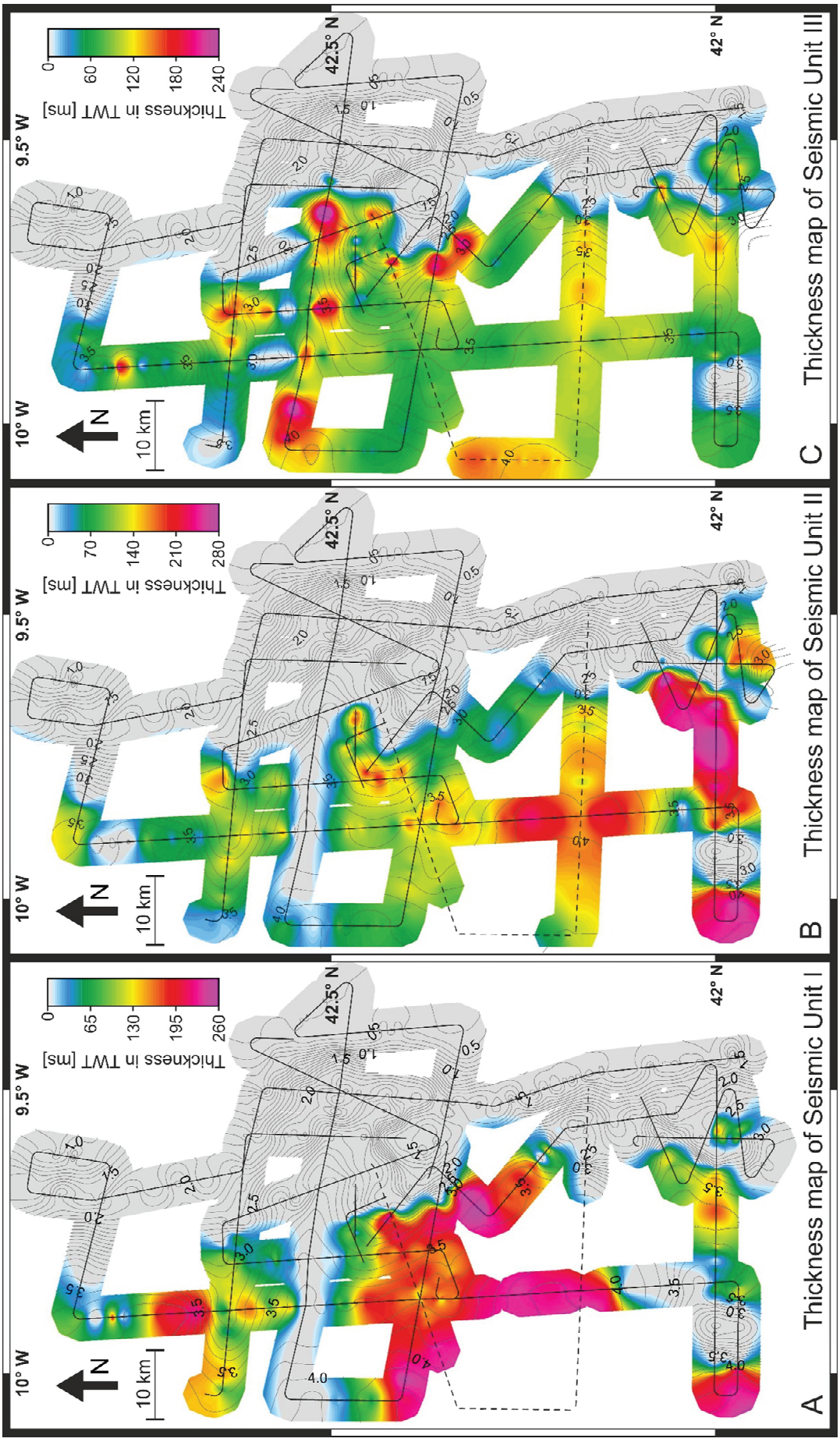

Figure 3.5 - Thicknessmaps of Seismic Units I – III. Contour lines represent the underlying topography (A: Unit I and H1, B: Unit II and H2, C: Unit III and H3).

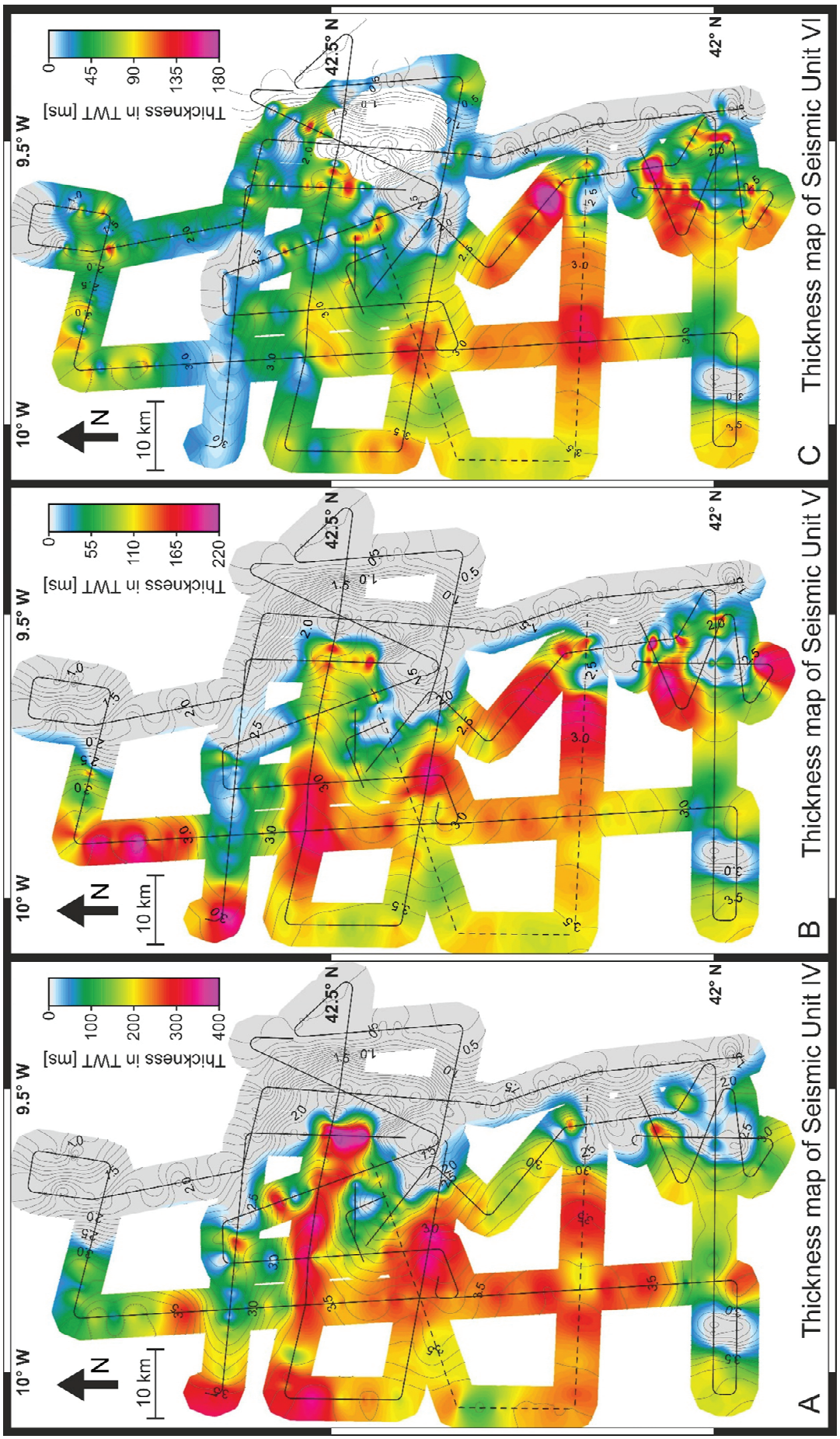

Figure 3.6 - Thicknessmaps of Seismic Units IV – VI. Contour lines represent the underlying topography (A: Unit IV and H4, B: Unit V and H5, C: Unit VI and H6).

In the remaining area of the Pontevedra Contourite, as well as the Lower Slope Basin and directly north of Ridge 1, thickness of SU IV varies between 0.2 and 0.3 s, thus is comparably thick in a large part of the study area (Figure 3.6A). The variations on a scale of a few kilometres are associated to MTDs and depressions in H4 (Figure 3.4). The contour lines of H4 distinctively show that Ridge 2 exists as a topographic feature (Figure 3.6A). On Ridge 1 thickness distribution is very patchy and spot-wise reduced to zero due to reflector truncations (Figure 3.4). Northwest of TO 1 another small patch which is less than 3 km in diameter and not covered by SU IV occurs. Furthermore the topographic obstacles and the middle and upper slope are not covered by SU IV. Compared to the SU III, the extent of the uncovered areas is smaller.

Seismic Unit V (SU V) is in vast areas build up from coarse sheeted drifts (facies A1) in the lower part and sheeted drifts (facies A2) in the upper part. MTDs occur in the Lower Slope Basin and in the canyons (Figure 3.4). Similar to the underlying unit SU IV, near topographic obstacles and above irregular topography in H5, mounded contourites are present (Figs. 3, 4). Thickness maxima reach up to 0.22 s and cover distances of 10 to 15 km along seismic profiles. Thickness maxima, associated to depressions in H5, are positioned in the Canyons 1 – 3 and in the gully north of TO 4 (Figure 3.6B). Others, which do not correlate to H5 topography, occur west and north of TO 2 as well as west of TO 1. Seismic data reveals, that, at TO 1, SU V does not onlap on the seismic basement, but is separated from the obstacle by a U-shaped erosional depression in the seafloor of about 2.5 km width (Figure 3.3). It furthermore shows reflector truncations at H6 west of the depocenter next to TO 1 (Figure 3.3) and at both sides of a through shaped depression in H6 in north south direction (Figure 3.4). Overall the Lower Slope Basin, the Pontevedra Contourite and the area north of Ridge 1 receive higher than medium thickness (~0.12 – 0.14 s). On top of Ridge 1 SU V is less than 0.06 s thin and in some spots not present. Northwest of TO 1 an area of about 3 km in diameter, which is not covered by SU V, occurs. Moreover TO 1, 2, 3 and parts of TO 4 are associated to null thickness values of zero.

Seismic Unit VI (SU VI) almost entirely consists of coarse sheeted contourite drifts (facies A1). Only partly sheeted contourite drifts (facies A2) occur and in the Lower Slope Basin some MTDs exist (Figure 3.3, Figure 3.4). Next to the topographic obstacles and on top of Ridge 1 mounded contourite drifts prevail. The main thickness maxima of SU VI on the Pontevedra Contourite, in the Lower Slope Basin and in the gully north of TO 4 are associated to depressions in H6 (Figure 3.6C). Only the depocenter in the gully reaches 0.18 s thickness, the other two only reach up to 0.135 s. Another thickness maximum north of TO 2, which is not related to H6 topography, reaches 0.18 s. SU VI is separated from TO 1 by the same seafloor depression as SU V (Figure 3.3). Furthermore the seismic data reveals that small wavy features overlie the location where SU V reflectors truncate at a step in H6 (Figure 3.3). In the northern part of the study area the thickness distribution is extremely patchy varying from 0 to 0.18 s over a distance of less than 2 km. In the Area of the Arosa Canyon (Canyon 3) several patches of low to zero thickness align along the seafloor expression of the canyon (Figure 3.6C). Seismic data shows that reflectors truncate at the canyon flanks (Figure 3.4). On the crest of Ridge 1 thickness is less than 0.02 s and several patches, which are not covered by SU VI, occur. It is furthermore noteworthy that TO 4 is covered by SU VI in approximately 2 km wide patches, which are elongated in north south direction, and alternate between very low (0 - 0.02 s) and medium (0.05 - 0.09 s) thickness values. The easternmost patch reaches even

0.18 s thickness. TO 1 – 3 and the southern part of middle and upper slope, in contrast, are not covered by SU VI. Very low (0.02 s) to zero thickness occurs in two small patches (<2 km diameter) northwest of TO 1.

3.6 Discussion

To discuss the evolution of the Galicia Margin, the changes in sedimentation pattern from one seismic unit to the next are linked to changes of the dominance of the respective external driving forces, such as ocean currents or tectonic activity, over time. The correlation of the successive stages characterized by a specific depositional unit with changes in large-scale oceanographic conditions in the Atlantic Basin allows for two things: establishing a solid stratigraphy across the margin on the one hand, and reconstructing which type of process had impact on margin sedimentation, on the other.

3.6.1 Basin morphology in the Mid-Eocene

H0 and H1 were dated by correlation to data from Murillas et al. (1990) to 89.9 Ma and 41 Ma, respectively. The deposits in-between these two boundaries were identified as hemipelagic post-rift sequence and are found in the GIB as well as on the Galicia Bank (Murillas et al., 1990; Ercilla et al., 2008). This observation proves that bottom currents were too weak to significantly influence sedimentation prior to the Mid-Eocene. The mid-Eocene basin topography (41 Ma) defines the surface of a sedimentary succession which deposited until then (namely H1) as well as areas which were bare of sediments at that time. The latter include the topographic obstacles (TO 1 - 4) and the steep middle slope. Combined with Ridge 1, these morphological features are the main constituents of the Mid-Eocene base topography, which still correspond well to the majority of features found on the modern bathymetric map. Correlation to main tectonic elements mapped by Murillas et al. (1990) reveals that these obstacles and ridges are probably associated with major faults and other tectonic features. Accordingly, Ridge 1 is related to an anticline while the topographic obstacles are associated to horst structures. TO 2 – 4 are linked to N-S trending horst and graben system in the south of the study area which presumably evolved during rifting and opening of the GIB in the early Cretaceous. Ridge 1 and TO 1 experienced uplift during the Pyrenean orogeny in the Mid-Eocene (Murillas et al., 1990). Erosional truncations at H1 on the ridge crest (Figure 3.4) indicate sediment failure, possibly caused by slope over-steepening as a result of this uplift. In contrast, Ridge 2 in the south does not follow the Eocene basin topography but overlays an N-S trending graben system. The recent canyons are not related to tectonic features, and only Paleo-Canyon 3 eroded as deep as into the Eocene basin topography. Since this paleo-canyon not erode into the late Cretaceous succession of horizon H0, it can have formed not earlier than 89 Ma ago. Paleo-Canyons 1 and 2 did not erode into the base topography, indicating that they formed after the Mid-Eocene.

3.6.2 Mid- to Late Eocene (41 – 35 Ma)

Seismic Unit I directly overlies the base topography, thus started to form in Mid-Eocene times. The location of major depocenters in the deep and low-gradient area of the Lower Slope Basin (Figure 3.5A) together with the occurrence of sheeted contourite drifts and MTDs (Figure 3.3, 3.4) suggests the existence of both gravity-driven downslope and contour current-driven along-slope sediment transport. Both processes levelled the topography by heightened sediment accumulation in depressions. No depositional fill is found in Canyons 1, 2 and 3 for the Eocene interval, which might be the case either because they eroded at that time, or material bypassed in the form of mass flows from the middle and/or upper slope, which in turn delivered material

into the deeper parts of the GIB. These potential mechanisms imply that the tectonic regime during Eocene triggered mass wasting much more frequent than reflected by preserved deposits. Additionally, downslope sediment creeping occurred particularly on top of Ridge 1 and to lesser extent at the Pontevedra contourite as indicated by small faults (Figs. 3, 4), which do not extend through all underlying strata. The creeping is interpreted as a result of the uplift of Ridge 1 and TO 1 during the Pyrenean orogeny in the Mid-Eocene (Murillas et al., 1990). The uplift also caused slope failures as indicated by headwalls on top of Ridge 1 (Figure 3.4). The overall patchiness in thickness distribution at the ridge is therefore attributed to the existence of scarps on its top and of MTDs at its southern flank. Furthermore, a convex contourite drift occurs around the Pontevedra Contourite. This drift thins out in northward direction towards the Arosa Canyon (Canyon 3). It can thus not unambiguously be answered to what extent and in which fashion turbidity currents passing through the canyon interacted with the bottom-current regime in the area. Consequently, a potential contribution to the drift built-up cannot be reconstructed. Further MTDs occur south of the drift (Figure 3.4). Although this drift body does not constitute a distinct thickness maximum, evidence exists for an impact of the bottom current on the deposition of SU I. Much older, Cretaceous contourite deposits at the deep Iberian margin were attributed to deep and saline Tethyan outflow water (Soares et al., 2014). Until the early Eocene however the Atlantic Ocean circulation changed significantly, deep water production took place in the southern-hemisphere high latitudes (Thomas et al., 2003; Robinson and Vance, 2012). There are reports on NCW outflow from the Norwegian Greenland Sea since 50 – 49 Ma (Hohbein et al., 2012) but neither a contribution of this water mass to the North Atlantic ocean circulation nor a contribution or existence of Tethys outflow water was detected (Thomas et al., 2003). Significant changes in this general situation are not known for the Eocene epoch at this point. It is thus, probable that the main source of bottom and intermediate waters was located in the South Atlantic until at least the termination of the Eocene. The topography-smoothing redistribution of sediment clearly points to an impact of bottom currents on sedimentation, but the lack of major contourite drifts in the study area suggests that the currents unlikely exceeded the minimum velocity required to redistribute material. Sheeted contourite drifts only require a weak to moderate velocity of about 5 cm/s (Faugères et al., 1999; Stow et al., 2008, 2009).

3.6.3 Late Eocene to Early Miocene (35 – 14 Ma)

The major part of the deposition of Seismic Unit II took place in the Lower Slope Basin and in local depressions in the H2 topography. However, the most marked change compared to Seismic Unit I is that the geometry of the contourite drift next to TO 1 changed from a sheeted to a plastered contourite drift at water depths greater than 3.4 s (~ 2550 m) (Figure 3.3). A reasonable explanation for this change in drift geometry is the presence of a water-mass boundary. The onset of NCW discharge through the Faeroe-Shetland channel at 35 Ma (Davies et al., 2001) is commonly acknowledged to generally mark the onset of NCW production. Since the Early Oligocene, NCW is present throughout the whole Atlantic Basin (Via and Thomas, 2006) but possibly less dense and shallower than today (Knutz, 2008). This water mass is, therefore, a good candidate for forming a water-mass boundary in the GIB with the still basinwide present southern source deep water. An alternative mechanisms for a change in current strength in these intermediate depths might lie in a changed supply of watermasses from the Pacific through the CAS, however no such variation is known for the Eocene-Oligocene Period. Hence it seems to be reliable to date the stratigraphic boundary between Seismic Units I and II to 35 Ma. However, the plastered contourite drift does not show

as maximum in the thickness map (Figure 3.5B). Contrastingly thickness maxima on the Pontevedra Contourite are of limited local extent and associated to MTDs intercalated into the drift (Figure 3.4), indicating that downslope processes dominated the depositional pattern. The largest thickness of SU II occurs in the depression, which underlies the modern Ridge 2. Most likely, the mid-slope gullies provided sediment to fill this topographic low. Particularly the gully located between TO 2 and TO 4 (Figure 3.2) is associated with intense downslope transport during the deposition of SU II, since it is thickly filled as well. In addition, TO 3 acted as a barrier hindering sediment transport further basinwards. As a result, the associated depression below Ridge 2 is filled up and the initial ridge topography is formed (H3 contour lines in Figure 3.5C). Mass wasting deposits occur in the Lower Slope Basin and on the Pontevedra Conoturite. While internal faulting occurred at Ridge 1 and the Pontevedra Contourite, similar to SU I. There are, in addition, no deposits preserved inside any of the canyons, and the sediment thickness distribution on Ridge 1 is still of patchy nature due to the presence of scarps (Figure 3.4). This observation shows that across-slope sediment transport was a dominant mechanism during the Oligocene, probably triggered by tectonic activity of the ongoing Pyrenean Orogeny.

3.6.4 Early Miocene to Early Pliocene (14 – 4.5 Ma)

The most profound change in sedimentation pattern between Seismic Unit II and Seismic Unit III is that the major depocenter did not only move from the Lower Slope Basin into the vicinity of TO 1 and into the Arosa Canyon (Figure 3.5C), but also that deposition maxima were concentrated to local areas compared to Seismic Units I and II (5 – 10 km). This change can be explained by the occurrence of small MTDs inside the canyon and around TO 1, but also by the built-up of mounded contourite drifts close to the obstacle (Figure 3.3). The existence of MTDs and headwalls, which are also found on Ridge 1, together with a significant number of faults points to a succession of slope failures and thereby ongoing tectonic activity. However, the first appearance of mounded contourite drifts separated by a moat from TO 1 gives evidence for an increasing impact of contour currents on sedimentation, and a particular focus of this bottom current against the slope due to Coriolis veering (Faugères and Stow, 2008; Rebesco et al., 2014). To achieve this slope-leaning current, a northward-directed water-mass flow is required. This change of sedimentation pattern was probably controlled by the reorganization of the global circulation pattern which included the establishment of the circum-Antarctic current system and the closure of the Tethyan-Indian connection terminating the circum-equatorial flow at 14 Ma (Stille et al., 1996; Rögl, 1999). The semi-enclosed Tethys basin already resembled the Mediterranean Sea at this stage; a general circulation pattern and exchange with the Atlantic Ocean similar to modern conditions is thus to be expected. Indications for surface Atlantic water inflow and intermediate Tethys water outflow were described for, at least, late Miocene times (Kouwenhoven and van der Zwaan, 2006). Since the mounded contourite drifts are attributed to Tethys outflow, the boundary between Seismic Unit II and III can be dated to 20 Ma. The MTDs were presumably triggered during the Betic Orogeny by the uplift of the Beiral de Viena Block, which underlies the southern part of the study area (Figure 3.1A) (Muñoz et al., 2003).

During the Miocene, the subsidence of the Iceland-Faeroe ridge opened a new pathway for NCW to contribute to North Atlantic bottom water (Stille et al., 1996). By 14 – 12 Ma, the prevalent bottom-water flow reversed into a southward-direction (Woodruff and Savin, 1989), a situation similar to the modern Atlantic Meridional Overturning. Shoaling of the Central American Seaway (CAS) 12 – 10 Ma ago restrained a Pacific-Atlantic exchange at low latitudes

to 1000 water depth (Duque-Caro, 1990), which further aided the southward transport of NCW (Preu et al., 2012; Nisancioglu et al., 2003). None of these changes however had a distinct impact on the deposits at the Galicia Margin. This fact underlines that water masses from nearby ocean passages tend to dominate the stratigraphic record.

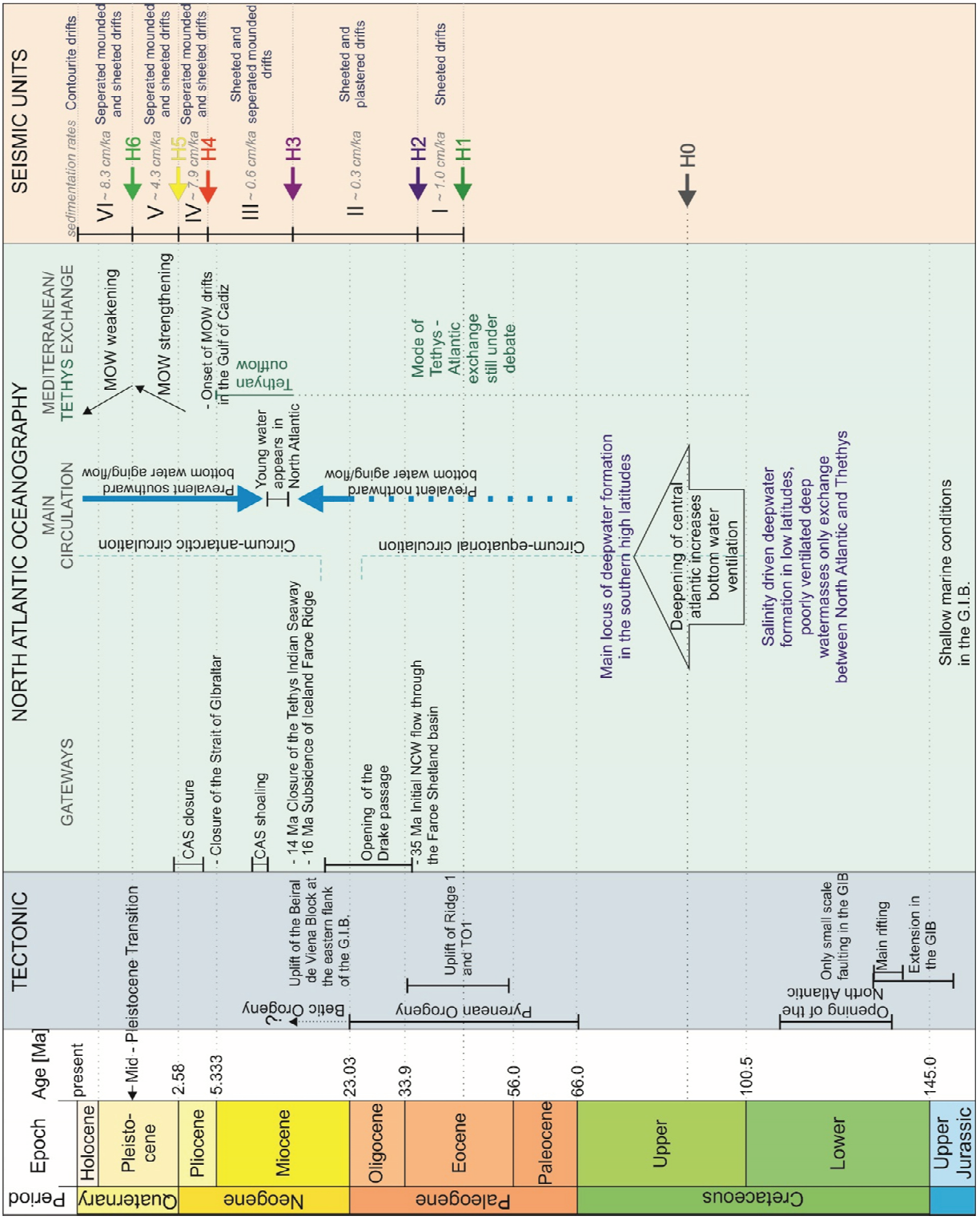

Figure 3.7 - Timeline of the evolution of the Galicia Continental Margin summarizing the tectonic evolution of the North Atlantic and the GIB (Boillot et al., 1979; Murillas et al., 1990; Muñoz et al., 2003) the Oceanographic evolution of the North Atlantic (Roth, 1986; Woodruff and Savin, 1989; Duque-Caro, 1990; Stille et al., 1996; Haug and Tiedemann, 1998; Rögl, 1999; Davies et al., 2001; Nisancioglu et al., 2003; Via and Thomas, 2006; Robinson and Vance, 2012; Hernández-Molina et al., 2014; Bell et al., 2015) as well as the findings from this study.

3.6.5 Early Pliocene to Early Pleistocene (4.5 – 2.4 Ma)

In Seismic Unit IV, contouritic activity is more intense and its control on sediment thickness stronger than in the older units. Also sedimentation rates rose substantially (Figure 3.7) implying that more sediment was supplied to the Galicia Margin. The Lower Slope Basin is covered by sheeted contourite drifts of ~ 0.25 s (~188 m) thickness. Minor variations in thickness are attributed to either mass-wasting deposits or filled depressions. Main thickness maxima are related to the infill of the Arosa Canyon. Next to the Pontevedra Obstacle, a fully separated mounded contourite drift developed (Figure 3.3). As a further effect of current-topography interaction, the area in the lee side of TO 1 was characterized by non-deposition. Locally higher current velocities, which do not allow deposition, are attributed to eddy shedding as a consequence of the interaction between bottom current and TO 1 (Boyer and Zhang, 1990; Hernández-Molina et al., 2006). Over the rugged topography of Ridge 1, which was formed by faulting and slope failures during the deposition of the preceding SU III, a wavy sediment pattern developed during deposition of SU IV (Figure 3.4). The patchy sediment distribution on top of Ridge 1 may, in a large scope, be credited to scarps and MTDs of the preceding SU III, in the way that these deposits shaped the local topography which modulated the current regime during the deposition of SU IV. The overall interaction of bottom currents with topography is indicative for a vigorous northward flowing water mass. MOW, as dense northward flowing water mass, is the prime candidate to interact with the middle slope and topographic obstacles at the Galician margin., It established after the reopening of the Strait of Gibraltar (5.33 Ma). Over the past 4.5 Ma, MOW was strong enough to build up contourite drifts in the Gulf of Cadiz (Hernández-Molina et al., 2014). This initiation is associated with the built-up of Seismic Unit IV in the working area. Since the closure of the Central American Seaway (CAS) from 4.2 to 2.4 Ma (Newkirk and Martin, 2009), Atlantic Meridional Overturning further enhanced and LSW reached the eastern North Atlantic Ocean (Nisancioglu et al., 2003). Hanebuth et al. (2015) identified ocean density fronts that migrate through the MOW-LSW transition zone, to be responsible for contourite drift built-up during the past deglacial-early Holocene time interval. It is possible that these density fronts are present and interact with the Galicia Margin since MOW and LSW are both present in the area.

3.6.6 Early Pleistocene to Mid-Pleistocene Transition (2.4 – 0.7 Ma)

The deposition of Seismic Unit V took place under an enhancing bottom-current regime. Overall sedimentation rates were reduced compared to Unit IV. The deep areas of the Lower Slope Basin accumulated around 0.12 s (~90 m) of sediments, modulated by H5 topography and MTDs (Figure 3.6B), which in this unit is still slightly higher than medium thickness. Spatially large thickness maxima are found over Canyons 1 to 3, which were completely filled after deposition of SU V (Figure 3.4). Wavy reflectors on the flanks of Ridge 1 in combination with the extremely thin and patchy sediment distribution on its crest indicate, that the current accelerated to overflow Ridge 1, thereby winnowing the seabed. Further depocenters are situated around the topographic obstacles TO 1, 2 and 4 and associated to separated mounded contourite drifts. At the contourite drift west of TO 1 (Figure 3.3), the moat is erosive and remained unfilled until modern times. A headwall located westward on the contourite flank indicates failure of contouritic sediments. Since no faults are present in that area the failure was presumably due to oversteepening of the slope. The associated scarp is visible in the thickness map (Figure 3.6B). The comparison of Seismic Unit V with Seismic Unit IV suggests that the interaction of the current regime with pre-existing topography technically remained the same but at an enhanced level. The uncovered patch at the TO 1 leeside is present and

occupies a slightly larger area. Overall amplitudes are stronger in the seismic record, which can be attributed to deposition of coarser material. Hernández-Molina et al. (2014) report a MOW strengthening in the Gulf of Cadiz during the lower Pleistocene. Thus a faster flowing bottom-current is expected along the entire flow path of MOW, which then is capable to redistribute coarser grains in the study area. Global cooling and the onset of Northern Hemisphere Glaciations (NHGs) about 3 – 2 Ma ago (Raymo et al., 1992) favoured continental erosion and led to the supply of coarser terrigenous material to the oceans.

3.6.7 Mid-Pleistocene Transition – modern (0.7 – 0 Ma)

The thickness distribution in Seismic Unit 6 is most variable while sedimentation rates are highest compared to all preceding units (Figure 3.7). The most widespread depocenter in the Lower Slope Basin is associated with two mass-wasting deposits and the fill of a depression of H6 (Figure 3.4). Further thickness maxima are located north of TO 2 and between TO 4 and TO 2. While the first maximum is associated with an elevation in the seafloor (Figure 3.2A), the second overlies a depression connected to a gully. The assumption in both cases is, that material was supplied by downslope transport and deposited in lee sides of obstacles where calm conditions prevail, thus they are small-scale contourite drifts. The crest of the separated mounded contourite drift of the Pontevedra Contourite migrates seaward during the deposition of SU VI (Figure 3.3). However, the thickness maximum of the Pontevedra contourite is not primarily related to the contourite drift itself, but filled in the scarp in H6. The wavy reflector pattern overlying the headwall, the existence of an area of nondeposition north of TO 1 which is attributed to eddy shedding and the extremely reduced sediment thickness on Ridge 1 (Figure 3.6C) associated with more wavy reflectors (Figure 3.4) provide further evidence for a lasting bottom current activity. Canyons 1 – 3 eroded into SU VI as indicated by reflector truncations and sediment thickness minima.

In summary, canyon activity, higher spatial variability, and overall higher amplitudes in the seismic sections are the main difference between Seismic Units VI and V. The boundary between these two units was associated with the Mid-Pleistocene Transition (MPT) when a 40-kyr glacial-interglacial frequency changed towards 100 kyr cycles. This change is also documented in the Le Danois contouritic depositional system at the Northern Iberian Margin (Van Rooij et al., 2010). The Gulf of Cadiz contourites show relative weakening in MOW intensity since the MTP (Hernández-Molina et al., 2014). These general changes in the depositional regime are thus attributed to weakening current conditions. The absence of faults indicates that slope failures and MTDs are not triggered by tectonic activity. High sedimentation rates rather suggest slope oversteepening as a reason for slope failures. These enhanced sedimentation rates can be attributed to an enhanced fluvial supply closer to the shelf break during the glacial intervals (Bender et al., 2012).

3.7 Summary and conclusions

The high resolution multichannel seismic dataset at the Galician margin in total spans 41 Ma and facilitates a first-time analysis of the interaction between continental margin topography and oceanographic regime prior to Pliocene times. Six seismic units are mapped, which reflect the evolution of across- and along-slope processes controlled by the North Atlantic Ocean circulation. Since data for an exact age determination of these units is not available (i.e. by drilling), their age control relies on a tied correlation with seismic data from Murillas et al. (1990) and especially on the carefully linkage to changes in the oceanographic system. This analysis gives clear evidence that changes in the North Atlantic circulation even caused by open and

closure of pathways far away have a distinct impact on the Galician margin sedimentary system. The stratigraphic evolution of the study area can be separated into six stages based on different interactions of bottom current with the topography:

- 41 – 35 Ma: A faint background currents smooths topography and fills depressions. No specific current topography interaction was observed.
- 35 – 14 Ma: Slight current strengthening and first interaction with topography of a northward flowing current possibly an early shallow NCW mode.
- 14 – 4.5 Ma: Development of initial separated mounded drifts related to Tethyan outflow water.
- 4.5 – 2.58 Ma: Establishment of quasi recent oceanographic conditions. Separated mounded drifts around topographic obstacles are fully developed and related to an interaction of MOW and LSW.
- 2.58 – 0.7 Ma: MOW strengthening and further drift build-up.
- 0.7 Ma – now: MOW weakening

During the built-up of the first three seismic units, the Pyrenean and Betic orogenic activity led to faulting and triggered mass wasting. The increasing interaction between bottom current and topography reflects the evolution of North Atlantic Ocean circulation but was never able to fully level out the pre-existing morphology designed by faulting. As soon as MOW starts to occur in the region, it dominates the sedimentation pattern. Reduced tectonic activity and enhanced continental sediment supply aid, in addition, to a more efficient built-up of contouritic drift depocenters. Since the Mid-Pleistocene-Transition, the amount of slope failures and downslope sediment transport increase due to enhanced material supply from the hinterland.

Acknowledgements

This study was funded through the DFG-Research Center/Cluster of Excellence “The Ocean in the Earth System” We would like to thank Captain Thomas Wunderlich, the crew of *R/V Meteor cruise M84/4* and Prof. Dr. Sebastian Krastel and his team of watchkeepers as well as Captain Michael Schneider and the Crew of *R/V Poseidon cruise PO 432* for their excellent work and support.

4 Morphology and evolution of contouritic depositional systems steered by the interaction of bottom currents with distinct seafloor topography at the Galicia Margin (NW Spain)

Haberkern, J.[a, *], Schwenk, T.[a], Hernández-Molina, F.J. [b], Hanebuth, T.J.J.[c], Spiess, V.[a]

[a] MARUM – Center for Marine Environmental Sciences and Faculty of Geosciences, University of Bremen, Germany

[b] Department of Earth Sciences, Royal Holloway, University of London, Egham, UK

[c] Department of Costal and Marine Systems Sciences, Coastal Carolina University, SC, U.S.A.

Abstract

Contouritic depositional systems (CDS), sedimentary structures which comprise depositional as well as erosional features, occur at the Galician Margin in various geometries and on relatively small horizontal scales (~2-20 km). They result from the interaction northward flowing contour currents with a complex basement topography, including isolated heights, a plateau attached to the upper slope and two east-west oriented ridges. Such topographic features act as obstacles, which locally perturb and amplify the bottom-currents, subsequently leading to the development of associated CDS, which record any change of the bottom current regime. To extract paleoceanographic information from this record the exact impact of bottom current interaction with topography on the size and shape of these CDS has to be understood first. The occurrence of various features within a small area renders the Galicia Margin a natural laboratory to study the interaction between bottom currents and small-scale topography, as the overall current regime can be expected to be spatially uniform. Hence the observed variability in sedimentation pattern must be solely attributed to the interaction of the current with the different topographic features.

In this study the effect of obstacle geometry on the evolution and shape of the contouritic depositional systems is targeted. In general, separated mounded drifts develop west of topographic obstacles whereby the shape and slope angle of the obstacle control the alignment of the moat and the height apparently influences moat width and depth. At the largest of the topographic obstacles flow detachment and eddy shedding occur at small protrusions of the obstacle. Under the influence of the eddy shedding a field sediment waves with crests in two different directions developed in the lee side of this obstacle. Further sediment waves with N-S aligned crests grow under the bottom current contouring one of the ridges. Another example of the strong control of topography on sediment deposition is a multi-crested drift, which consist of several elongated mounded drifts built under multiple bottom current cores. The current splits into several cores at steps and heights in the topography underlying the multi-crested drift. Contouritic terraces at the middle slope might be forming under the influence of another

water mass boundary than all other features. It is furthermore shown that the contouritic features on elevated positions react more sensitive to variation in current strength, which once more shows the importance of small-scale drifts for paleoceanographic reconstruction. All in all, the abundance of different processes on a small scale at the Galicia Margin makes it a good area not only to study the different processes and their interaction but also their contribution to the shape of a larger system which will finally be a step towards a more holistic understanding of the role of bottom currents in shaping continental margins.

4.1 Introduction

The influence of preexisting topography on bottom currents and thereby on the sediments accumulated under the influence of these bottom currents is known as a crucial parameter controlling drift geometry (Faugères et al., 1999). Such Contourite deposits have been studied extensively since their discovery more than 50 years ago (Heezen and Hollister, 1964, Rebesco et al., 2014). As they provide paleoceanographic archives, especially paleocurrent markers, hold implications on slope stability and are of interest in hydrocarbon exploration (Rebesco et al., 2014), they yield valuable information for different fields of research. However reconstruction of paleocurrents is not a straightforward process, as size and shape of a drift are not only controlled by bottom current velocity but also by the topographic framework, sediment supply and the time period available for drift construction (Faugères et a., 1999). Additionally, today a large variety of oceanographic processes is known to influence the bottom current velocity and impact sediment distribution. These processes include persistent abyssal circulation, changed by opening and closure of large oceanic gateways (Knutz, 2008) over brine formation on glacial shelves (Rebesco et al., 2016, Lantzsch et al., 2017) to the short lived passing of oceanographic density fronts (Hanebuth et al., 2015, Zhang et al., 2016). Moreover, changes in topography have a crucial influence on the characteristic traits of drift geometry, i.e., changes in slope angle may control the depsosit of either a plastered or a separated mounded drift (Vandorpe et al., 2016).

For an unambiguous paleoceanographic reconstruction utilizing contourite depositional systems it is paramount to decipher if changes in drift geometry are controlled by changes in the regional current system, or by changes of the local topography, maybe even by the drift construction itself, as it has been shown by Van Rooij et al. (2010). There is especially a lack of studies analyzing the complex interaction between currents, topography and resulting drift geometry at slopes with strongly dissected topography.

This study concentrates on a study area at the Galicia Margin, which inherited multiple topographic structures from phases of tectonic activity. The oceanographic regime interacts with several topographic obstacles, two ridges and the middle slope which is incised by numerous gullies. A dense net of high resolution multichannel seismic profiles in combination with bathymetric and Parasound data not only allows to map contouritic features in high detail, but furthermore enables to capture their small-scale spatial variations and reconstruct the evolution of these deposits. Also the small size of the study area allows for the assumption, that the primary current regime did not change spatially throughout the area, thus spatial changes in geometry from drift to drift can be solely attributed to the topography. An additional advantage is, that although the contourites are not active under modern oceanographic regime, the regime under which they build up is well known through modeling at one of the topographic obstacles (Hanebuth et al., 2015; Zhange et al., 2016).

In this study the interaction of the bottom current with all topographic features in the area is tackled. Different conceptual models, including the dependency of flow focussing and slope angle, flow splitting, flow detachment, and eddy shedding, are applied and refined based on the findings. Finally a classification of the different topographies and interaction processes which lead to the deposition of various contourite drifts is performed. Additionally, the paleoceanographic information known from the model is expanded to fit entire area.

4.2 Geology of the study area

The study area at the Galicia Continental Margin is situated at the eastern flank of the Galicia Interior Basin (GIB) and comprises water depth from 300 to 2700 m (Figure 4.2, Figure 4.1). The GIB itself formed during a rifting phase in the early Cretaceous, preceding the opening of the North Atlantic Ocean Basin (Muñoz et al., 2003; Murillas et al., 1990). The seafloor of the GIB is characterized by horst and graben blocks, which are the product of hyperextension and sequential faulting during rifting (Brune et al., 2017; Pérez-Gussinyé et al., 2003). Especially E-W orientated structures have been reactivated in Neogene times during the Pyrenean and Betic orogenies (Muñoz et al., 2003). Sediment supplied to the margin mainly originates from

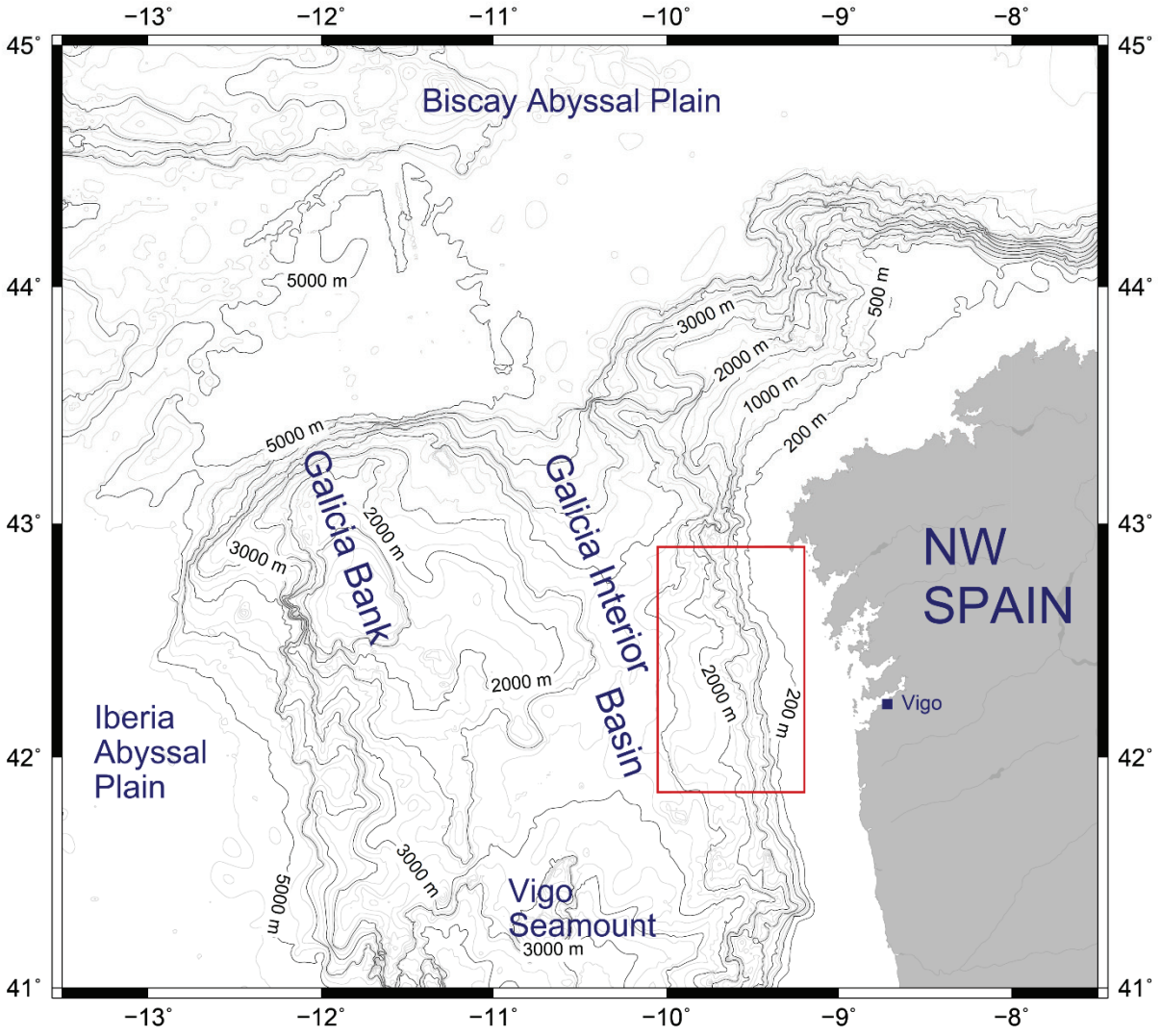

Figure 4.1 - Overview map of the Galicia Continental Margin, including the Galicia Interior Basin (GIB), and the Galicia Bank. The red rectangle marks the working area of this study.

Portuguese rivers (Duoro, Minho) and is intermittently stored in a mid-shelf mudbelt (Dias et al., 2002a; Dias et al., 2002b; Lantzsch et al., 2009; Lantzsch et al., 2010; Oberle et al., 2014a; Zhang et al., 2016a). Shelf export is accommodated by resuspension during storm events and subsequent seaward transport in nepheloid layers (Dias et al., 2002b; Oberle et al., 2014b; Oliveira et al., 2002; Vitorino et al., 2002). Throughout the Quaternary, sedimentation pattern on the slope were governed by hemipelagic deposition in the intergalcials, increased turbidite activity during sea-level fall, enhanced input of terrigenous material during glacials (Bender et al., 2012) and intermittent contouritic activity during deglacials (Bender et al., 2012; Hanebuth et al., 2015; Zhang et al., 2016b).

4.3 Oceanography of the study area

Source **Watermass**	Hernández-Molina et al. (2011)	Fiúza et al. (1998)	McCave and Hall (2002)	Varela at al. (2005)
Mixed Layer				
		200 - 700 m	50 -100 m	100 m
EANCW	~350 m	subtropic subpolar	400 - 500 m	subtropic <300 m subpolar <450 m
	600 m	500 - 600 m	800 m	
MOW	MU 500 - 700 m ML 800 - 1400 m	MU 780 m ML 1100m		MU ~800 m ML ~1100 m
	1500 m	1600 m	1400 m	1500 m
LSW	1800 m			
	2200 m	2200 - 2300 m	*2150 m*	3000 m
NADW				
	4000 m			
LDW				

Table 4.1 - Overview over water masses at the Iberian margin presented in different studies, compiled from Hernández-Molina et al. (2011) and references within, Fiúza et al. (1998), McCave and Hall (2002) and Varela at al. (2005).

The Galicia Margin at the eastern flank of the GIB is bathed by at least four watermasses and a mixed layer on top. Various studies measured different depths for water mass boundaries, which may be attributed to different measurement locations, seasonal variability or short term displacement of water mass boundaries by internal waves, tides or passing eddies.

Table 4.1 provides an overview of the different depths provided by different studies. In general the mixed layer extends down to around 100 m depth, underlain by the East North Atlantic Central Water (ENACW) until a depth of 500 – 800 m. Below that, the Mediterranean Outflow Water (MOW) is found until a depth of 1400 – 1600 m. Some studies defined two cores of MOW in different depths. The two lowermost watermasses in the GIB are the Labrador Sea Water (LSW) until a depth of 2200 – 3000 m underlain by the North Atlantic Deep Water

(NADW). High current speeds are expected for the MOW in the study area, simulated current speeds are higher than 10 cm/s and very locally they even exceed 50 cm/s (Hernández-Molina et al., 2011). However contourite deposits in the working area situated deeper than all records of modern MOW (Hanebuth et al., 2015). Moorings which recorded the hydrodynamic conditions in 2000 m depth over a time span of 18 months on the flank of the Pontevedra contourite in the study area, reveal current velocities exceeding 0.15 m/s only for 0.3% of the recorded time. For 76% of the timespan velocities were less than 0.07 m/s, which is not enough for the resuspension of the contouritic material, thus the modern oceanographic regime is unlikely responsible for the build-up of the contourite depositional system observed in the study area (Hanebuth et al., 2015; Zhang et al., 2016b). Indicators for 300 - 700 m deeper flowing MOW during glacials and deglacials are found around the Iberian Margin (Hanebuth et al., 2015; Rogerson et al., 2005; Schönfeld and Zahn, 2000; Zhang et al., 2016b). Modelling of oceanographic conditions with a 300 m displaced transition zone of MOW to LSW showed that passing oceanic density fronts interacting with the local topography creates sufficiently high current velocities (up to 0.38 m/s) for the buildup of the observed contouritic features (Hanebuth et al., 2015; Zhang et al., 2016b).

4.4 Material and Methods

This study integrates high resolution multichannel seismic data as well as Parasound echosounder data and multibeam bathymetry acquired during RV METEOR cruise GALIOMAR III (M84-4; Hanebuth et al., 2012). Multichannel seismic (MCS) was acquired using a 2 x 1.7 l GI Gun with a shotrate of 7 s and a 400-m long Syntron Streamer with 64 channels. The recorded data have a usable frequency range of 100-300 Hz. Data processing included binning to an along-track resolution of 5 m, normal moveout correction with a constant velocity of 1500 m/s, static corrections, despiking, Ormsby filtering, CMP stacking, white noise reduction and migration. It was performed with the Vista seismic processing suite (Schlumberger). Parasound data of the 4 kHz signal were converted using the custom made software ps32sgy and transformed to envelope data. The multibeam bathymetry grid is a merge of data collected with the swathsounder Kongsberg Simrad EM 122 and EM 710. Data were processed and gridded to a resolution of 100 x 100 m using the open-source software MB system and FLEDERMAUS (QPS).

A joint data interpretation was carried out using The Kingdom Software (IHS Global Inc.). For the identification of features at the seafloor and in the subsurface, bathymetric data, an absolute slope map as well as an azimuth dipmap were integrated with Parasound and MCS data. For a detailed interpretation of seismic data the stratigraphy and seismic facies definition of Haberkern et al. (in prep) (Chapter 3) were used.

4.5 Results

4.5.1 Identification of structural features

The bathymetric data presented in this study (Figure 4.2A) was already utilized by Hanebuth et al. (2015) and Zhang et al. (2016b). Their studies focused on the largest topographic obstacle in the area and combined hydrodynamic modelling with sediment core and Parasound echosounder data. This study will, in contrast, present an overview of all topographic features as well as detailed spatial analyses of the sedimentary pattern of several selected examples. The utilization of multichannel seismic data allows this analysis to go further back in time.

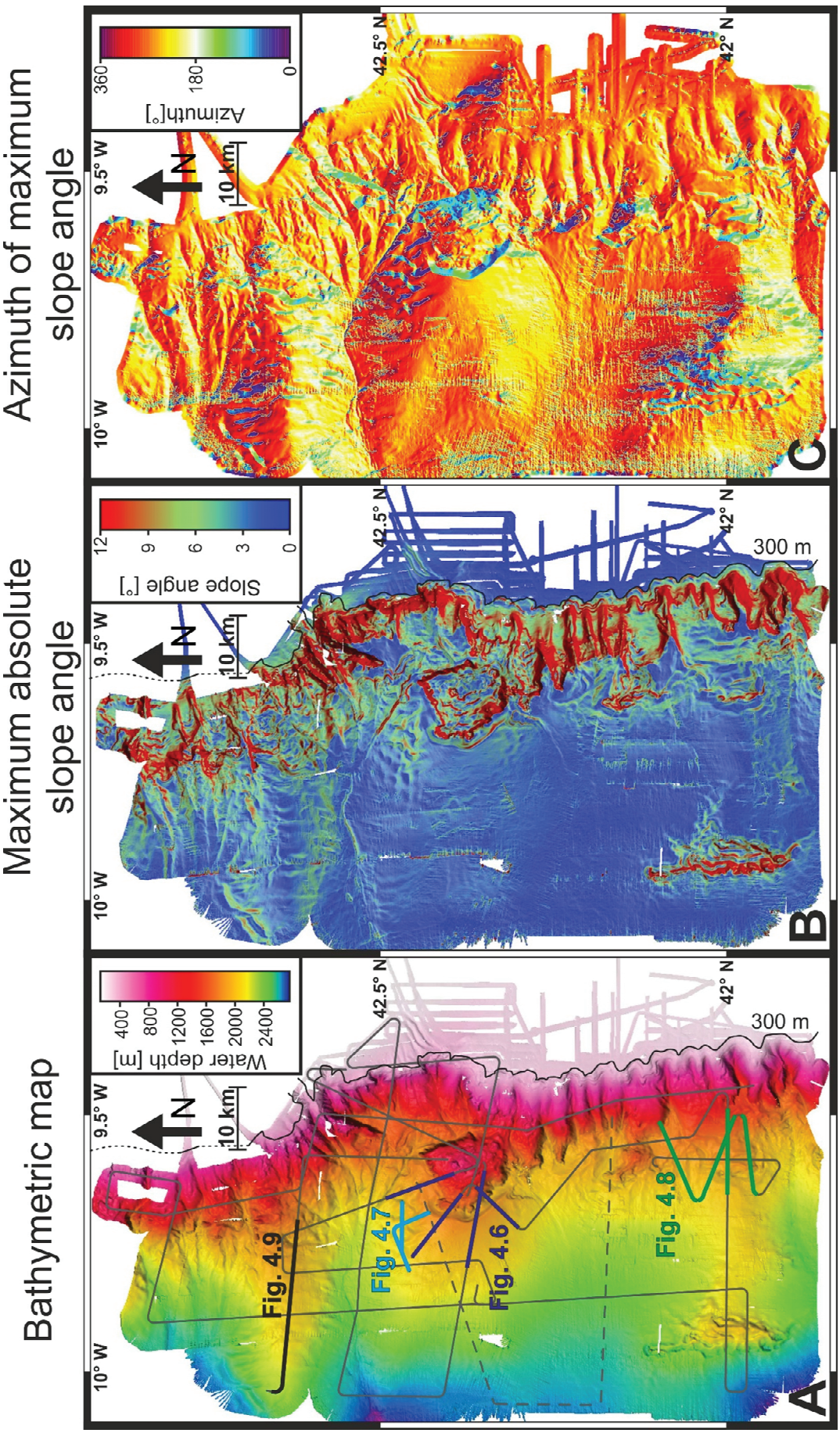

Figure 4.2 – Three maps based on bathymetry data, which were used in the integrated data analysis for the identification of morphologic features at the seafloor. A: Bathymetric map of the study area, including the location of all shown seismic profiles. B: Maximum absolute slope angle map calculated from the bathymetry. The color scale was clipped at 12° to visualize variations of lower gradients better. C: Azimuth map of maximum gradient, calculated from the bathymetric map.

The following structural features have been identified in a joint interpretation of the different bathymetric maps (Figure 4.2) and Parasound and MCS data and combined to a morphosedimentary map (Figure 4.3).

Morphologically the working area is structured twofold. The primary structure are the different slope areas: the slope is roughly meridional oriented and partitioned in upper, middle and lower slope characterized by different slope angles (Figure 4.2B). The secondary structure is exerted on the lower slope, which is again structured by the occurrence of different topographic heights. These heights have been categorized as four topographic obstacles (TO 1 – 4), and two ridges (Ridge 1, 2) (Figure 4.3). The following paragraph will describe the different partitions of the area in more detail.

The upper slope is characterized by low gradients (< 5 °) until 300 m water depth (compare Figure 4.2B and Figure 4.4). The middle slope reaches down to a water depth of 1300-1800 m. It is steeply inclined with gradients of 10° and higher, and is dissected by numerous gullies with extremely steep flanks (Hanebuth et al., 2015). Around 42.5° N the middle slope forms an embayment of 30 km width. South of the embayment gullies occur regularly and almost parallel aligned in East-West direction. In the embayment and north of it, the gullies acts as tributaries to three canyons**,** which are oriented from east to west. A similar canyon with tributaries is found at the southern end of the study area (Figure 4.2).

A large E-W trending ridge occurs in the north, as well as in the south of the working area (Figure 4.2A, Figure 4.3). Ridge 1, in the north, extends from the middle slope to the western end of the study area. It is about 15 km wide. Near the slope it is elevated 500 m above the surrounding seafloor, but towards the west its relief decreases to only 300 m (Figure 4.2A). The surface of Ridge 1 is overall wavy, with wave-crests oriented nearly perpendicular to the ridge axis (Figure 4.2B, C). They show maximal heights at the flanks (~70 m), while on the ridge crest the heights diminish to 40 m. Overall, the waves have a length of 1.5 – 2 km. In the south, Ridge 2 extends in-between two topographic obstacles, namely TO 4 near the slope in the east, and TO 3 in the West (Figure 4.3) (the detailed description of obstacles follows in the next paragraphs). Ridge 2 is about 20 km wide, elevated by about 300 m above the surrounding seafloor (Figure 4.2A). On its southern flank the surface is wavy in a few areas (Figure 4.2B, C). Again the wave-crests are oriented nearly perpendicular to the ridge. Compared to Ridge 1, the waves on Ridge 2 are less regular and their reliefs are less as 50 m, however, the wave lengths are similar to the waves observed on Ridge 1.

In the very north of the study area the seafloor morphology is dominated by the occurrence of two E-W oriented canyons as well as the gullies cutting middle and lower slope. Two more E-W oriented canyons occur within the study area, both are situated directly south of each of the ridges. For further reference, canyons are labeled Canyon 1 - 4 from north to south (Figure 4.3).

Four topographic obstacles (so-called “TOs”) have been identified primarily by their steep flanks and rough surfaces in the bathymetric map. In the above described embayment a large, almost circular isolated topographic obstacle (TO 1) with a diameter of 12 km arises up to 800 m higher than its surroundings (Figure 4.2A), which was already described and named as *Pontevedra outlier* by Hanebuth et al. (2015). Obstacle TO 2 is found south of the *Pontevedra outlier*, it is characterized by a very irregular shape and is significantly smaller as TO1 with an area of 6 x 9 km² and a maximum height of 400 m.

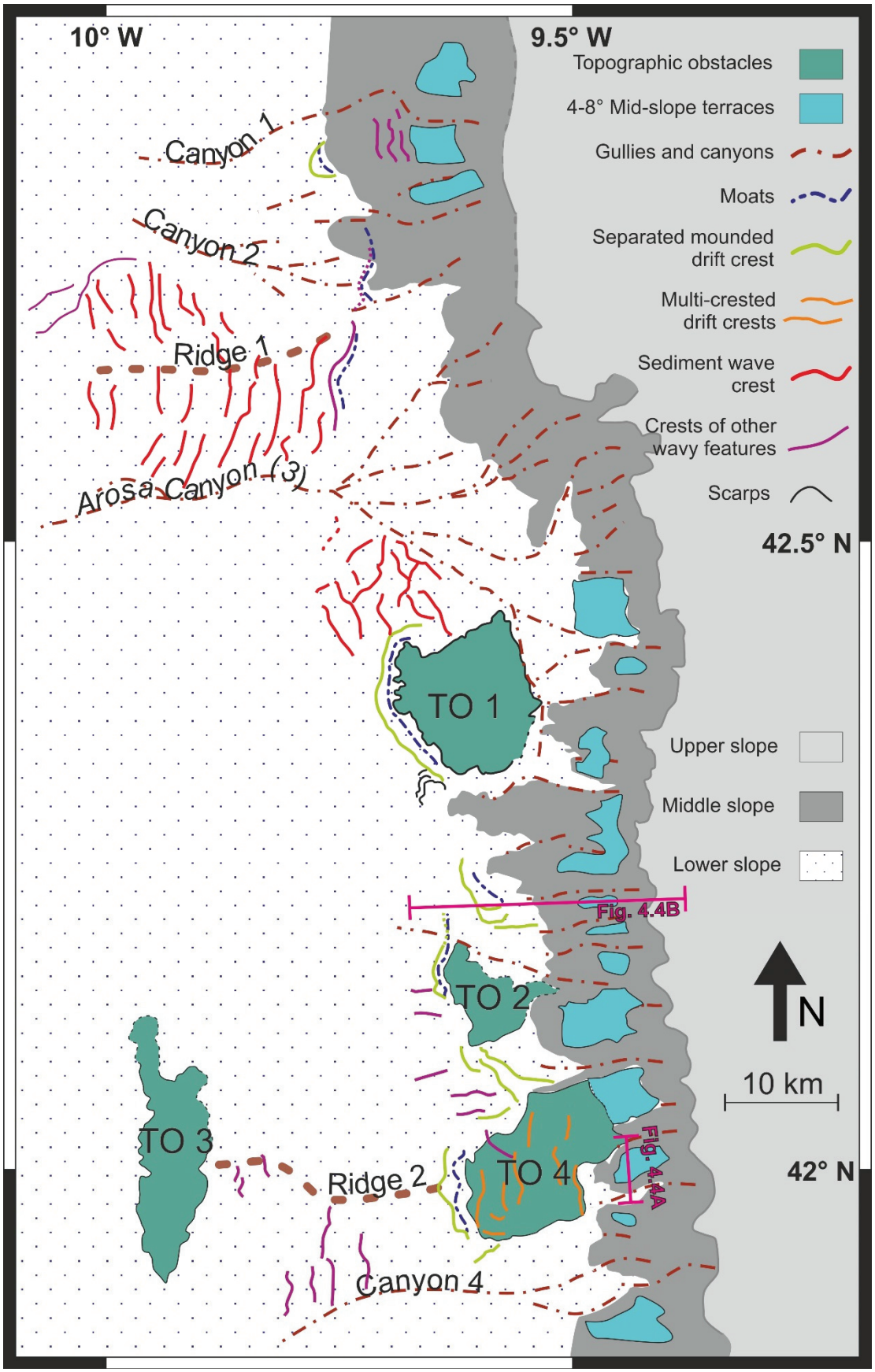

Figure 4.3 - Morphosedimentary map derived from the integrated data interpretation of the study. It shows the structure of the study area in upper, middle and lower slope. Within this structure the map shows the location of canyons and gullies, the different topographic obstacles, crests and moats contributing to the various CDS as well as sediment waves and other wavy features.

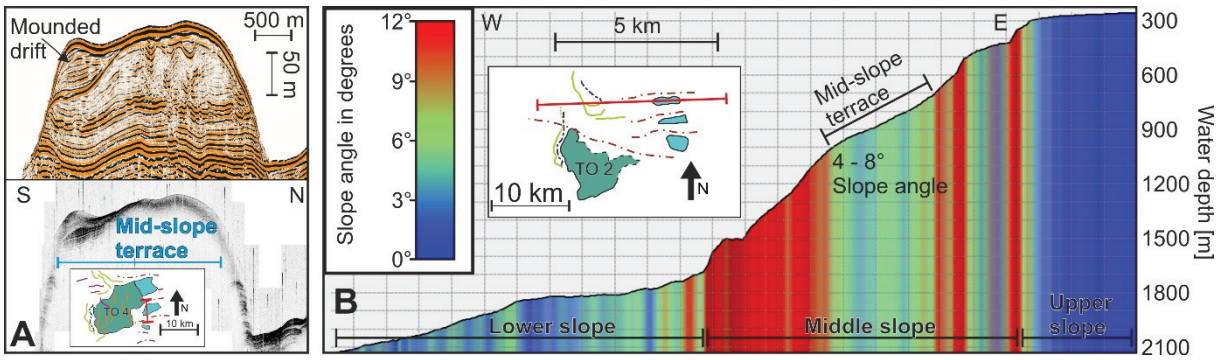

Figure 4.4 - Illustration of the identification of Mid-slope terraces. A: MCS (upper part) and Parasound (lower part) data showing the morphology and structure of a Mid-slope terrace in S-N direction. B: Bathymetric profile showing the general slope angle variation across the Galicia Margin. The Mid-slope terrace is clearly visible as an area of reduced slope angles at the middle slope. For location also see Figure 4.3.

TO 3 is located in the southwest of the study area and elongated to 21 km in north-south direction with a maximum width of 6.5 km. Its highest point is 480 m above the surrounding seafloor. TO 1 – 3 are isolated topographic obstacles, furthermore one non isolated topographic obstacle (TO 4) occurs as a plateau connected to the middle slope in the southeast of the study area. The surface of TO4 is slightly tilted seaward, in a water depth between 1600 - 1800 m and protrudes the slope by ~10 km. In along-slope direction it has a width of ~12 km. To the north it is transitioning into the mouth of a gully with a depth difference of only 50 m, while in the south it features some terrace like steps but south of those, the seafloor drops down by 200 m into Canyon 4. On top of TO4 some crests occur, which are up to 60 m high and strike subparallel in N-S orientation. Opposed to the topographic obstacles there are areas, which are characterized by their overall low slope gradients. First, in many of the wider gully mouths the slope of the seafloor drops below 4 degrees (Figure 4.2B). Furthermore slope angles in a range of 4 to 8 degrees occur at the middle slope in water depths between 400 and 1500 m. This leads to the light expression of a terrace at the middle slope, which is hard to recognize in the slope angle map (Figure 4.2B) as it is interrupted by the incising gullies and thus appears as several low angle patches lined up along the middle slope. The change in slope angle is also evident in bathymetric profiles (Figure 4.4B). Their appearance in the Parasound data is characterized by low penetration, and a chaotic signature of medium to high

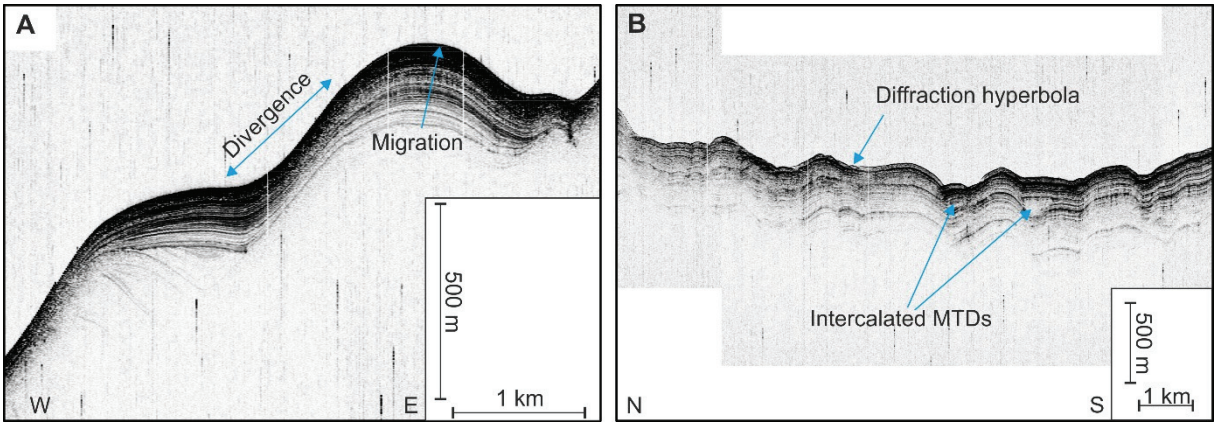

Figure 4.5 - Examples of the different types of wavy features identified by means of Parasound data. A: Example of features classified as sediment waves. B: Example of the features classified as other wavy features.

amplitudes (Figure 4.4A). They are indicated as mid-slope terraces in Figure 4.3 (see interpretation and discussion in Section 4.6.5).

In addition to the waves on the ridges and on TO4, wavy topographies occur in various expressions throughout the working area (Figure 4.2, Figure 4.3). Their signature in the Parasound data was utilized to classify them as either sediment waves or other wavy features (Figure 4.3). Wavy topographies which show continuous reflections, divergence and a migration direction were classified as sediment waves (e.g. Figure 4.5A). Whilst features which lack these characteristics and instead may display parallel and or discontinuous reflectors, even reflector truncations, diffraction hyperbolas and intercalated transparent patches were ranked as other wavy features (e.g. Figure 4.5B). One example of wavy topographies, which shall be discussed further is found northwest of the TO1, where two crossing alignments of wave crests are found. The reliefs of theses waves are averagely 20 to 40 m, but can peak up to 150 m. Furthermore on the western side of the topographic obstacles TO1, TO2 and TO4

Name	Continuity	Amplitudes	Reflector spacing	Reflector geometry	Example	Interpretation
A1	Highly continuous	High	Large	Subparallel	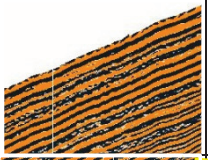	Coarse sheeted contourite drifts
A2	Highly continuous	Medium	Dense	Subparallel	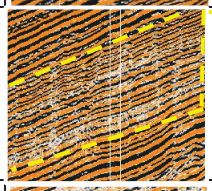	Sheeted contourite drifts
B	Semi continuous	Low to medium	Medium to large	Subparallel to contorted	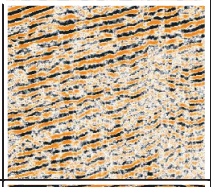	Altered sediments of different origin prevalently sheeted contourite drifts
C1	Discontinuous	Medium to transparent	Medium	Contorted to chaotic	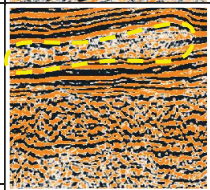	Mass waste deposits with disturbed to no internal structure
C2	Discontinuous	High	Medium	Contorted to chaotic	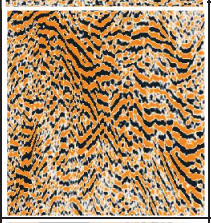	Tectonically altered sediments, seismic basement
D	Highly to semi continuous	High to low	Dense to large	Divergent and convergent	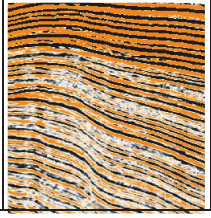	Other contouritic drifts including plastered and mounded drifts

Table 4.2 - Seismic facies description defined by Haberkern et al. (in prep) (Chapter 3).

mounded topographies of different heights and extents are observed (Table 4.4), they are separated from the TOs by elongated depressions.

4.5.2 Multichannel seismic data

For the analysis of the multichannel seismic data the seismic facies interpretation (Table 4.2) as well as the definition of seismic units (SU) I – VI (Table 4.3) were adapted from Haberkern et al. (in prep) (Chapter 3).

Seismic unit	Epoch	Age [Ma]
SU I	Mid- to late Eocene	41 - 35
SU II	Late Eocene to early Miocene	35 - 14
SU III	Early Miocene to early Pliocene	14 - 4.5
SU IV	Early Pliocene to early Pleistocene	4.5 - 2.58
SU V	Early Pleistocene to Mid-Pleistocene	2.58 - 0.7
SU VI	Mid-Pleistocene to modern	0.7 - now

Table 4.3 - Seismic units and their deposition periods at the Galicia Margin (Haberkern et al. in prep, Chapter 3).

Pontevedra obstacle - TO 1

Insight into the sedimentary structures around TO 1 is provided by four multichannel seismic profiles (Figure 4.6), radially oriented around the topographic obstacle. The southernmost profile strikes SW-NE, the orientation of the following profiles is rotating clockwise as they are placed further to the north. The topographic obstacle is characterized by the seismic signature of the seismic basement (facies C2). Its characteristic steep flank continues in the sub seafloor. All other seismic units onlap on that flank.

SU I and II are only identifiable in the three southernmost profiles (Figure 4.6A-C). Whilst in Profiles GeoB11-034 and 019 they consist of altered sediments and are of roughly constant thickness, in Profile GeoB11-035 both units consist of mass transport deposits (MTDs). The upper boundary of SU I forms a step on which SU II onlaps thus it thins out and terminates towards TO 1. SU III in contrast is present in all four profiles and onlaps directly on TO 1. It shows high variability in thickness together with variations in the topography of the upper unit boundary. In all profiles SU III thickness is increased near the obstacle. Southwest of the obstacle (Figure 4.6A) SU III reveals a plastered drift. West of TO 1 (Figure 4.6B) SU III has a similar but gently mounded outer geometry, internally MTDs and subparallel reflectors alternate. Northwest of TO 1 (Figure 4.6C) the outer geometry of SU III shows several mounded features, which internally are related to contorted reflectors, mounded drifts as well as reflector truncations. In the northernmost profile (Figure 4.6D) no mounded features occur in the outer geometry of the unit and internally, MTDs dominate. SU IV prevalently consists of sheeted and mounded contourite drifts southwest and west of the obstacle (Figure 4.6A-C). In Profiles GeoB11-034 (Figure 4.6A) and 035 (Figure 4.6C) the topography of the upper unit boundary features a depression between the obstacle and a mounded body In Profile GeoB11-19 (Figure 4.6B) similar geometries can be found in the internal reflectors. North of TO 1 (Figure 4.6D) a mix of sheeted contourite drifts and MTDs result in some mounds in the topography of its upper boundary. At one of the mounds, reflector truncations are present. SU V and VI are separated from TO 1 by a depression in the southern three profiles (Figure 4.6A-C). In Profile GeoB11-034 and GeoB11-019 (Figure 4.6A, B) it is U-shaped with reflector truncations at the seaward flank. Apart from the mounded drift next to the depression which migrates downslope or aggrades, SU V and VI consist of sheeted drifts. In Profile GeoB11-035 (Figure 4.6C) the depression appears V-shaped, generally not as wide as the U-shaped examples and bare of any reflector truncations at the seafloor. Instead SU V is present beneath the depression, parallel layered to its seaward flank. West of the crest, reflectors

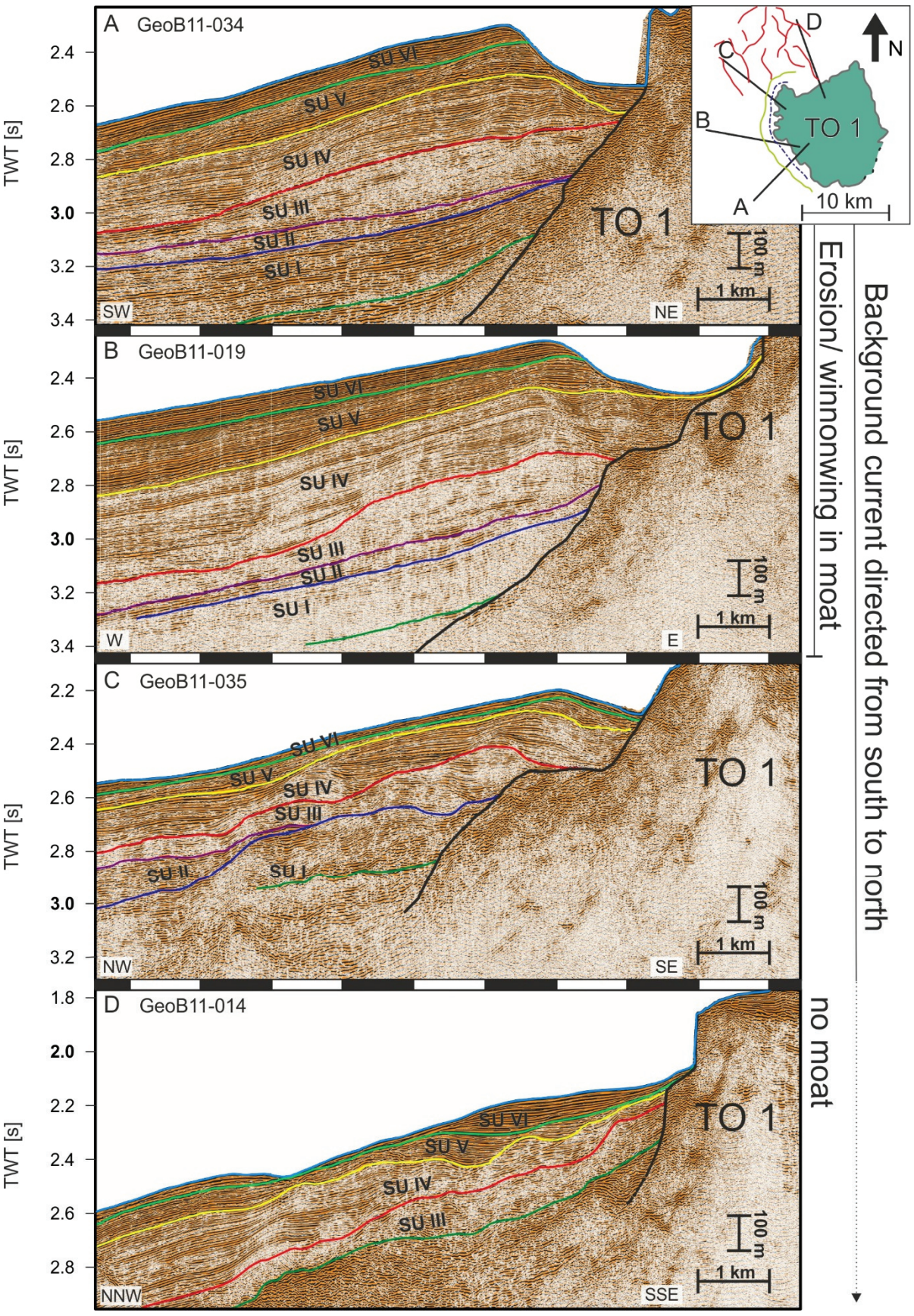

Figure 4.6– Seismic profiles A: GeoB11-034, B: GeoB11-019, C: GeoB1-035, D: GeoB11-014 around TO 1 in the order of current direction from south to north clockwise around the obstacle, see map in the upper right corner. Seismic units following terminology as shown in (Table 4.2). Thick black line represents seismic basement. For location see also Figure 4.2A and Figure 4.3.

truncate at its upper boundary. Further west SU V is only 0.01 s thick, but towards the western end of the profile, it thickens up to almost 0.1 s. SU VI thinly (0.03 s) drapes the underlying topography with only minor thickness variations. North of the obstacle no depression exists (Figure 4.6D). The sheeted contourite drifts of SU V onlap on the variable topography of SU IV. SU VI forms a lenticular contourite drift body near the obstacle and a small mounded topography in the northern end of the profile shown in Figure 4.6D.

Wavy features north of TO 1

The subsurface structure of the wavy features northwest of TO 1 is revealed by three MCS profiles, GeoB11-036, 026 and 025b (Figure 4.7). The seismic basement is discernible by its chaotic transparent internal structure. Seismic Units I – III are characterized by a mix of MTDs and altered sediments. SU I and II onlap on the seismic basement and are almost conformably overlain by the other units. However, onlapping reflectors can be found locally. The upper unit boundaries of SU III to VI express an undulating topography, which only locally is associated to reflector truncations or onlaps. The most remarkable example occurs at the eastern end of Profile GeoB11-036 (Figure 4.7A), where the upper boundary of SU III forms a pinnacle associated to truncation of internal reflectors. The general relief of the unit boundaries increases from the upper boundary of SU III to the seafloor, although locally depressions are smoothed out by divergent reflectors in overlying units. SU IV entirely consists of altered

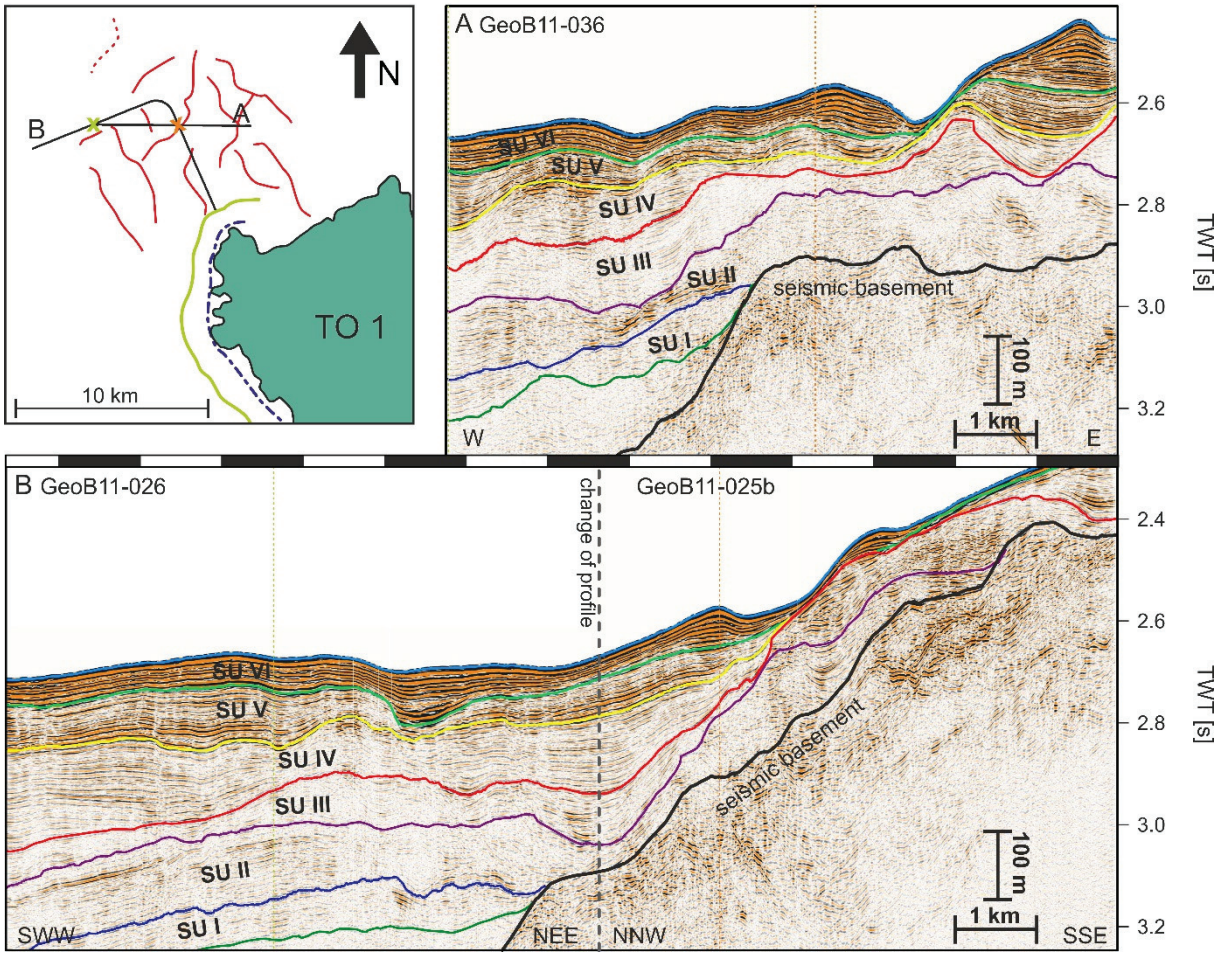

Figure 4.7 — Seismic profiles A: GeoB11-036, B: GeoB11-026/025b showing the wavy features north of TO 1. Seismic units following terminology as shown in (Table 4.2). Thick black line represents seismic basement. For location see also Figure 4.2A and Figure 4.3.

sheeted drifts, SU V mostly of sheeted drifts and SU VI mostly of coarse sheeted drifts, however, small mounded or wavy features (< 2 km) occur in all three units (Figure 4.7A, B).

TO 4

The seismic profiles GeoB11-039, 030, 040 and 041 reveal the internal structure of TO4, which is attached to the middle slope in the southeast (Figure 4.8). In the southern three profiles (Figure 4.8A-C) the base topography represented by the seismic basement has a steep flank towards the west in the central and the eastern parts of the profiles, exhibiting a variable topography including horst structures and a shallow graben. Additionally to the usual chaotic and transparent appearance of the seismic basement, locally high amplitude and semi-continuous, subparallel reflectors are incorporated below the horst and graben topography. The northernmost Profile GeoB11- 041 (Figure 4.8D) is located off the plateau in a gully exit (see Figure 4.2A). There the base topography is steeply inclined to the west with a change to lower slope angles in a depth of 2.8 s TWT (Figure 4.8D). This profile is presented here as a reference profile for the depositional architecture unrelated to TO 4. Of the Seismic Units west of the plateau (TO 4) only the Seismic Units II - VI are regarded, whereas Seismic Unit II is only shown in Figure 4.8B and C. In all cases the units in onlap on the steep flank of the base topography. The Profile GeoB11-039 (Figure 4.8A) poses an exception, there the base topography is draped even on its steep flank by a transparent unit in which the boundary between SU II and III cannot be recognized. On top of the strongly dissected base topography in the southern part of TO 4 (Figure 4.8A) the internal acoustic facies of units I – IV is dominated by the occurrence of MTDs. In the profiles in the centre of the plateau (Figure 4.8B, C) SU I-III also incorporate MTDs but furthermore display the internal seismic facies of sheeted contourite drifts, and SU IV also shows evidence of mounded drift deposits. In general SU I and II fill the depressions of the base topography, only in GeoB11-040 (Figure 4.8C) SU I is absent on top of TO 4. In Profile GeoB11-030 (Figure 4.8B) a U-shaped depression incises SU I in the middle of the profile. SU II only occurs east of the depression and its reflectors truncate at flank of the depression. SU III occurs over the whole plateau. In the south (Figure 4.8A), it forms two relatively steep, pointy elevations, in the middle parts of the plateau (Figure 4.8B, C) its outer topography has less relief, still at all steeper parts of upper boundary reflector truncations occur. West of the southern part of TO 4 SU IV and V are restricted to the eastern steep part of the profile, whilst on the remaining parts, SU IV is split into one part on the eastern (steep) part and another SU IV deposit on the western part of TO 4. The thinning in the middle of the plateau and mounded topographies in SU IV are associated to reflector truncations. Furthermore SU V is only present on top of TO 4 in the very southeast (Figure 4.8A). SU VI overall has the appearance of either coarse sheeted contourite drifts or mounded contourite drifts. In the south (Figure 4.8A) mounded features fill the depressions between the steep elevations. Further to the east more mounded drifts occur. On the middle and northern parts of TO 4 several mounded drifts occur in the western as well as the eastern parts, the latter are associated to reflector truncations on their western flanks. In the middle of TO 4 SU VI is very thin. The Profile GeoB11-041, which cuts into the gully exit north of TO 4, presents a very different pattern: The base topography slope is steep in the east and does not feature a plateau, only a distinct change in the slope angle. SU I is not shown in (Figure 4.8D). SU II and III are mostly consisting of MTDs with few continuous reflectors onlapping the base topography. SU IV consists of altered sheeted contourite drifts with a few MTDs, its upper boundary has a mounded topography associated to reflector truncations. SU V internal

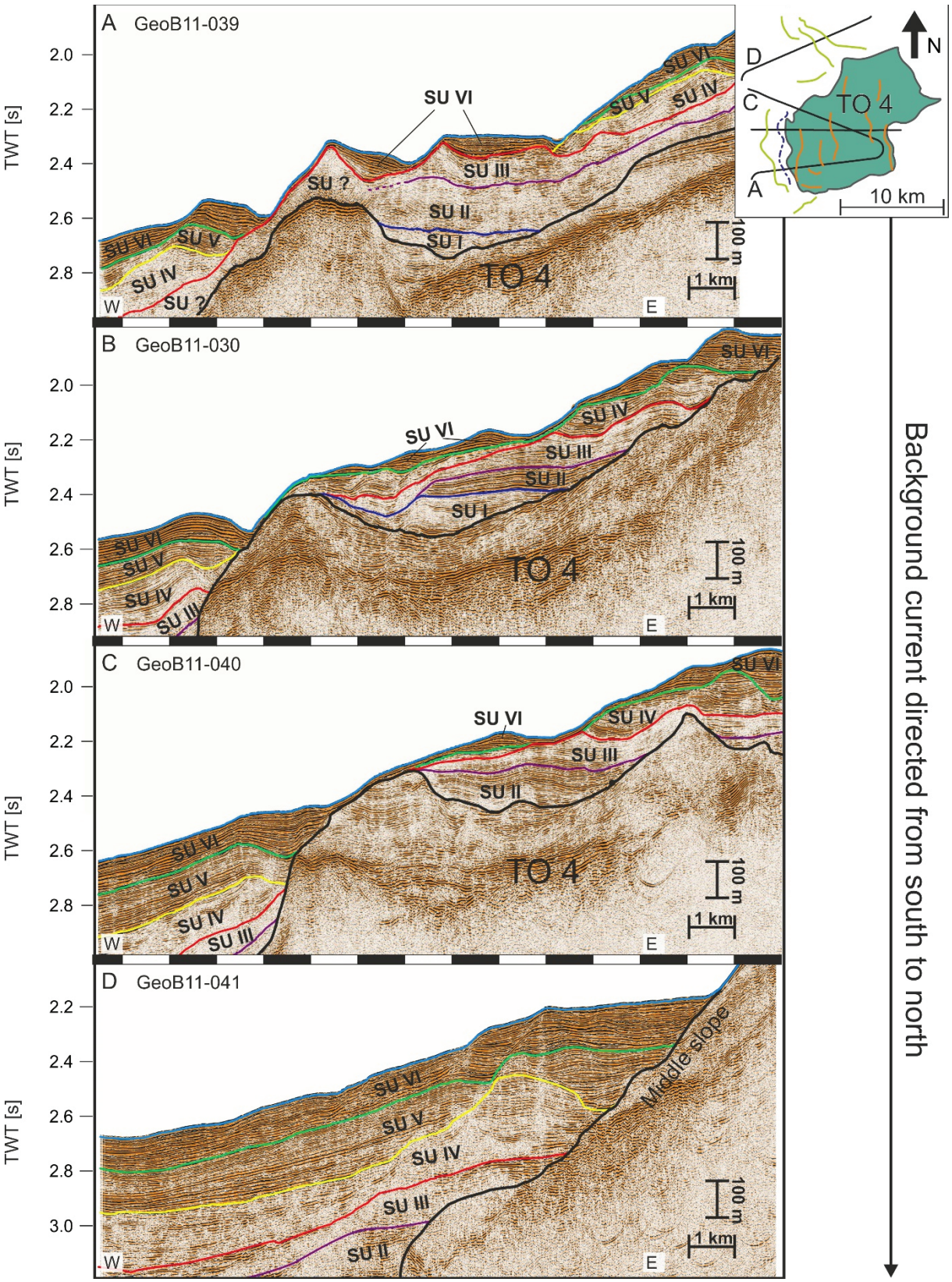

Figure 4.8 - Seismic profiles A: GeoB11-039, B: GeoB11-030, C: GeoB11-040, D: GeoB11-041 covering TO 4. Profiles are sorted in current direction from south to north. Thick black line represents seismic basement. For location see also Figure 4.2A and Figure 4.3.

reflectors onlap on the mound, as well as on the a smaller slightly mounded topography over the mounded feature in the underlying unit. In SU VI reflectors representing coarse sheeted drifts smooth out the topography of the mounded feature built by SU V to a certain extent. In the western part of the profile reflectors are partly contorted.

Wavy features on Ridge 1

Seismic Profile GeoB11—017 images the subsurface along the crest of Ridge 1 (Figure 4.9). Overall the topography and underlying structures dip towards the west. The seismic basement is characterized by contorted to chaotic internal reflectors. In the eastern part of the profile, the seismic basement represents the middle slope, which exhibits a very steep slope on which most seismic units onlap. In the middle part of the profile the slope of the basement is quite flat, but steepens again to the western end. SU I and II consist of low amplitude reflectors and were altered by tectonic movement, thus they incorporate numerous columnar low amplitude zones and a few MTDs. Both units closely follow the topography of the underlying seismic basement, however their upper boundaries have very rugged surfaces and are associated to single reflector truncations. SU III is very thin in the western part of the profile and much thicker, up to 0.2 s, in the middle part. There, its upper boundary exhibits a very variable topography associated to various reflector truncations. In the east SU III onlaps on the basement. Internally it consists of altered sediments but the amplitudes of SU III are higher compared to the underlying units SU I and II (Figure 4.9). Unit IV generally reveals the internal seismic facies of sheeted drifts however, it also expresses a multitude of wavy internal geometries, onlaps on lower boundary as well as truncations at the upper boundary. Thickness is very irregular and as a result the topography of the upper boundary of SU IV is smooth and has an overall

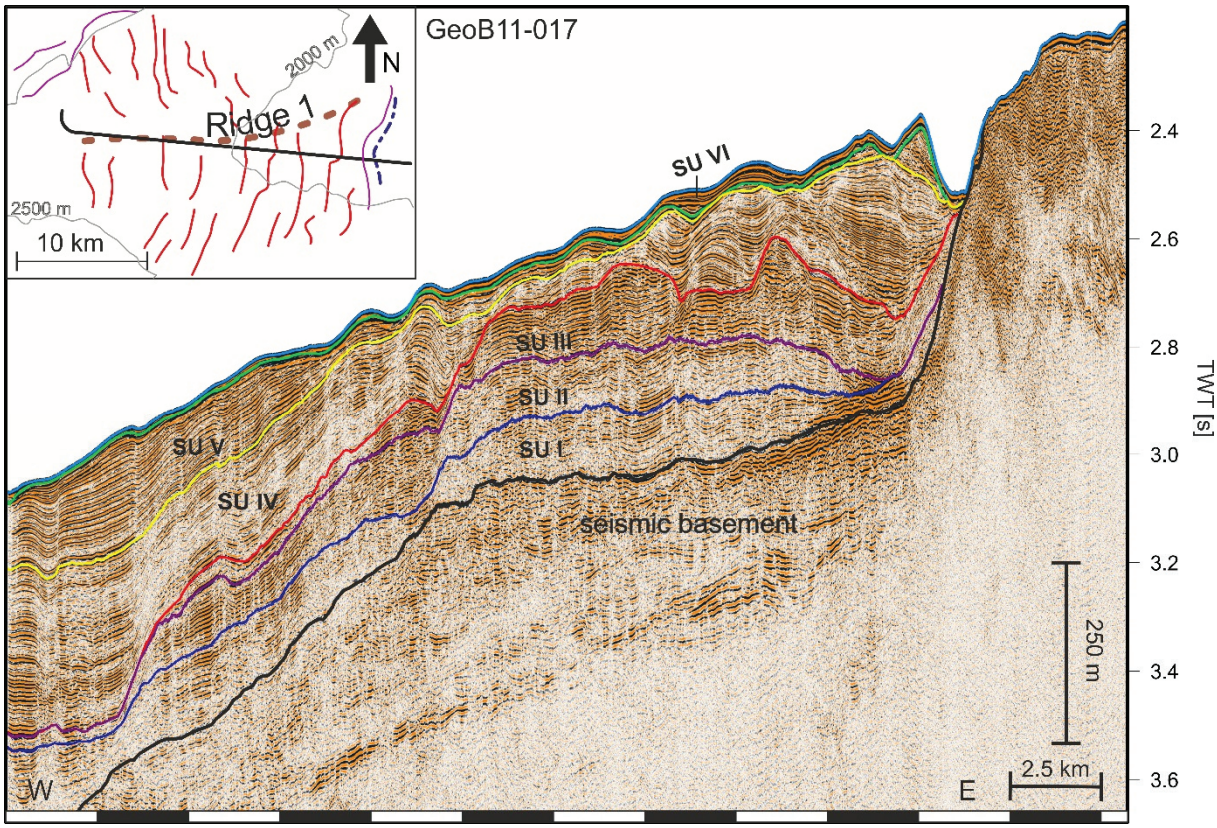

Figure 4.9 – Profile GeoB11-017 along the crest of Ridge 1, providing insight into the wavy features on the Ridge 1. Thick black line represents seismic basement. For location see also Figure 4.2A and Figure 4.3.

moderate seaward inclination over the western and middle part of the profile. This surface is furthermore modulated by the occurrence of small wavy features, around 1 km wide with a variable relief ranging from 0.002 to 0.01 s (Figure 4.9). SU V shows the same seismic facies as SU VI, but its thickness variation differs extremely. In the middle part of the profile it is extremely thin except for a small mounded feature close to the steep slope of the seismic basement. In the eastern part of the profile in contrast its thickness increases up to almost 0.2 s. Internal reflectors are subparallel to the lower unit boundary and truncate at the upper boundary, which therefore is much less inclined compared to its lower counterpart (Figure 4.9). Unit VI internal reflectors meet the criteria of coarse sheeted drifts, however some mounded and wavy features are incorporated in the unit. It is overall very thin. Unit V and VI are separated from the steep slope of the seismic basement in the east by a depression (Figure 4.9).

4.6 Discussion

4.6.1 Identification and classification of contouritic depositional systems

Mounded crested sedimentary deposits together with associated erosional features are identified as contouritic depositional systems (CDS). CDS which form under the influence of the same watermass are considered to be a contourite depositional complex (CDC) (Hernández-Molina et al., 2008b).

The classification of bottom current influenced sedimentary features in the study area revealed three main categories: **Separated mounded drifts** are identified by a lateral sequence of a topographic obstacle, a moat and a mounded drift from east to west. Separated mounded drifts occur west of TO 1, TO 2 and TO 4 (Figure 4.3). A **multi-crested drift** occurs on top of TO 4. It consists of several elongated drift bodies separated by contouritic channels as well as elongated winnowed and eroded areas. Current influenced **wavy features** were identified north of TO 1 as well as on Ridge 1.

4.6.2 Separated mounded drifts

The largest CDS is associated to the topographic obstacle TO 1 (Pontevedra Outlier). Its development over the last 50 ka is already described in Hanebuth et al., 2015. The moat and the crest of the separated mounded drift are half circling around the obstacle (Figure 4.3). Where the current entered the moat in the south, it eroded drift sediments (Figure 4.6A, B), but further to the north the moat is draped by sediments (Figure 4.6C). Furthermore the moat relief decreases from more than 100 m down to 20 m from south to north. These findings indicate that current intensity weakened along the flow path, which is in agreement with model results from Hanebuth et al. (2015). The E-W extent of the contourite is less 28 km (Hanebuth et al., 2015). As the along slope extents are restricted to the extents of the obstacle amounting for 11 km it is regarded to be a patch drift following the definition of Hernández-Molina et al. (2006) and Rebesco et al. (2014) (Hanebuth et al., 2015).

In the following paragraph the spatio-temporal evolution of the drift is analysed, therefore the stratigraphic framework of Haberkern et al. (in prep) (Chapter 3 (Table 4.3) is applied. The seismic units SU I and SU II have been deposited under the influence of a bottom current, which did not strongly interact with TO 1. In **Miocene** times **(SU III)** a plastered drift developed southwest of the TO 1 (Figure 4.6A), further around, west of the obstacle the drift is slightly mounded and sediments failed on the contourite flank (Figure 4.6B). Northwest of TO 1 mass wasting and erosion obscure the depositional geometry of the drift, nonetheless an initially

mounded geometry and a shallow moat can be inferred. North of the obstacle only MTDs were deposited in the Miocene (Figure 4.6D). The shallow and only locally developed moat indicates that the interaction of the bottom current with the topographic obstacle did not produce current velocities high enough to inhibit sediment deposition or even cause erosion around the entire obstacle. In the **Pliocene (SU IV)** a distinct separated mounded drift developed southwest and west of TO 1 (Figure 4.6A, B). Northwest of TO 1 initially two mounded bodies formed, subsequentially their topographic expression was smoothed out by drift sediments (Figure 4.6C). North of the obstacle, the deposition is still dominated by mass wasting resulting in a rough topography. In the early **Pleistocene (SU V)** erosion took place in the moat south and west of TO 1 while the separated mounded drift was mostly aggrading or migrating seaward (Figure 4.6A, B). This indicates that the current was strongly focused in the moat. Northwest of TO 1 the drift initially migrated upslope, thereby deposited in the moat. Erosion took place at its seaward flank. Therefore, there, SU V is locally extremely thin (Figure 4.6C). Thus, current strength within the moat must have decreased around the obstacle, however, current strength on the contourite flank northwest of TO1 was increased. North of the obstacle (Figure 4.6D) sheeted drifts, which smoothed out the underlying topography, indicate a changing current regime. Enhanced thickness of SU IV Is interpreted to be the result of additional sediment input from the Arosa Canyon. A similar spatial pattern of current variation around TO 1 imprinted in the drift deposits, which formed since the **Mid-Pleistocene transition (SU VI)**. The mounded drifts south and west of TO 1 migrated seaward while erosion lasted in the moat (Figure 4.6A, B). Northwest of TO 1, the entire drift body is thinly draped with slightly elevated thicknesses on the contourite (Figure 4.6C). Since at that location the sediments of the underlying seismic unit SU V were eroded, it is assumed that the local current velocities did decrease to allow for the deposition of the thin drape. North of TO 1 a thicker plastered drift built up close to the obstacle (Figure 4.6D) which again reports sediment supply from the middle slope.

The sediment covered TO 4 also acted as an obstacle to the flow as indicated by the moat and separated mounded drift along its seaward (western) flank in water depth deeper than 2.4 s (Figure 4.6). The initial mounded drift, which appeared in the **Miocene (SU III)**, was restricted to the central part of the drift in N-S direction (Figure 4.6B) and was still subdued. In the **Pliocene (SU IV)**, a separated mounded drift formed along the entire obstacle flank (Figure 4.6A-C). In the **Early Pleistocene (SU V),** in the southern part west of TO 4, the drift migrated mostly upslope, whilst seaward of the mound another winnowed area occurs (Figure 4.6A), in the central part the moat in the preceding unit was filled and a narrower moat developed further upslope (Figure 4.6B). North of it, the mound is migrating slightly seaward (Figure 4.6C). In the **Upper and Middle Pleistocene (SU VI),** in the southern part west of TO 4, the drift migrated further upslope and the local winnowing was even more pronounced (Figure 4.6A). In the central part of TO 4 the mounded drift aggraded (Figure 4.6B), and north of it the moat was filled. The moat filling starts at a knickpoint where the slope angle of the obstacle decreases in upslope direction (Figure 4.6C). It is assumed that the slope angle there is too low to focus the bottom current and therefore the moat was filled.

West of the very irregular shaped TO 2 a moat and a separated mounded drift only occur along the northern half of the obstacle (Figure 4.3).West of the elongated TO 3 no elongated separated mounded drift was found.

The construction of distinct drift bodies associated to TO 1and TO 4 began in the Middle Miocene under the influence of outflow water from the Tethys (Haberkern et al., in prep). This Tethys outflow was considerably weaker than its successor the MOW, which started to flow in the Pliocene (4.5 Ma) in the Gulf of Cádiz (Hernández-Molina et al., 2014). Thus drift building under the influence of MOW at the Galicia Margin is assumed to start also at 4.5 Ma (Haberkern et al., in prep Chapter 3). Then a distinct separated mounded drift was established from the southwest to the northwest around TO 1.

However not the MOW core, but the deglacially shoaling transition zone between LSW and MOW was identified as the effective zone of contouritic activity (Hanebuth et al., 2015; Zhang et al., 2016b) at the Galicia Margin. The current strength variation reflected in the sedimentary deposits thus recored the dynamic of this transition zone but still correlates well to the variations in MOW strenght recorded in the Gulf of Cádiz (Haberkern et al., in prep; Chapter 3) There MOW strength increased from Pliocene to Pleistocene but decreased after the Mid-Pleistocene transition (Hernández-Molina et al., 2014). The increase only clearly shows in the erosional patches northwest of the obstacle.

Conceptual implications of the interaction of bottom currents with topographic obstacles

Apart from TO 3, the water depth west of all remaining topographic obstacles is within the interval of 1800 and 1900 m. West of TO 3 the seafloor slopes down to 2450 m. The lack of a separated mounded drift next to TO 3 is conclusive evidence, that the transition zone between LSW and MOW never was displaced far enough downward to interact with TO 3. The presence of separated mounded drifts at TO 1, TO 2 and TO 4 reports a displacement until at least 1900 m.

A comparison of the obstacle height and width, with the width and depth of the moat shows that the largest obstacle (TO 1), in both height and width, is associated to the deepest and widest moat, and the smallest obstacle (TO 2) to the shallowest and narrowest moat (Table 4.4).

Mapping of the crests and moats of the separated mounded drifts (Figure 4.3) shows that both contour the shape of the obstacles at least partly. This is attributed to the current focusing due to the Coriolis force veering the current against the obstacle flank. However in the case of TO 2 only the northwestern tip of its irregular shape is contoured. At TO 4, which has a rounded rectangular shape, moat and drift only exist at the N-S striking part of its flank. Only at the largest obstacle the moat is observed to half circle the obstacle. Vandorpe et al. (2016) proposed that a threshold in obstacle slope angle is required to successfully focus the bottom current and develop a moat. And indeed the slope angle of TO 4 is highest along the N-S striking part of its flank (Figure 4.2B). At TO 3 there are many patches of high slope angles, however the part which is contoured by moat and drift crest exhibits continuously high slope angles. Around TO 1 the slope angles are also continuously high (Figure 4.2B).

Furthermore, around TO 1 the erosion on the contourite flank northwest of the obstacle (Figure 4.6C) is evidence that the flow is changing around the obstacle. The fact, that the moat is erosive in the southwest and west of the obstacle but depositional northwest of it suggests that the current velocity in the moat is decreasing around the obstacle.

Obstacle					Moat			Drift	Waterdepth
	Height	Width		Shape	Depth	Width	Alignment	Migration	West of the obstacle
		N - S	E - W						
TO 1	810 m	~11 km	~ 12 km	subcircular	75 - 170 m	925 - 2770 m	half circle	Variable	1800 m
TO 2	445 m	up to 9 km	up to 7 km	irregular elongated (NW-SE)	0 - 55 m	25 - 1330 m	N-S slightly bent	upslope	1900 m
TO 3	575 m	23 km	10 km	elongated (N-S)	no distinct drift body				2450 m
TO4	775 m	~ 10 km	attached to middle slope	rounded rectangular	0 - 70 m	95 - 2470 m	N-S	aggrading	1900 m

Table 4.4 - Shape, sizes and water depth of topographic obstacles and associated separated mounded drifts measured from their seafloor expression in bathymetric data. The depth of the moat was measured from the drift crest to the deepest point, whilst the width was measured from the drift crest to the flank of the obstacle in the same water depth.

The decrease of current speed around TO1 and the absence of a moat north of it, can be attributed to flow detachment. Batteen et al. (2007) formulated a condition which initially was applied to current flowing around large capes in the Gulf of Cadiz. It constrains the maximum radius R of a cape, from which a current is still able to detach. Vandorpe et al. (2016) showed that a simplified condition may be applied to submarine obstacles:

$$R < \sqrt{\frac{U}{f\frac{\nabla h}{H}}}$$

With R being the minimum radius for detachment, U being current velocity, f represents the Coriolis parameter, ∇h the tangent of the slope angle in degrees, and H the water depth next to the obstacle in the moat. Solving for U and applying suitable parameters allows to deduce the maximum velocity of a current, which is able to flow around an obstacle without detaching (Vandorpe et al., 2016).

$$U_{max} = R^2 f \frac{\nabla h}{H}$$

Applying water depth and radius for the Pontevedra obstacle (Table 4.4) as well as a Coriolis parameter of $f = 9.85 \times 10^{-5}$ and a slope angle of 25 ° (Figure 4.2B) results in a maximum velocity of 0.77 m/s, which unlikely is ever reached in the area. The maximum velocity captured in the mooring data, analysed in Hanebuth et al. (2015) and Zhang et al. (2016b) is 0.188 m/s.

The maximum modelled velocity amounts to 0.35 m/s. Thus the current should have fully flown around the obstacle at all times. However, if the irregular shape of the obstacle is taken into consideration, the radii of smaller protrusions, which range from 1500 to < 1000 m (Figure 4.10) have to be accounted for. This calculation shows that U(R=1500) just reaches 0.014 m/s, a value that is frequently exceeded in the model and in the modern regime (Hanebuth et al., 2015; Zhang et al., 2016b). Consequently it can be assumed that the current, which was responsible for drift build-up in the deglacial detached from the obstacle at one of the protrusions.

In the direction in which the current presumably detached, northwest-north of TO1, wavy expressions at the seafloor with two different orientations provide evidence for even higher spatial variability of the current regime (Figure 4.3). The seismic data reveal prevalent mass wasting in that location until the beginning of the Pliocene (SU I – III) (Figure 4.7). In the Pliocene (SU IV) slightly mounded drift bodies built up, which cannot be correlated to underlying or close-by topography. During the Pleistocene (SU V – VI) build-up of several mounds and winnowing, even erosion occur on small spatial scales within an area smaller than 10 km² and evolve into an undulating, upslope migrating topography (Figure 4.7). Therefore the features were interpreted to be sediment waves which developed under a complex current pattern presumably involving flow in more than one direction. This cannot be explained by current detachment only. Hernández-Molina et al. (2016) suggested that the wavy features might have built up under the influence of internal waves. Moreover, eddies which shed in the lee of TO 1 and travel north might modulate the current velocities and directions at that location. The model of Zhang et al. (2016b) includes eddies being shed behind TO 1. Boyer and Zhang (1990) identified the Rossby number (R_O) as most significant criterion for eddy shedding behind a seamount. In general R_O expresses the impact of the Coriolis force versus inertial forces. Their model shows that eddy shedding occurs for:

$$R_O = \frac{U}{fD} > 0.1$$

U is the current speed, f is the Coriolis parameter and D the length of the obstacle or phenomenon. Rossby numbers for TO 1 with D=11km and $f = 9.85 \times 10^{-5}$ have been calculated using different threshold velocities (Table 4.5).

The largest value of 0.38 $\frac{m}{s}$ corresponds to the maximum current speed of the model of Zhang et al. (2016b), while the other values represent the velocities occurring in the modern oceanographic regime of the area the lowest value thereby prevails for 76% of the time (Hanebuth et al., 2015). Results show that during recent oceanographic conditions eddy shedding is probably a rare phenomenon, however, just slightly higher velocities enable eddy shedding. Therefore it is assumed that eddy shedding was most likely a prevalent phenomenon

Current speed $\left[\frac{m}{s}\right]$	0,38	0,15	0,12	0,07
Rossby number	0,35	0,14	0,11	0,06

Table 4.5 - Threshold velocities and Rossby numbers for eddy shedding.

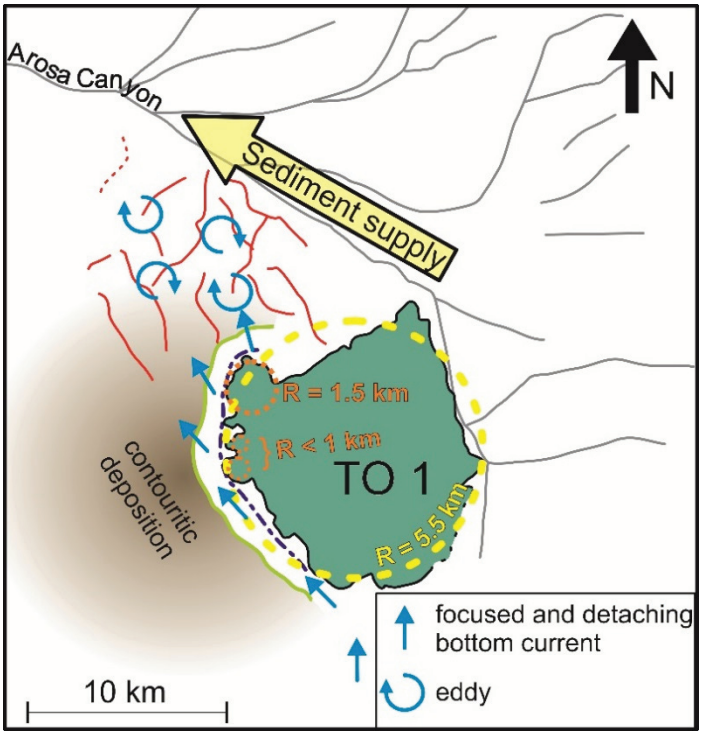

Figure 4.10 - Conceptual sketch of processes resulting from the interaction of bottom currents and TO 1. Compare Figure 4.3 for location in the study area.

in times of contouritic deposition. Furthermore a stronger oscillatory component in the current velocity, caused for example by internal tides could lead to larger eddies being shed (Boyer and Zhang, 1990; Turnewitsch et al., 2013).

In conclusion, the occurrence of flow detachment and eddy shedding are expected to be responsible for the variability observed in the drift deposits including sediment waves with different orientations around TO 1 from south to north (that is from luv to lee). Thickness increases to around the obstacle to the north is partly induced by sediment input from the Arosa Canyon and its tributaries, making the northern part of the drift a mixed system of along- and downslope transported sediments (Figure 4.10).

4.6.3 Multi-crested drift

Seismic data reveal that the seismic basement beneath TO 4 has a dissected topography (Figure 4.8). The western flank of TO 4 is underlain by a small horst structure, which is connected to a gentle slope in the east, via a shallow but wide depression. The depression shallows from south to north (Figure 4.8A - C). From Mid-Eocene to Early Miocene times, the depression was filled up. Indicators for mass wasting on top of the plateau, such as MTDs and associated headwalls in SU I-III, provide evidence that the area was affected by the tectonic activities of the Pyrenean and Betic Orogenies from Eocene to Miocene (Muñoz et al., 2003; Haberkern et al., in prep Chapter 3). Both, MTDs and headwalls contributed to the very variable topography of SU IIIs upper boundary. This is most pronounced in the south, where SU III forms two distinct heights, which do not correlate with underlying topography of SU II (Figure 4.8A). The overlying Pliocene Unit (SU IV) then deposited under the influence of MOW (Haberkern et al., in prep, Chapter 3) with the contribution of small MTDs. In the southern part of TO 4, SU IV only occurs in the east and was eroded on the western part of TO 4 (Figure 4.8A), whilst in the middle and northern part of TO 4, erosion in the central part divides SU IV in an eastern and a western patches (Figure 4.8B,C). Early Pleistocene sediments (SU V) are missing on TO 4 except for a small patch in very southeast (Figure 4.8A). This observation indicates that enhanced current velocities in the Early Pleistocene (Haberkern et al., in prep Chapter 3) in combination with the elevated position of TO 4 created a hydrodynamic regime too energetic to allow for sedimentation on top of the obstacle.

After the Mid-Pleistocene transition, when current velocities decreased, sediments deposited again on top of TO 4. This unit (SU VI) consist of small drift bodies separated by zones of erosion or at least non-deposition. These bodies are elongated in along slope direction on the

Plateau (Figure 4.2, Figure 4.3), parallel to the main current direction. Changes in drift geometry along that path are apparently related to changes in the underlying topography. In the south, the two distinct heights built by SU III are underlying SU. On top of their surfaces, drift sediments fill the topography. The seaward inclined slope parts remain exposed to the current (Figure 4.8A). Further north the underlying topography changed to being overall seaward inclined with steps. On the areas with low gradients, mounded drifts migrate upslope, whilst steeper gradients are only thinly draped by probably winnowed sediments (Figure 4.8B, C).

The build-up of the observed drift bodies is assumed to be the result of decreasing current velocities of the MOW in the Late Pleistocene (see Hernández-Molina et al., 2014). The observed spatial pattern of erosion/winnowing and deposition, finally creating several small mounded contouritic drifts can be explained by the existence of several current cores which are pushed against the slope due to Coriolis veering causing erosion on their upslope side and deposition on their downslope side. The distribution of the drift sediments on the either flat or eastward inclined surfaces, whilst steep and westward dipping areas in underlying topography are left blank and in some cases are eroded, hints that the topography causes the focusing of the bottom current into the several cores. Multi-crested drifts developing from a single separated mounded drift have been described in the Rockall Trough (Stoker, 1998). However the multi-crested drift presented here is an extreme example for the control of underlying small-scale topography on the drift geometries.

4.6.4 Wavy features on Ridge 1

Another example for complex current-topography interaction is found on Ridge 1. Similar to the multiple crested drift on TO 4 the underlying topography is very rugged and was presumably formed by tectonic activity during the Pyrenean and Betic Orogenies in Miocene times (Muñoz et al., 2003), as evident from small-scale faults and erosional truncations which are interpreted to be headwalls (Figure 4.9). In the Pliocene (SU IV) the topography was mainly filled up and wavy features formed above steep heights and mounded topography, both indicating bottom current influence. During the Early Pleistocene the impact of the current increased. In areas shallower than 2.8 s (around the crest of Ridge 1) only a thin sediment package was deposited. In deeper parts of Ridge 1 a thicker deposit is found, which is eroded on the top. In combination with the lack of Early Pleistocene deposits on TO 4, this leads to the conclusion that the current regime was too intense to allow for significant deposition on elevated areas, and the erosional surface representing the Mid-Pleistocene transition suggests that current speed even increased at the end of the Early Pleistocene. Since the Mid-Pleistocene transition also only a thin cover of sediment deposited, but it is clearly visible that the wavy features migrate upslope in both Pleistocene Units (SU V and VI). To evaluate if the wavy features are sediment waves sensu stricto, in the following it will be discussed if they fulfill the criteria for sediment waves as adapted from Lee et al., 2007; Lee et al., 2002; Wynn and Stow, 2002: (i) Differential accumulation rates resulting in either up- or downslope migration, in the case of the wavy features on the northern ridge upslope migration is observed. (ii) Reflector continuity throughout all sediment waves extending even further than the sediment wave field. This can only be confirmed for areas where no erosion took place. (iii) Reflector geometry such as the dip of flanks and crest/trough width should display some degree of regularity. The width of crest and through is quite regular for the waves on the Ridge 1, however since their height varies considerably the dip of the flanks is not very regular

(Figure 4.9). (iv) Linear surface expression with varying degrees of sinuosity and bifurcation. This criterion is met by the wavy features on Ridge 1 (Figure 4.3). Furthermore sediment waves formed under bottom currents are usually oriented oblique to the regional slope and perpendicular to the current direction, turbidity current waves are usually oblique to the turbidity current overspill and therefore very often parallel to the regional slope (Wynn and Stow, 2002).

The occurrence of erosion and mounded features are definetly strong evidence for a current impact on the ridge, however, the irregularity of the wavy features on Ridge 1 together with their N-S orientation - parallel to the primary current direction – may on a first glance strongly contradict the assumption that these features are sediment waves. . Therefore a possible interpretation could be, that the irregular (paleo) seafloor topography split the current into fast flowing cores, analogue to the mechanism acting on top of TO 4. Consequently the wavy features on Ridge 1 would have to be interpreted as a multi-crested drift.

However, it is more likely that the ridge does have a significant impact on the bottom current pathway. Assuming a strictly contour parallel current direction, most of the wavy features are oriented perpendicular to the current direction, as typical for the formation mechanisms of sediment waves. Furthermore the irregularity of the waves might be inherited by the complexity of the topography the current encounters. This is furthermore supported by the fact that the regularity in wavelength is increased after the deposition of SU V (Figure 4.9). Thus the features are interpreted to be sediment waves which are modulated by small-scale underlying topography.

4.6.5 Contourite terraces

Slope angle analysis identified some areas at the middle slope between the gullies where the gradients vary between 4 to 8 degrees. These mark exceptional areas on the overall significantly steeper middle slope. They cover water depths inbetween 400 and 1300 m, and their appearance in Parasound data suggests that they are prevalently formed through winnowing (Figure 4.4). Terraces related to contouritic activity, so-called contourite, terraces are mostly situated at water mass boundaries and comprise erosional as well as depositional features (Hernández-Molina et al., 2009; Preu et al., 2013; Rebesco et al., 2014). Depositional features were mapped only in along slope direction at the borders of the terraces to the gullies (Figure 4.4). Furthermore the depth of the terrace corresponds to the depth of the modern MOW upper core thus, the terrace cannot be forming actively under the current oceanographic regime. Therefore it is suggested that it formed under the influence of the upper boundary of MOW when it was displaced during glacial times. This would require a displacement of up to 800 m. Under the assumption that the vertical extent of the water masses and transition zones is not affected during glacial interglacial variation and furthermore considering, that the topographic obstacle TO4 in a depth of 2450 m is not affected by the MOW LSW transition zone this would constrain the maximum displacement of MOW to a value between 800 and 950 m.

4.7 Conclusions

In this study the strong control of pre-existing topography on the position and shape of contouritic depositional systems is shown at the example of the Galicia Margin. The small size of the study area guarantees that the observed changes in the depositional pattern are not a function of a change in the background hydrodynamic regime but solely result from the interaction of the current with the local topography. Hence the observed interaction processes

can serve as representative examples for analogue settings. The analysis of the distribution of different types of contouritic deposits, in relation to distinct topographic features resulted in a classification of four types of feature combinations.

(i) Next to topographic obstacles separated mounded drifts formed. One of the topographic obstacles is situated too deep to be influenced by the highly energetic bottom current regime and thus is not associated with a separated mounded drift. At the highest obstacle the associated moat is the deepest and widest, at the obstacles with the smallest height it is vice versa. The along slope extent and shape control the orientation and length of the moat. Furthermore, at the largest obstacle, TO 1 the flow detaches due to the irregular shape of the obstacle and eddy shedding leads to the build-up of wavy features northwest of TO 1. (ii) A multi-crested drift formed under several bottom current cores. Steps and distinct heights in underlying topography split the bottom current into the several cores, which focused against steeper parts of the topography, causing erosion or winnowing upslope and deposited mounded drift bodies in downslope direction. (iii) Wavy seafloor topographic features occur in multiple locations in the study area. North of TO 1 their formation is assumed to be controlled by eddy shedding lee of TO 1. (iv) On Ridge 1 sediment waves form under a bottom current that contours the ridge. Irregularities in wave height are associated with the underlying topography.

Furthermore contourite terraces at the middle slope potentially result from the interaction of the boundary between ENACW and MOW. In terms of paleoceanographic significance, the analysis of the positions of all contouritic features in the area allows to constrain the possible glacial and deglacial MOW displacement to a value between 800 m and 950 m. Additionally, the fact that the sediment waves on Ridge 1 and the multi-crested drift are the only areas, which are affected by erosion during MOW strengthening in the Lower Pleistocene confirms that they react more sensitive to changes in the current regime, thus fortifies the importance of studying small-scale contouritic features for paleoceanographic reconstruction.

In future, the concepts which were semi-quantitatively applied to reconstruct the current topography interaction in the area, as there are the dependency between flow focussing and slope angle, flow splitting, flow detachment, and eddy shedding, could be on the one hand modelled to determine thresholds in topography and current strength under which they act. But furthermore, in future studies comparison to other areas, which exhibit similar pre-existing topography but differ in the hydrodynamic regime or sediment supply could provide valuable insight on how these factors impact the resulting sedimentary record of the topography current interaction. Furthermore there is still a need to understand the interaction of processes on even smaller timescales. At the Galicia Margin for instance the contribution of downslope transport guided by the numerous gullies to the shape of the margin is still not fully understood and can potentially be studied by means of high resolution echosounder data as is available from the *RV Meteor Cruise M84-4.*

Acknowledgements

This study was funded through the DFG-Research Center/Cluster of Excellence “The Ocean in the Earth System” We would like to thank Captain Thomas Wunderlich, the crew of *R/V Meteor cruise M84/4* for their excellent work and support.

5 Fault controlled contouritic depositional systems beneath and around Cold Water Corals – an example from the salt rafted Angola Margin

Haberkern, J.[a], Schwenk, T.[a], Wintersteller, P.[a], Wenau, S.[a], Wienberg, C.[a], Hebbeln, D.[a], Spiess, V.[a]

[1] MARUM – Center for Marine Environmental Sciences and Faculty of Geosciences, University of Bremen, Germany

Abstract

Due to the necessity of ambient bottom currents to form contouritic depositional systems or Cold Water Coral (CWC) mounds the presence of both under the influence of the same bottom current is a quite common occurrence. Up until now CWC mounds have been mostly discovered in the North Atlantic whilst contouritic depositional systems are ubiquitously known throughout the world oceans. In the salt rafted Kwanza Basin at the shallow Angola continental margin, CWC mounds occur in chains in water depths between 200 and 500 m, comprising heights up to >100 m and widths between 400 and 1000 m. During *R/V Meteor Cruise M122* in 2016, high resolution multichannel seismic data have been acquired to investigate the spatio-temporal evolution of sedimentary architecture and CWCs as well as the role of faulting related to salt tectonics. Integrated data analysis of high-resolution multichannel seismic data and multibeam bathymetry allows to identify indicators for an active bottom current regime, including contourite channels, separated mounded drifts and erosional surfaces, from the seafloor to 300 mbsf related to a fault bordering a salt raft. Furthermore, active and buried faults are ubiquitous in the study area. CWCs appear to be rather recent features since only few superficially buried mounds have been found restricted to shallow water depth (<300 m). The architecture of the Contouritic Depositional System (CDS), however, is older and CWC growth starts late within the active CDS, indicating that it has developed a habitable environment for CWCs. This study presents a detailed analysis of the contourite channels as well as separated mounded drifts on both sides of the most prominent mound chain. The so-called Anna Ridge is 13 km long and approximately N-S oriented. The eastern channel was formed much earlier than the CWCs and underwent several cycles of channel filling and erosion, suggesting significant changes in the regional current regime over time. Contrastingly, the western channel succeeds the CWC formation, which suggests that it is formed by the interaction of bottom currents with the CWC mounds. This study presents a conceptual evolutionary model for the interaction of bottom currents with the active salt rafting process including eventual CWC mound formation and subsequent changes of the topography-current interaction process.

5.1 Introduction

The concept of contourites as sedimentary deposits forming under the influence of bottom currents has been advanced since the first discovery of bottom current influence on deep sea sediments (Heezen and Hollister, 1964). Nowadays contouritic depositional systems (CDS) are studied in water depths from shallow water (e.g. Rebesco et al., 2016) down to the abyssal plains and even in lacustrine environments (e.g. Ceramicola et al., 2001). Also, in addition to persistent thermohaline currents, a multitude of forcing mechanisms are recognized including internal tides (Vandorpe et al., 2016) and oceanic fronts (Hanebuth et al., 2015). Despite all these advances, the essential motivation to study contouritic deposits have remained the same over more than 50 years. Besides slope stability implications and their relation to the formation, storage and sealing of hydrocarbons, the potential of contourites to provide paleoceanographic archives draws major scientific interest (Rebesco et al., 2014). Contouritic drifts record paleoceanographic changes as their composition and/or geometry of deposition reflects variations in the current under which they form. However, when it comes to CDSs in areas where bottom currents interact with topography such as seamounts or outliers (Roberts et al., 1974; Hanebuth et al., 2015), mud volcanoes, ridges (Vandorpe et al., 2016), slide scars, capes or marine promontories (Martorelli et al., 2010; Falcini et al., 2016), a change in drift geometry may also result from a change in the interaction process. In the simplest case, this happens when drift sediments start to bury the topography and thereby remodel the topography encountered by the bottom current (Van Rooij et al., 2010). The interaction of processes is even more complex if the encountered topography itself changes through time, as would be the case for tectonically active regions or biogenic structures such as Cold Water Coral (CWC) mounds. Fault related contouritic drifts are actually regarded as a distinct sediment drift type (Rebesco and Stow, 2001; Rebesco, 2005; Rebesco et al., 2014) although documented examples are rather rare (Ceramicola et al., 2001; Rebesco et al., 2014). Also, the co-occurrence of Cold Water Corals and contourite drifts has gained attention lately (De Mol et al., 2002; Van Rooij et al., 2003; Hebbeln et al., 2016). Up to date CWC mound research is mostly concentrated on the North Atlantic and Mediterranean which is unlikely to reflect their actual distribution (Hebbeln et al., 2016).

The working area of this study is located in the western South Atlantic, in the Kwanza Basin offshore Angola, where salt-tectonic activity creates a multitude of faults (Fort et al., 2004; Marton et al., 2000) and furthermore large chain building CWC mounds have been found. This study uses high-resolution multichannel seismic for the reconstruction of a CDS, which initially formed through the interaction of a large normal fault at the border of a salt raft in the Kwanza Basin. A stacked sequence of elongated separated mounded drifts developed in the raft graben. Subsequently CWC growth took place along the fault on the footwall block, which is the salt raft and further modulated the hydrodynamic regime so an additional elongated separated mounded drift developed along to the coral ridge on top of the salt raft. This unique setting reveals valuable implications for the growth and constraints of fault controlled drifts and furthermore on the interaction of contouritic drifts and CWCs. Finally it indicates where suitable CWC habitats are situated in a CDS.

5.2 Geologic setting of the Kwanza Basin offshore Angola

The Kwanza Basin offshore Angola is underlain by a thick (up to 1500 m) Aptian evaporite formation, which deposited after initial rifting in young shallow basins of the South Atlantic Ocean (Duval et al., 1992; Ala and Selley, 1997). All post-salt strata are deformed through salt tectonics, which essentially comprise an extensional regime on the upper slope and a

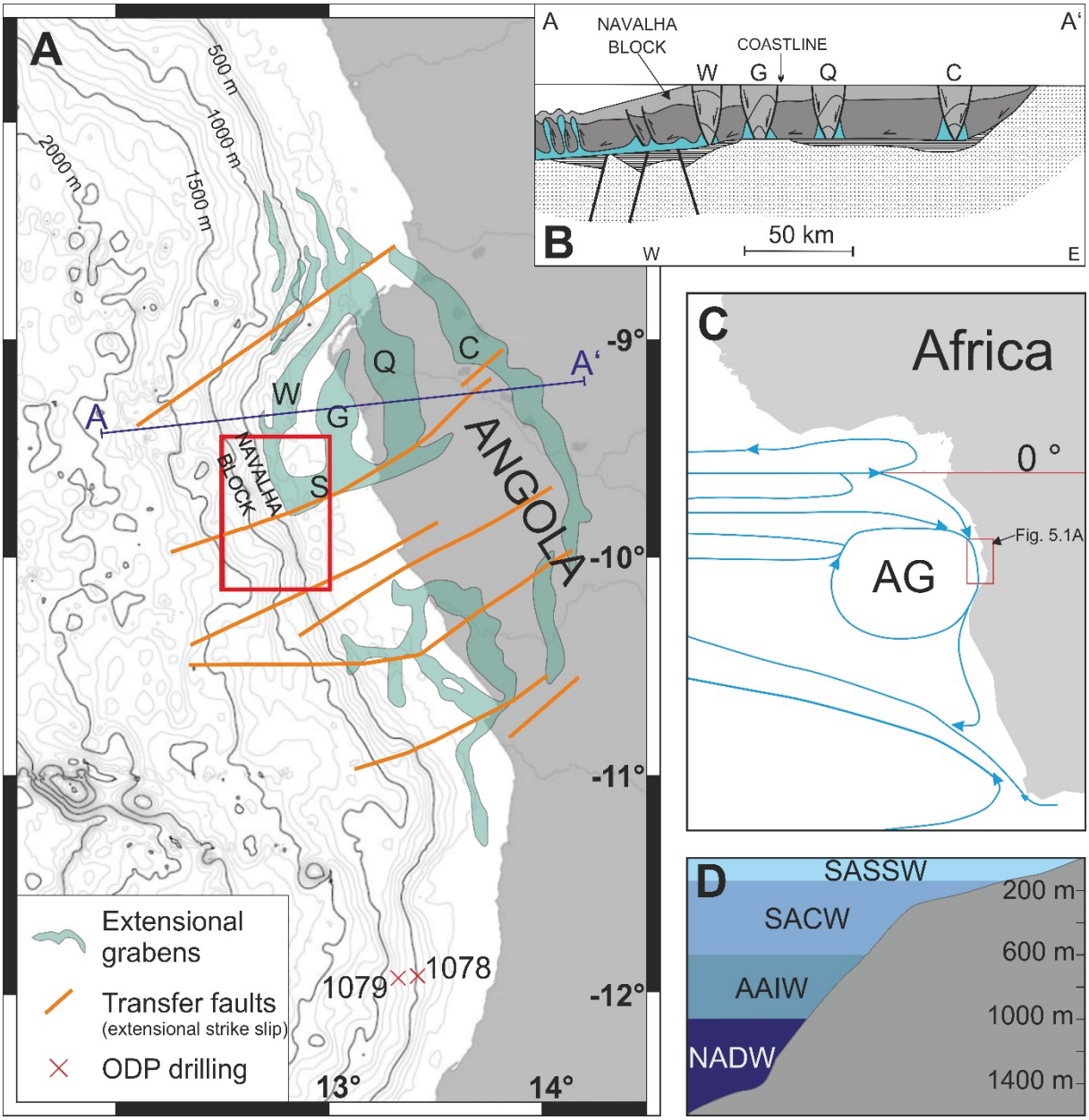

Figure 5.1 – A: Overview map of the Angola working area, overlain with different structural features: outline of sedimentary grabens formed by salt rafting redrawn from Lundin (1992), transfer zones redrawn from Hudec and Jackson (2004). The red rectangle indicates the area of interest of this study. The names of the extensional grabens are (C) Calombaloca, (G) Gaviota, (Q) Quenguela, (S) Sangano and (W) Western. B: Structural transect across the Angola Margin redrawn from Lundin (1992) showing the sedimentary depocenters in the extensional grabens. C: Overview map showing the location of A, and the major circulation features of the South Atlantic Central Water adapted from Stramma and Schott (1999). D: Water masses at the Angola Margin.

contractional domain on the lower slope connected by a translational domain (Cramez and Jackson, 2000; Marton et al., 2000). In this study, the focus lies on the extensional regime, which is characterized by extensive salt rafting. Gravity-driven mobilization of salt started after an overburden of a few hundred meters was deposited, resulting in two phases of salt rafting (Duval et al., 1992). Phase 1, or pre-rafts, of Middle to Upper Cretaceous age have been conjoined by further Upper Cretaceous sedimentation after their formation (Duval et al., 1992; Marton et al., 2000). Phase 2, or mega-rafts, formed since the Middle Eocene due to increased sediment load and regional basinward tilt of the margin (Duval et al., 1992; Lundin, 1992; Marton et al., 2000). These rafts are believed to form from an initial fault in which salt rises

upwards and thereby separates the blocks, which both move in downslope direction (Lundin, 1992). Subsequently the salt recedes again and the resulting depression is filled by sediments. Since the seaward raft block is presumably moving seaward faster than the landward block, and the salt is still sinking, the graben between both rafts widens and the sediment fill subsides. At first the subsidence is stronger at the landward side of the graben resulting in a landward expanding sequence in graben filling. Once the salt is completely removed under the landward raft and the graben filling, both weld to pre-salt sediments and the landward subsidence diminishes. Thus any widening of the graben is subsequently accommodated by seaward subsidence of the graben filling while expanding the sequence in seaward direction. In the final stage of the model (Lundin, 1992) the seaward raft also forms a weld to pre-salt sediments and subsidence in the graben ceases. The graben is now filled by a domed sedimentary structure. In the onshore Inner Kwanza Basin and the shallow parts of the Outer Kwanza Basin four grabens have been identified from east to west: Calombaloca, Quenguela, Praia and Western graben. They reach widths of ~15 km (Figure 5.1) and depths of ~3 km (Lundin, 1992; Hudec and Jackson, 2004). Their along slope extent amounts to ~70 km and their terminations correlate with the occurrence of a ENE-WSW trending transfer zones where they merge into the Sangano Graben (S in Figure 5.1A and B) (Lundin, 1992; Hudec and Jackson, 2002; Hudec and Jackson, 2004; Lundin, 1992). Due to uplift in the Paleo- and Neogene the Calombaloca and Quenguela Graben are now situated onshore and together with the Praia trough have reached their final stage of development. Subsidence is still ongoing only at the seaward flank of the Western Graben and the Navalha Block, the raft west of the Western graben is still gliding downslope (Lundin, 1992).

5.3 Water masses and circulation offshore Angola

The Angolan slope down to 1000 m water depth is influenced by four main water masses (Figure 5.1.D), which were also found in CTD casts of M122 (Hebbeln et al., 2016). South Atlantic Subtropical Surface Water (SASSW) is present down to a depth of ~75 m and underlain by South Atlantic Central Water (SACW) which is present in the depth interval from 75 to 500 m. The core of Antarctic Intermediate Water (AAIW) is situated at 700 to 800 m whilst below 1000 m North Atlantic Deep Water (NADW) occurs (Mohrholz et al., 2001). Circulation offshore Angola is dominated by the presence of the cyclonic Angola Gyre, the Angola Current and the Angola Benguela Front (Figure 5.1C) (Gordon and Bosley, 1991; Stramma and England, 1999; Stramma and Schott, 1999). The Angola Benguela Front is detectable as a thermal front in the upper 50 m and in salinity measurements until 200 m at 20° to 18° south (Gordon and Bosley, 1991; Stramma and Schott, 1999). The Angola Current is also restricted to surface water masses (Stramma and England, 1999; Stramma and Schott, 1999). The Angola Gyre however exists as a weakened and southward shifted version in the central water masses (Figure 5.1C) and also below (Gordon and Bosley, 1991; Stramma and England, 1999; Stramma and Schott, 1999).This results in a southward directed current in all water depths in the position of the study area.

5.4 Material and Methods

The data used in this study was collected during *RV Meteor* Cruise M122 ANNA (Hebbeln et. al., 2016). It includes high resolution multibeam bathymetry data acquired with a hull-mounted Kongsberg Simrad EM 710 swath sounding system. Necessary processing steps were carried out on board with the open source software MB systems and the data were gridded to a resolution of 15 m. Furthermore, sub-seafloor structures were imaged using high resolution multichannel seismic (MCS) data. A Sercel Mini-GI gun with a chamber volume of 2 x 0.49 l

was employed as a seismic source and shot every 4.5 seconds. For recording a 120-m long Hydroscience Technologies Inc. (HTI) digital streamer with 96 channels was used. Data processing of the MCS data included CMP-binning to an along track resolution of one meter, static correction, interactive velocity analysis, NMO-correction, bandpass filtering and despiking prior to CMP-stacking. Post-stack white noise reduction and FD migration were carried out. All processing steps were performed using the Vista seismic processing suite (Schlumberger). Horizon and fault picking were performed in the Software Kingdom (IHS Global Inc.).

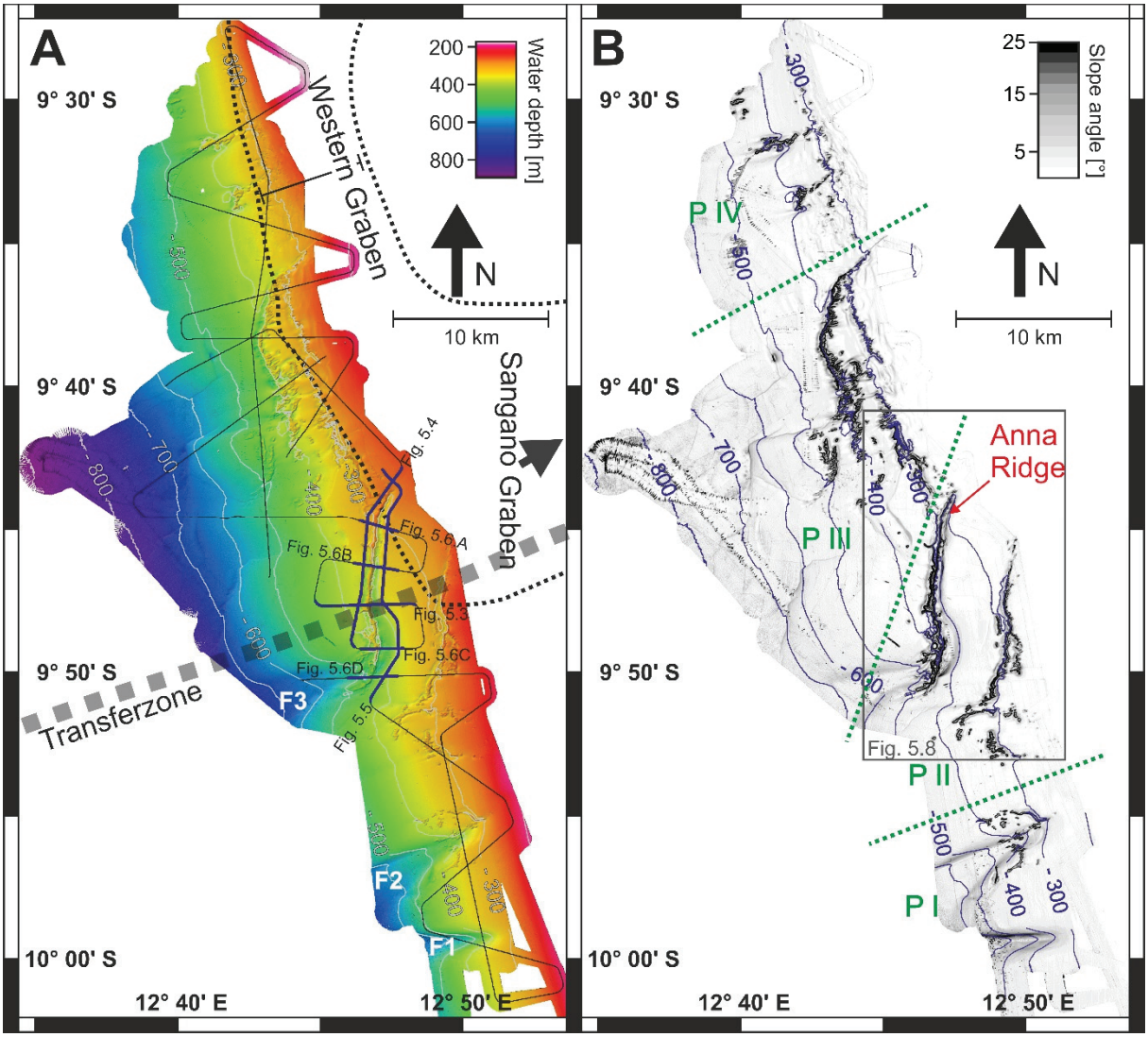

Figure 5.2 – A: Bathymetric map of the working area, showing the location of the multichannel seismic data collected during RV Meteor cruise M122. It covers water depth from 175 to 900 m and mounded structures and ridges occur at the seafloor. It furthermore shows the location of the transferzone and the extensional graben shown in Figure 5.1A. B: Slope angle map of the working area. The area was divided in four provinces (P I – P IV) by different size, shape and orientation of the seafloor structures.

5.5 Results

5.5.1 Bathymetry – Distribution of cold water corals

The working area of *RV Meteor* cruise M122 extends for about 70 km along-slope in water depths from 175 to 900 m offshore Angola (Figure 5.2A). Overall the slope is gently inclined with dips of less than 4° in west southwest direction. The highest slope angles in the working area (Figure 5.2B) are attributed to ridge and mound structures of various shapes and sizes which are usually contoured by depressions at one or both sides (Figure 5.2B). Individual

mounds range in size from less than 100 m to a few kilometres and are mostly of circular or elliptic shape. At some places they cluster to form irregular shapes whilst in other places ridges occur, in which individual mounds are not recognizable (Figure 5.2B). Their occurrence is restricted to water depths shallower than 550 m. Furthermore, in the southern part of the study area, three funnel-shaped depression (F1, F2, F3 from south to north in Figure 5.2B) incise the seafloor in across-slope direction from depths of 300 – 400 m downward. F2 and F3 reach a width of 2.5 km, whilst F1 is narrower with only about 1.5 km width. To provide a better overview over the mound structures they have been grouped in to four provinces (P I – P IV) (Figure 5.2B), which will be described in the following paragraph from south to north.

In P I in the south of the working area, around the head of F1 a few individual mounds and patches as well as two short (<2.5 km) ridges occur. Their heights range from 15 m for the smaller mounds up to more than 50 m for the ridges. P II hosts the most prominent elevated structures in the southern central part of the study area. Two parallel ridge structures strike N-S roughly 5 km apart from each other (Figure 5.2). Thus they are oriented in an acute angle (~ 20°) to the overall slope directions. The eastern ridge extends for 12 km and has a frayed appearance with scattered mounds at its southern end (Figure 5.2). Disregarding the frayed parts the distinct ridge is only ~500 m wide but up to 75 m high. The western ridge was named Anna Ridge during the *RV Meteor cruise M122* for the acronym of the cruise (Hebbeln et. al., 2016). It is almost 14 km long and whilst it is only up to 400 m wide at its northern end, in the south it widens up to 1.5 km. In average it rises up to 100 m over the surrounding seafloor. Compared to its counterpart to the east it has a much smoother and more linear shape while it is only frayed at its southern end where it appears to be slightly bending downslope. The eastern ridge has one wide channel to its west and a narrower and less continuous channel on its eastern side. The western ridge is framed by channels on both sides and from its southern end a wide (1.2 - 3 km) cone shaped depression extends further downslope. As the highest, most linear and most continuous feature this ridge and its underlying geology will be the focus of this study.

In P III further mounds extend from the northern tip of the Anna Ridge in several parallel chains towards north-northwest in along slope orientation. Along the 300 m isobath two separate chains of 7 and 6 km length occur 2 km apart from each other. Near the Anna Ridge, the southern chain forms a winding convoluted morphology. Towards its northern end it becomes more frayed and less coherent. It actually consists of a row of numerous small (100 m wide) mounds which are each elongated up to 300 m in downslope direction. The northern one of the two chains exhibits this morphology along its entire length. Along the 400 m isobaths a longer and wider chain occurs. South of it some scattered mounds, some mound patches and two short ridges occur until a depth of 500 m. Towards the north the chain bends upslope and merges with northern tip of the 300 m isobath chains. Its appearance is frayed in upslope direction and in downslope direction contoured by a channel.

In P IV in the north of the study area in shallow depth numerous very small (~100 m diameter) mounds are distributed in the areas shallower than 350 m water depth. At 400 m depth two larger irregular mound patches occur. One is elongated to more than 1.5 km in along and the other in across slope direction. Some more elongated mounds of shorter height (20 – 30 m) occur in two patches in 500 m depth.

5.5.2 Sedimentary units below and around the Anna Ridge

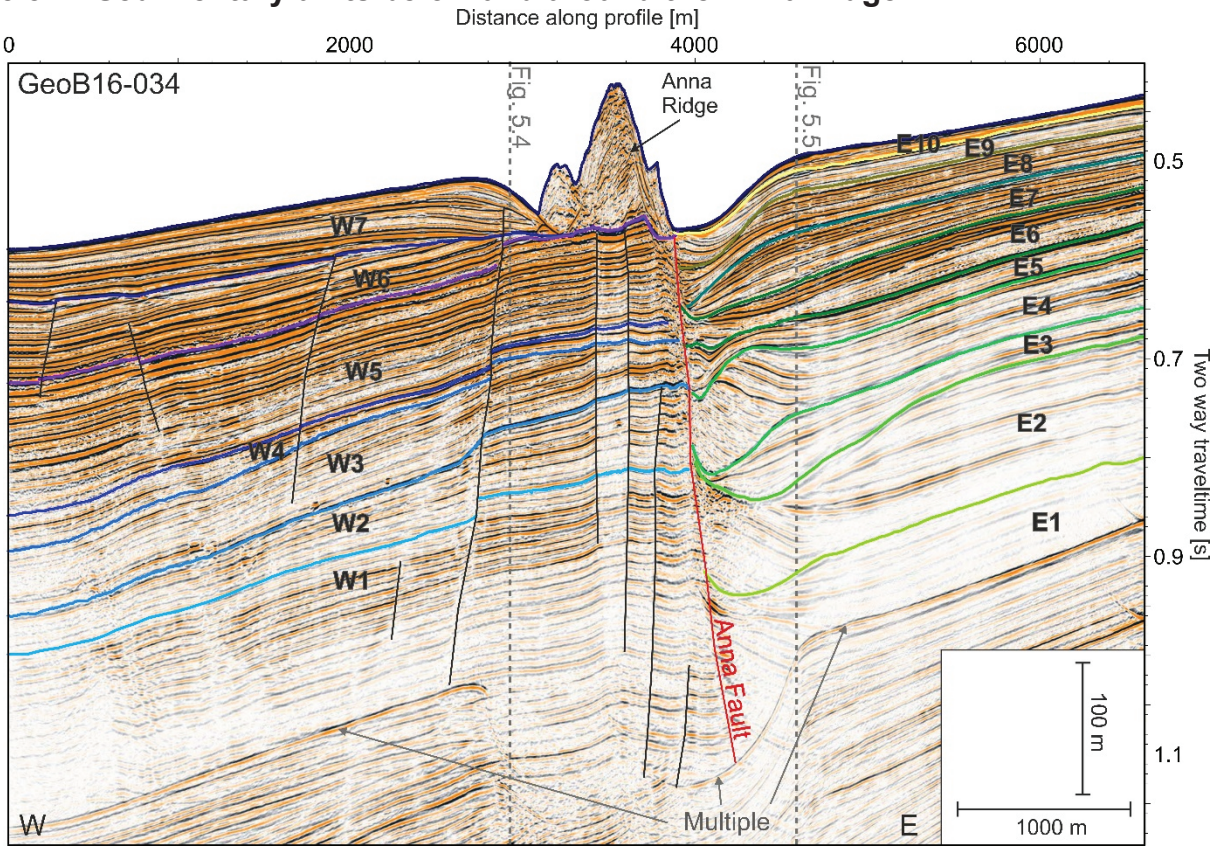

Figure 5.3 – MCS profile GeoB16-034 crossing the Anna Ridge in E-W direction, for location see Figure 5.2. It shows the succession of the Eastern Seismic Units E1 – E10 and the Western Seismic Units W1 – W7. The Anna Ridge appears as contorted to chaotic body.

The Anna Ridge in multichannel seismic data is associated with contorted to chaotic internal reflectors and is situated on an unconformity that truncates underlying reflectors (Figure 5.3). The multichannel seismic data furthermore reveals that the surface expression of the ridge is underlain by a lateral discontinuity and none of the identified seismic units on either side can be traced to the opposite side (Figure 5.3). The lateral discontinuity is here termed Anna Fault. Due to his apparent separation between sedimentary deposits on either side of the Anna Ridge and Anna Fault, seismic units were defined based on their occurrence in relation to the ridge. On the eastern side of the structure ten major seismic units have been identified, which are bounded by local unconformities. They are labelled E1 – E10 from the deepest unit upwards (Figure 5.3). West of the discontinuity, seven different main units occur. They are as well bounded by unconformities and have been named W1 – W7 from bottom up upwards (Figure 5.3, 5.4).

Western Seismic Units (W1-W7)

The western seismic units W1 – W7 are characterized by prevalently parallel to partly subparallel internal reflectors, which are in general highly continuous. Faults occurring throughout the seismic units show offsets of up to 25 ms (Figure 5.3). Reflector spacing and amplitudes are overall variable even within each unit, however, amplitudes are generally increasing from bottom up whilst reflector spacing is only large in the deeper parts of unit W1 and medium to dense further up (Figure 5.3, 5.4). The upper boundary of unit W1 was not detectable in the southern and northern areas of the occurrence of the western units. It is conformable throughout most of the area and apparently dips toward the west in the E-W

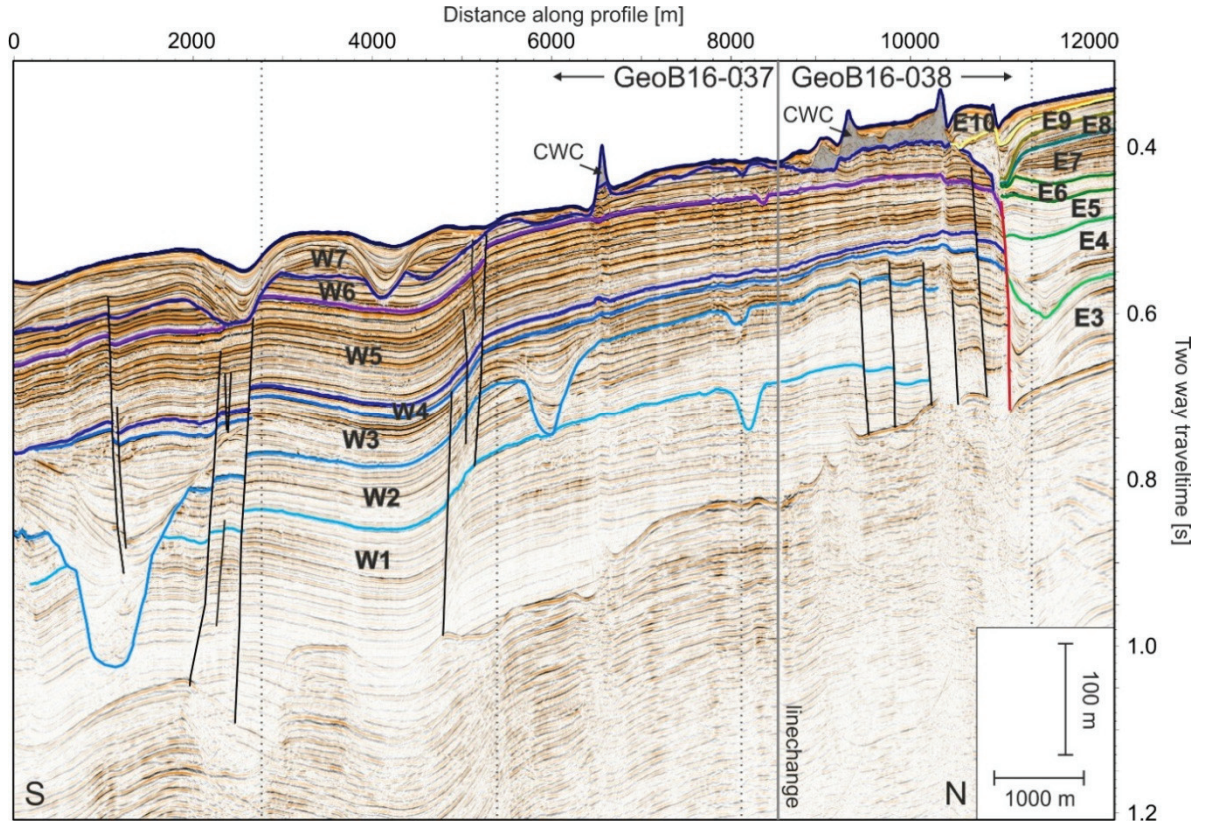

Figure 5.4 - Composite N – S oriented MCS profile west of the Anna Ridge consisting of GeoB16-037 and GeoB16-038. For location see Figure 5.2.This profile shows the Western Units W1 – W7 along the Anna Ridge. At the northern end of the profile the Eastern Units E3 – E10 are visible.

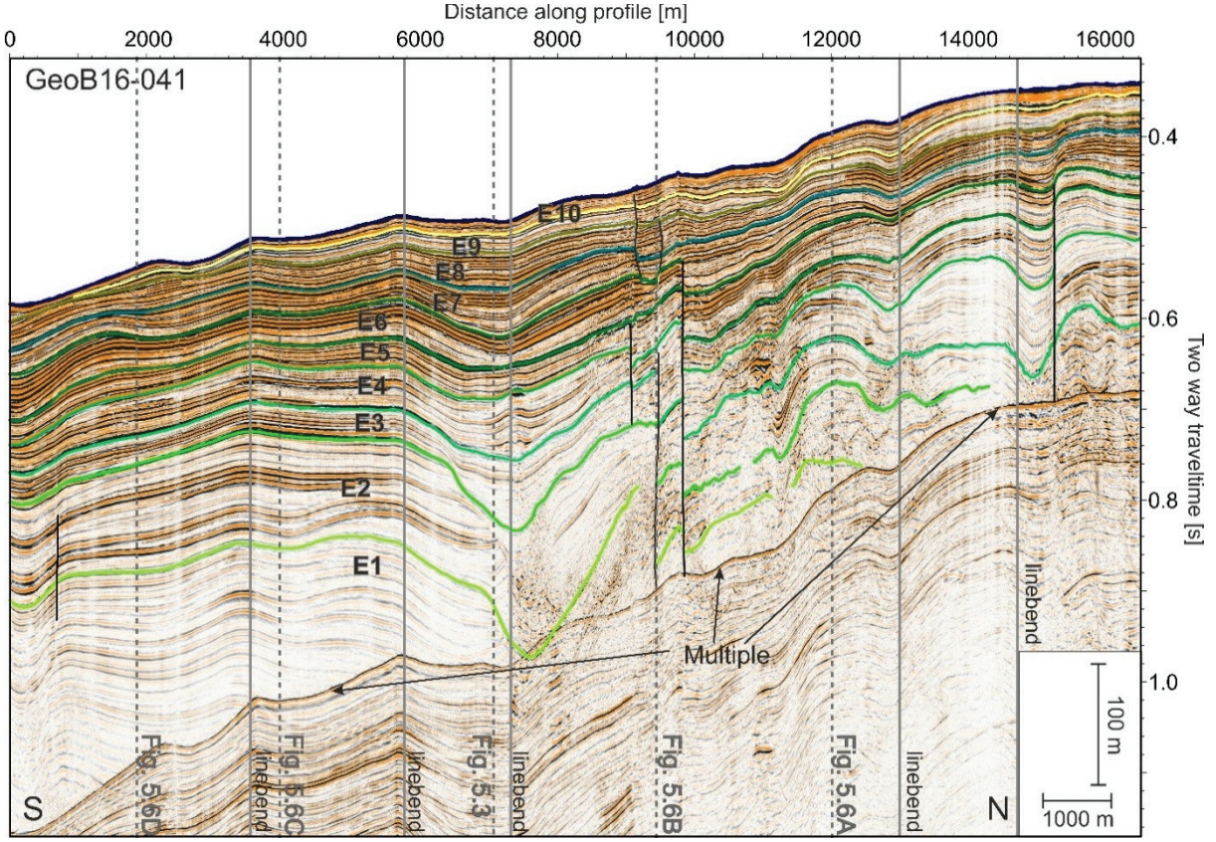

Figure 5.5 - N-S striking MCS profile GeoB16-041 east of the Anna Ridge. For location see Figure 5.2. Profile GeoB16-041 shows the Eastern Units along the Anna Ridge.

striking Profile GeoB16-034 (Figure 5.3). The N-S oriented profiles (Figure 5.4) reveal that the apparent dip changes along the lines, the change in dip direction is accompanied by reflector displacements. Furthermore two U-shaped depressions incise Unit W1 where internal reflectors are truncated at the upper unit boundary. The larger one of these depression in the very south, actually also cuts through the overlying unit W2. W2 appears in the E-W striking profile (Figure 5.3) as a wedge shaped unit converging to the west, therefore the upper boundary is stronger inclined to the west than the lower one. It is affected by the same reflector offsets as the underlying unit W1 and undergoes the same changes in apparent dip along the N-S line (Figure 5.4) whilst maintaining a constant thickness in that direction. Reflectors truncate at the large incision in the south (Figure 5.4). The underlying depression in the north is filled by slightly divergent W2 reflectors. Furthermore, two small incisions occur in the upper boundary of W2, both associated to truncations of W2 reflectors, which are in one case inclined to form wedge shaped subunits which converge with distance from the incision (Figure 5.4). W3 is of roughly constant thickness in E-W direction and apparently dips eastward (Figure 5.3), while reflectors are truncated at the upper boundary in the area under the Anna Ridge. The thickness in the N-S trending line is highly variable since W3 fills all underlying depressions with divergent reflectors (Figure 5.4). In the largest depression in the south several divergent bodies are stacked asymmetrically. W4 is a very thin unit (< 40 ms) which diverges to the west (Figure 5.3) but converges and thins out in the south (Figure 5.4). W4 is overlain by the very thick (70 - 110 ms) Unit W5, which increases in thickness slightly south along Anna Ridge (Figure 5.4) and towards the west (Figure 5.3). Finally unit W6 is characterized by many reflector truncations at its upper boundary. In E-W direction the upper boundary is quite straight and dipping to the west while in N-S direction it is variable with many small incisions. W7 as uppermost unit shows a stark contrast to the underlying strata. In the E-W trending profile it onlaps on the discontinuity separating W6 and W7 on which also the ridge resides (Figure 5.3). It is separated from the ridge by a depression and next to it formed a mounded body, which migrates towards the east. One internal discontinuity associated with reflector truncations can be found in the mounded structure (Figure 5.3). Along the N-S profile further internal discontinuities can be found as well as divergent infilling of underlying depressions (Figure 5.4). Furthermore this unit is hardly affected by any reflector displacements.

Eastern Seismic Units (E1-E10)

The eastern seismic units E1 – E10 follow the trend of strengthening amplitudes and diminishing reflector spacing from bottom up that is observed in the western part. The lowermost unit E1 is characterized by low amplitude widely spaced reflectors. Units E2 – E5 show medium to widely spaced, low amplitude reflectors with occasional occurrences of medium to high amplitude reflectors. The upper units E6 – E10 consist of a mix of low to high amplitude reflectors which are medium to densely spaced (Figs 5.3, 5.5). However they are not only separated from the Western units by the Anna Fault and in the case of W7 the ridge, but their geometry poses a strong contrast to the western units. The internal reflectors of the eastern units are overall subparallel. Most strikingly in Profile GeoB16-034, each Eastern Unit is separated from the Anna Fault by a depression (Figure 5.3). In some units (E2, E4, E8 and E9) internal reflectors truncate at the flank of the depression, in others the depression is the product of converging internal reflectors (E1, E3, E6, E7). Usually the overlying units fill underlying depressions either through inclined onlapping reflectors (E2, E4) or more conformably (E5, E6). The adjacent units may be mounded or slightly divergent (Figure 5.3).

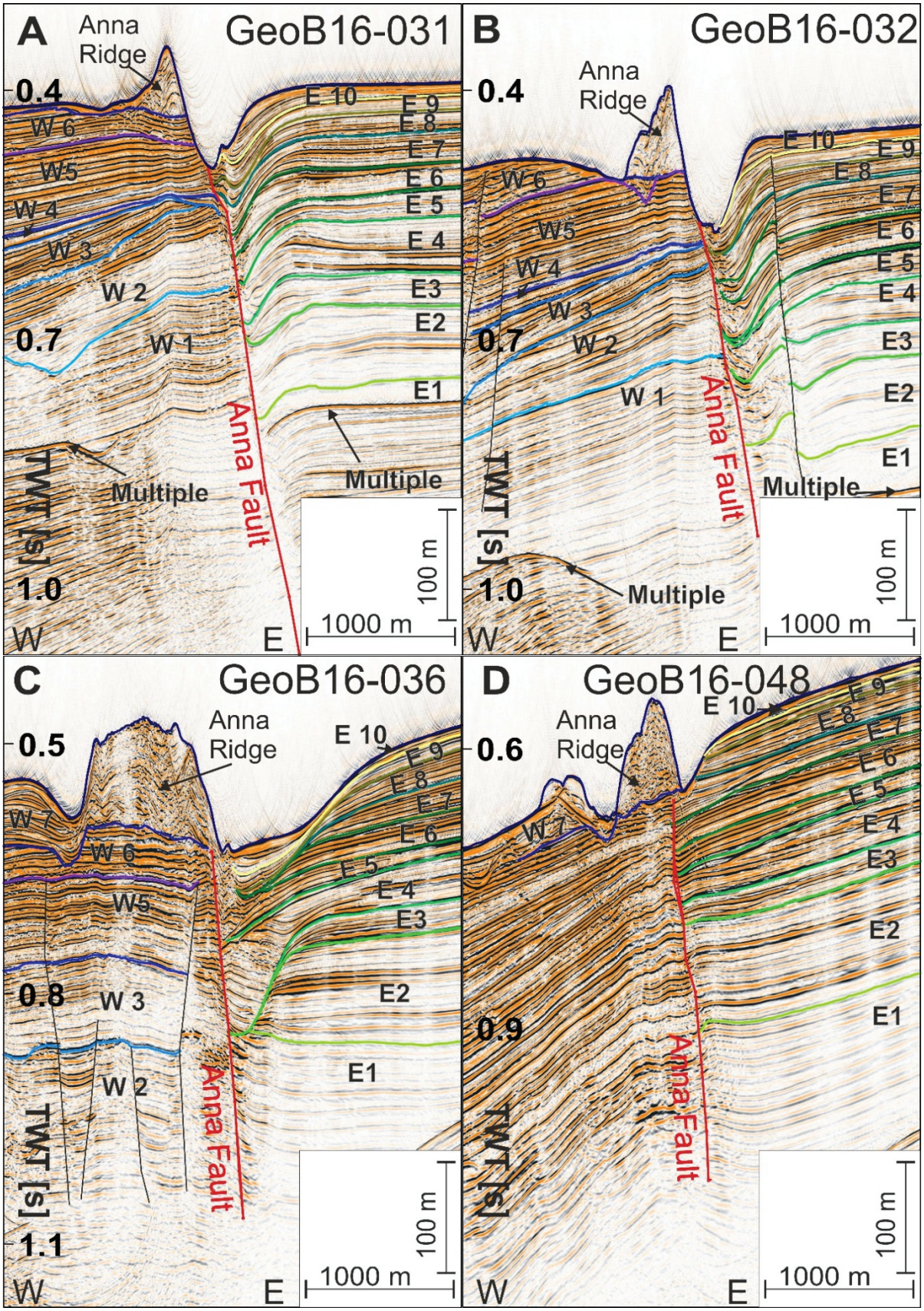

Figure 5.6 - Synthesis of all MCS profiles crossing the Anna Ridge in E-W direction sorted from north to south A and B are situated north of GeoB16-034 (Figure 5.3) and C and D are situated south of it. For exact locations see Figure 5.2.

Comparison of different profiles cutting the Anna Ridge in E-W direction, reveals that the characteristics of the depressions and adjacent reflector geometry, do vary along the Anna Fault (Figure 5.6). In the south (Figure 5.6D) no such depression is observed for the lower units E1 – E3 whilst it exists very subdued in units E4 – E6. One profile further north (Figure 5.6C) unit E1 is not associated with a depression and units E2 and E3 truncate at the flank of one deeply incised depression, which is filled by steeply inclined reflectors of E4, which again truncate at the upper boundary. E5 fills the depression more conformably with a thickness maximum caused by divergent reflectors. Units E6-8 again truncate at the flank of one and the same depression, which then is again covered by units E9 and E10. In the northern two profiles (Figure 5.6A, B) less variation is present as the shape of the depression is very similar in all units and differences are restricted to different degrees of divergence and amount of reflector truncations. Considering all that variation, the only trends which are evident, are on the one hand the lack of depression in the southern deep part of the record, and the decrease in variation in the northern part. Moreover in north south direction (Figure 5.5) all eastern units are continuously present, their thickness is varying slightly and reflector truncations occur in units E1-3 at the flanks of an incision in the southern third of the profile (Figure 5.5) and in E6 associated with a small mounded topography, furthermore they are affected by reflector offsets up to 90 ms for the lowermost unit boundaries diminishing in upward direction (Figure 5.5). In the areas of reflector offsets as well as in a depression in the lowermost unit, chaotic and contorted reflector pattern as well lateral phase reversals occur locally on a scale of around 2 km.

5.6 Discussion

The main aim of this study is to unravel the relationship between the Anna Ridge on the seafloor and the Anna Fault, which separates the eastern seismic units E1 – E10 from the western seismic units W1 – W7. Sampling and ROV observations during *RV Meteor* Cruise M122 confirmed that the ridge structure was built from CWCs prevalently of the species Lophelia Pertusa (Hebbeln et. al., 2016). All seismic profiles crossing the Anna Ridge show it as a chaotic body on top of an erosional surface and in each case reveal the Anna Fault directly under the eastern boundary of the ridge (Figure 5.3, 5.6). A fault-offset cannot be determined across the fault as the reflector pattern in the Eastern and Western Seismic Units are fundamentally different. The depressions and mounded deposits are interpreted as separated mounded drifts. The CWC ridge, contourite drift and the fault thus appear to coincide. In the following, a model that integrates fault activity, contourite deposition and CWC growth will be presented. To clearly distinguish the fault below the Anna Ridge from other faults it will be referred to as Anna Fault.

5.6.1 Structural setting

The location (Figure 5.1) and extent of the Anna Fault suggest that it is part of the boundary between the Navalha block and the Western Graben or the Sangano Graben, as the southwestern-most extent of the salt rafting zone in the Kwanza Basin (Lundin, 1992). Thus, the western units W1 – W6 are associated to the salt raft, the Navalha block, and the eastern units to the graben filling, which is still undergoing subsidence (Lundin, 1992). The orientation of Anna Ridge might be controlled by the transferzone, which bounds the area of raft grabens to the south (Hudec and Jackson, 2002; Hudec and Jackson, 2004; Lundin, 1992) (Figure 5.1). The N-S oriented Anna Fault is not strictly a part of the raft graben, at least in the orientation it was mapped by Hudec and Jackson (2004), but rather represents a south-westward extension of the graben which developed under the influenced of the transfer zone (Figure 5.1). In summary the Navalha Block, bounded locally by the N-S oriented Anna Fault moves

downslope in southwest direction. Whether this movement is associated with a transfer movement along the Anna Fault cannot be evidenced by data of this study. Moreover, for the model presented here, the subsidence associated to the normal fault movement is much more important and since subsidence is reportedly ongoing at the Western Graben (Lundin, 1992) the Anna Fault is likely still active. Thus, accommodation space for the deposition of separated contourite drifts within the graben is currently being created.

5.6.2 Environmental conditions during sediment deposition

The raft block is build up by the seismic units in the west of the Anna Fault (W1-W6) and underlying strata which were not imaged in the MCS data. The western units are either characterized by different degrees of divergence or bounded by erosional discontinuities. Variation in the depositional pattern might be attributed to nature of sediment supply, the creation of accommodation space through subsidence or tilting, whilst erosion was either caused by local uplift, which subjected the seafloor to the forces of wave movement or a stronger influence of bottom currents. These mechanisms in any case occurred on a relatively large spatial scale (> 10s km). Additionally these units underwent faulting under the extensional stress exerted by movement of sediments on the Aptian salt layer (Fort et al., 2004; Hudec and Jackson, 2004; Marton et al., 2000), which is a potential driver for tilting and subsidence. On top of the raft block, the uppermost western unit W7 is interpreted as a separated mounded drift due to its shape and internal reflector geometry (Figure 5.3). It is situated on top of the same erosional discontinuity that the CWC ridge is rooted on but thins out towards the north (Figure 5.3, 5.4, 5.6). Presumably it developed after the corals had grown high enough to focus the bottom current regime, which is generally southeast-ward directed, along the ridge. The eastern part of the sub seafloor is characterized by a vertically stacked sequence of moats and corresponding separated contourite drifts (Figure 5.3). Thus reporting a current core capable of moat winnowing and erosion, which with the prevalently southeast-ward along-slope flowing bottom current regime needed structural guidance to develop in north south orientation. Such guidance, and the major cause for the difference in sediment deposition styles across the Anna Fault might be topography at the seafloor produced by a fault offset, which focuses the local current regime (Rebesco, 2005). In a normal fault, such as the Anna Fault, in locally subsiding parts accommodation space is created. The increase in volume of the water column in that area causes lower current velocities generally favouring deposition of sediment. Since the current is pushed against the foot wall of the fault due to Coriolis veering, it focuses in northward direction and the moat is developed while sediment is deposited as separated mounded drift. On the foot wall anything from reduced deposition over winnowing to erosion might take place. Such a form of interaction of salt-tectonically induced topography at the seafloor and the prevailing current regime in the area causes a distinct change in sedimentation rates east and west of the fault. The reflector truncations of unit W6 reveal that the top of the salt raft is affected by erosion in the area of the western units. Thus, the eastern units are presumably much younger than the western units W1 – W6. Hence the entire system is regarded to be a formerly undescribed setting of a *fault-controlled contouritic depositional system* (Rebseco, 2005; Rebesco et al., 2014). Fault-controlled CDSs are up to now only sparsely described which renders the Anna Fault an important example.

The diverse geometries of moat and contourite deposition east of the Anna Fault documented the activity of the bottom current core, which is focussed along the Anna Fault and the raft block. This core varied temporally during the deposition of units E1 – E10. Since the style of drift and moat observed in the profiles over the Anna Fault differ not only between seismic units, but also spatially within one seismic unit along the fault (Figure 5.6) it is not possible

separate temporal trends from spatial variation in the activity of the current core. Temporal changes which occur similarly along the entire ridge could hint at changes in the background hydrodynamic regime, whilst spatial trends might be attributed to spatial variation in fault movement. However, since they seem to mask one another a contemporaneous occurrence of both processes has to be assumed. Only the absence of a moat in Unit E1 – E3 at the southern part of the fault (Figure 5.6D) indicates a reduced current influence in deeper water at the time of deposition. The fact that reflectors cannot be traced across the Anna Fault even where the bottom currents did not impact sedimentary deposition, indicates that the fault offset exceeds the penetration limit of the seismic data and that the equivalent eastern units to the western deposits must lie deeper than ~400 mbsf. Faults have been observed abundantly throughout the study area (Figure 5.4) and probably originate from the extensional salt-tectonic regime in this part of the Kwanza Basin (Fort et al., 2004; Hudec and Jackson, 2004; Marton et al., 2000). Most faults show minor displacements up to 20 m and reflectors can easily be traced across (Figure 5.3, 5.4, 5.5).

5.6.3 Stratigraphic framework

When it comes to building a stratigraphic framework and amounting for the lateral age difference of units two main questions arise. One is the balance between local subsidence and sedimentation rate and the other is the local variation of sedimentation rate or relation between sedimentation and erosion rate across the fault. As the subsidence of the graben is compensated by ongoing sedimentation, the sedimentation rate must balance the subsidence rate. Spathopoulos (1996) claims that raft grabens in the Kwanza Basin are filled rapidly with sediments. Furthermore, variations in accommodation space were found to have a much larger influence on the amount of sediment deposited than the sediment supply (Rouby et al., 2003). Hudec and Jackson (2004) report ages of 5.33 and 8.3 Ma in the sediments of the Navalha raft block at approximately 75 and 325 mbsf respectively, in a water depth of around 400 m. The location of their findings is situated about 30 km north northwest from the Anna Ridge. Taking the distance and the thickness variation and tilting observed in the Western Units only along 3 km (Figure 5.3) into consideration an adaption of these values to date the sediments of the Western Unit would be unreliable. Nonetheless an estimation that the sediments observed in the Western Units until depth of 800 – 900 mbsf at least reach until the Pliocene but are probably not much older than Late Miocene can be made.

Establishing a stratigraphic framework for all observed units still poses a special challenge since neither sedimentation rates nor the rates of salt-induced subsidence are known. In order to constrain the range of values and eventually get an idea of the amount of time recorded in the sediments, subsidence and sedimentation rates have been integrated from adjacent areas.

Sedimentation rates from neighbouring areas of the study areas are similarly very variable. To exclude samples with influence of sediment supply from the Congo River only sites south of the study area were considered. However, none is closer than 200 km to the study area. One value from a short (10 m) core from a water depth of 3411 m amounts to 4.6 cm/ka (Schneider et al., 1995). Further sedimentation rates are available from the ODP sites 1078 and 1079 in water depth of 427 m and 738 m respectively. They contain long time intervals with peak values up to 60 and 40 cm/ka for the interval from 100 – 260 ka and 100 – 280 ka respectively (Wefer, Berger, Richter et al., 1998a, b).Since sedimentation rates generally decrease with water depth and distance from the coast it may be expected that the depth interval between 200 and 800 m still receives a rather high amount of sediments.

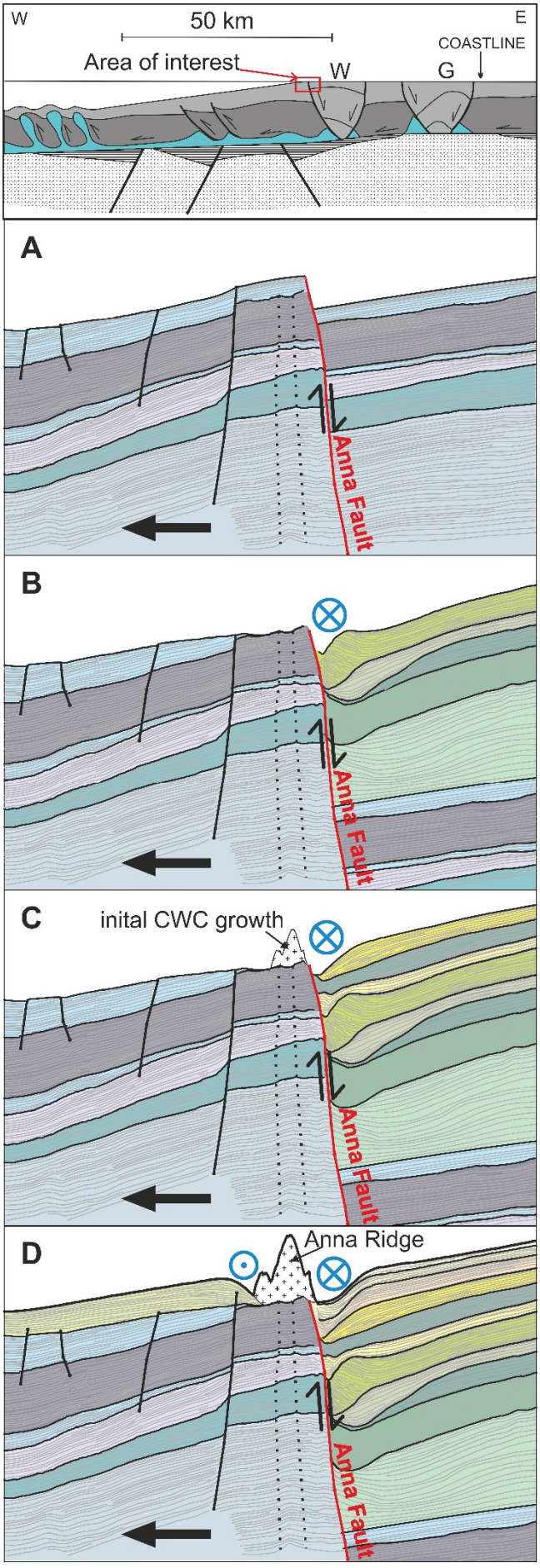

For contouritic sedimentation in general a sedimentation rate higher than 60 cm/ka under calmer current conditions is considered still ordinary (Stow, 2001). All in all, a sedimentation rate of 40 cm/ka would suffice to produce the averagely 400 m thick deposit observed in the graben within the last 1 Myrs. In that case the variation between the ten contouritic sedimentary units in the graben filling would fit to the 100 ka glacial-interglacial cyclicity, which established during the Mid-Pleistocene Transition (Zachos et al., 2001). This would furthermore require that the subsidence of 400 m also took place within 1 Myr. In the Congo-Cabinda Basin subsidence rates have been inferred from accommodation variation and vary between 30 m/Ma to up to 250 m/Ma on short timescales (Rouby et al., 2003). In contrast, subsidence rates for the Western Graben have been calculated from reflector offsets and range from 5.27 to 7.45 m/Ma in an area 50 km north of the Anna Fault (Hudec and Jackson, 2004). However, since the graben and fault there appear as a rollover with extensional faults and not as a raft graben (Hudec and Jackson, 2004) the structural setting is somewhat different. Nonetheless the above mentioned subsidence rate of 400 m/Ma is higher than any of the observed values thus suggesting that, the real age of the lowermost imaged Eastern Unit is first of all older than 1 Myr and furthermore controlled by the subsidence rate. Considering this, the paleoceanographic

Figure 5.7 - Evolutionary model of the Anna Fault as the border between the Navalha Block and the Western Graben. Units on the left (western) side of the Anna Fault belong to the Navalha Block and the Units on the right (east) belong to the sediments filling the western graben. The evolutionary phases include the following steps A: pre-contouritic subsidence phase. B: contouritic deposition in the subsiding graben C: initial CWC growth D: contouritic sedimentation in the subsiding graben and west of the CWCs on the salt raft (modern situation).

variability is seemingly more complex and a better age control is required before the record may be interpreted.

5.6.4 Evolutionary model

The following paragraph should briefly summarize the sequence of processes leading to the build-up of the observed features. In the initial setting of the scenario salt rafting is already in progress (Figure 5.7A). Thus the western graben is formed, the raft block is moving downslope and subsidence in the graben is ongoing. However there is no distinct impact of bottom currents on the sedimentation leading to the roughly horizontal layered units being subsided in the raft graben whilst their counterparts on the raft move downslope. This step basically refers to the strata which are expected to be situated under the penetration limit of the MCS data used in this study. The second model stage represents the onset of bottom currents which interact with the fault offset, erode sediments on the raft and cause the formation of separated mounded contourite drifts in the graben (Figure 5.7B). In a third step after contouritic deposition in the graben has been ongoing whilst on the raft winnowing or erosion prevailed, at some point in time Cold Water Coral growth starts on the erosional surface on top of the raft (Figure 5.7C). West of the CWC winnowing prevails for a while until the CWC mound is high enough to modulate bottom currents sufficiently to cause the build-up of another separated mounded drift on its western side which is captured in the final step of the evolutionary models (Figure 5.7D). Separated mounded drift build-up is active and ongoing in the graben since the second phase.

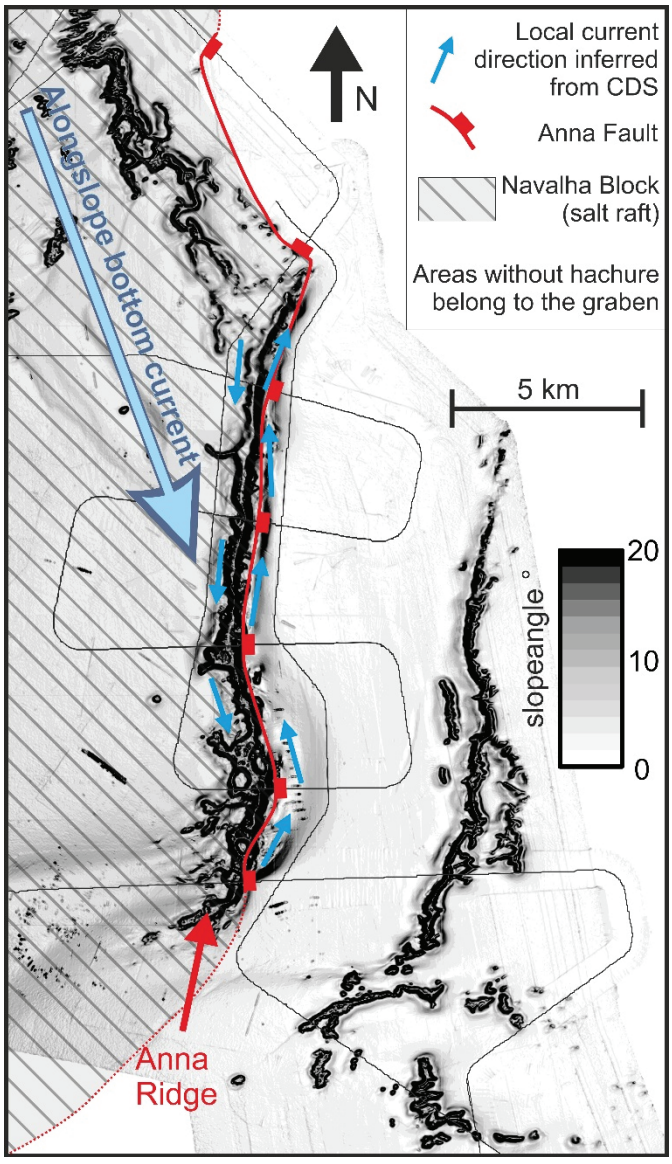

Figure 5.8 - Compilation of tectonic and hydrodynamic processes beneath and around the Anna Ridge. The background is a slopeangle map from. The Anna Fault and extents of the Navahla Block were mapped from the seismic data. The along slope bottom current was drawn parallel to the slope and local current direction follows the small-scale morphologic expression of the drifts.

5.6.5 Position and timing of CWC growth within the fault-controlled CDS

The alignment of the Anna Ridge parallel to the fault-controlled CDS and the salt raft is a new and unique example for the co-occurrence between CDS and CWC mounds. It is still under discussion whether hardground formation, nutrient supply or sediment input is the most important environmental factor for CWC mound formation, it is however well known that all of them are provided under the influence of an enhanced bottom current regime

(Hebbeln et al., 2016). Consequently the focused bottom current along the Anna Fault created a habitable environment for CWCs. Therefore it should have been active before mound formation started. However for the exact timing a better age control for the seismic data together with a good estimate of the erosional periods is required. The formation of the second CDS west of the Anna Ridge in turn is an important example for the capability of biogenic topography to modulate the current regime, and shows that they act as a topographic obstacle analogue to small-scale seamounts.

5.7 Conclusions and outlook

This study outlined the co-occurrence of a fault-controlled CDS and a CWC ridge in water depth between 200 and 600 m. The fault has been identified as the border of a salt raft with its orientation being controlled by the occurrence of a transferzone, which marks the transition from the salt rafting zone to a part of the continental margin where no salt rafting occurs. This unique setting evidences for the first time that significant influence of bottom currents may be involved in the filling of extensional grabens which open in the process of salt-rafting. Variations of contouritic deposition were grouped into ten phases of which the first three only imprinted on shallower water depth. Future studies with a valid stratigraphic framework may reveal whether the recorded variation is linked to paleoceanographic changes, movement at the fault or a mix of both processes.

This study concentrated on the most extreme example of both, faults and CWC mounds. However numerous faults and CWC mounds occur in the working area. To sufficiently constrain environmental factors governing CWC growth, further research is required. An overall correlation of faults, CWC mound and CDS occurrences would provide valuable insight whether the features are linked through a genetic process or simply mutually benefit in some locations. In addition a densely spaced Parasound Echosounder dataset was gathered during *RV Meteor cruise M122.* Analysis of this high resolution dataset would facilitate an assessment of the interplay of CWC mound and CDS growth on much smaller timescales.

Last but not least, the general mechanism of drift building due to current-topography interaction at the border of a raft graben likely also occurred at other raft grabens. Due to the lower resolution of conventional seismic systems these drifts might have been overlooked until today. However since nowadays two raft grabens are situated onshore in Angola, these potentially provide a location to study contourite deposits on land.

Acknowledgments

This study was funded through the DFG-Research Centre/Cluster of Excellence “The Ocean in the Earth System”. We would like to thank Captain Rainer Hammacher and the crew of *R/V Meteor cruise M122* for their excellent work and support.

6 Summary and Conclusion

This thesis tackled the impact of the interplay between bottom currents and seafloor topography on the paleoceanographic record in contourite deposits. Contourites, forming under the influence of topography-current interactions, are highly complex and, thus, the retrieval of paleoceanographic information is not trivial; however, worthwhile as deposits in such extreme conditions react much more sensitive to changes in the ambient hydrodynamic regime. Based on three case studies from two different working areas at the Galicia and Angola continental margins, the understanding of the processes associated with the interaction between topographic features and hydrodynamic regime was significantly advanced. In both areas the spatio-temporal evolution of the deposits was analysed using multichannel seismic and bathymetric data. For the Galicia Margin Parasound echosounder data was utilized in addition.

The first study area at the Galicia Margin presents a setting at the flank of an intraslope basin with a strongly dissected seafloor topography. Topographic obstacles and ridges on the seafloor interact with the hydrodynamic regime, whilst downslope sediment transport is supplied through canyons and gullies. In combination with mass wasting deposits found on other parts of the slope this leads to a sediment distribution which is highly variable in both space and time.

The first study at the Galicia Margin comprises a paleoceanographic reconstruction of the Atlantic circulation as it impacted the area throughout the last 40 Myrs. The impact of different stages of the evolution of Cenozoic Atlantic circulation is for the first time resolved in in this study, thus it fills a gap in the paleoceanographic record. To get a grasp on the relatively long term variation in the overall current regime that affects the area, the sediment distribution in six distinct timespans was evaluated on the basis of thickness maps derived from the analysis of the seismic data. The approach for this study was to unravel the sedimentary processes acting in the working area simultaneously and estimate their contribution to the thickness distribution in the area. To thus identify a hierarchy of processes for each timespan resolved in the reconstruction. The lower boundary of the first of the six phases dates to the Mid-Eocene, revealing a weak background current, which redistributes sediments to the deep basins in the area and inhibiting deposition at the steep middle slope and topographic obstacles. It furthermore is a phase of active downslope transport in which the canyons are characterized through erosion. After the subsidence of the Iceland-Faroe Ridge at 38 Ma, plastered drifts build under the influence of young Northern Component Water, which at that time flew in shallower depth than the modern North Atlantic Deep Water. 14 Ma ago, the eastern end of the Tethys Ocean closed rendering the Tethys a semi-enclosed basin. This presumably led to an outflow of Tethys water to the Atlantic in intermediate depth. At the Galicia Margin this is marked by the onset of drift building associated to topographic obstacles. The Tethys outflow ceased when the basin was fully closed during the Messinian Salinity crisis 5.33 Ma. After the opening of the Strait of Gibraltar and circulation of the Mediterranean Outflow Water the built-up of distinct separated mounded drifts at topographic obstacles started at around 4.5 Ma. The timing is furthermore influenced by the availability of Labrador Sea Water in the study area, as the drift formation is driven by density fronts travelling through the downward deplaced transition zone between MOW and LSW. Ultimately drift formation is driven by the interaction of the density front with the obstacle. Drift formation only occurs during the deglacial shoaling of said transition zone. Further variations in drift construction reflect waxing and waning flow

conditions of MOW which presumably contribute to background flow conditions in the transition zone. From the start of the Pleistocene it grows stronger until the Mid-Pleistocene Transition (~0.7 Ma). This is recorded in the strongest phase of drift formation in the area. After the Mid-Pleistocene transition the MOW strength decreases again, in that phase the contourite buildup is reduced, but sustained. This successful reconstruction not only filled a gap in the paleoceanographic record, but for the first time clearly shows the influence of Cenozoic Atlantic circulation on the Galicia Margin. The same or at least a similar influence can be expected to act on the entire north eastern Atlantic Margin. Furthermore the similarity of the Miocene Tethys outflow to the Plio-Quaternary MOW was found to be distinctly recorded in the drift sediments. Last but not least it provides a good stratigraphic framework for the second study of this thesis and future work.

The second study at the Galicia Margin dealt with a detailed analysis of the topography-bottom-current interaction processes at the different types of topographic features. For that purpose, morpho-sedimentary features in the area were mapped based on bathymetric, and a dense net of multichannel seismic data, complemented by Parasound echosounder profiles. Different types of topographic features such as topographic obstacles, canyons and ridges were classified and the products of their interaction with the hydrodynamic regime identified. The analysis showed, that topographic obstacles in a specific water depth interval are associated with separated mounded drifts. A deeper lying obstacle however, does not have a drift deposit. Furthermore, the variation in the separated mounded drift around the largest obstacle showed that the current detaches from the obstacle at smaller protrusions in the obstacle shape. Eddy shedding, mainly caused by short term hydrodynamic processes such as internal waves interacting with the obstacles, was interpreted to be responsible for the formation of an extraordinary arrangement of sediment waves, which exhibit crossing crests in the lee side of the largest topographic obstacle. Additional sediment waves, locally occurring on one of the ridges, are aligned perpendicular to the contours lines which the current was expected to follow, while irregularities in underlying topography lead to a relatively irregular spacing of the wave crests. Additionally, a unique example of a multi-crested drift is found on top of another topographic obstacle. It comprises several elongated mounded drifts, which are separated from each other by zones of winnowing and erosion. The distribution of the drifts is controlled by the underlying topography, which splits the bottom current in several current cores. The dominant control of topography on the shape of drifts and, moreover, the lack of distinct drift morphologies in the areas of rather gentle slopes, indicate that at the Galicia Margin, the interaction of the bottom currents with topography are a prerequisite for drift build-up and underlines the exemplary character of this margin for these processes.

The second study area is situated at the shallow Angola Margin, which is strongly influenced by salt rafting. The study focused on one particularly peculiar fault situated beneath a Cold Water Coral ridge at the seafloor. It was shown to be an, up to now, undescribed form of a fault-controlled contouritic depositional system. Seismic facies analysis showed that east of the fault a sequence of separated mounded drifts is developed, whilst the units west of the fault do not reveal a considerable current influence in their genesis. The structural analysis revealed, that the fault is the border between a salt raft and a sediment filled graben and interacts with the bottom current regime in the way that the fault offset at the seafloor focuses the bottom current. Since salt rafting is still ongoing, the extension causes the sediments in the graben to subside, creating accommodation space. This accommodation space is filled under the influence of the focused bottom current resulting in a drift deposit which his separated from

the fault by a moat. In the data presented in this study an up to 400 m thick deposit of contouritic sediments was discovered, indicating that the interaction process is active for more than 1 Myr. The whole system, as a new and unique setting for a fault controlled drift, furthermore implies that contouritic activity might be a common and up until now overlooked process when it comes to the filling of extensional grabens formed by salt rafting. Moreover the position of the Cold Water Corals along the fault on its western side implies that fault controlled drifts are able to provide a suitable habitat for CWC. It is known that CWC prefer locations influenced by highly energetic bottom currents. Thus the ability of the fault to focus the bottom current, which is most likely linked to its offset, can be seen as seen as the initial provider of a suitable habitat for the CWC. However a second drift, which developed west of the corals overlying the same discontinuity on which the corals grow, shows that the morphology of the corals is just as well capable of modulating the bottom current regime.

Both study areas presented in this thesis combined, provide a multitude of examples for different kinds of topographies, which through interaction with the bottom currents lead to the build-up of contouritic drifts. The second study at the Galicia Margin showed, that the drift size corresponds to the obstacle size at least in along slope or along flow direction. At the fault related drift in Angola this cannot be tested since the data do not cover an end of the fault. The depressions, which contour the CWC structures moreover confirm, that erosion and winnowing as processes leading to the formation of the moat are restricted to the extents of the topographic obstacle. This shows that without the presence of topographic obstacles, cold water coral mounds or faults deforming the seafloor, the contourites would deposit in the form of sheeted drifts without a specific morphologic expression.

In terms of geologic setting, this project regarded two very different examples of passive margins. Tectonic activity at the Galicia Margin is restricted to the rifting phase which concluded in the Cretaceous, and reactivation of faults during the Pyrenean and Betic orogenies. However, in combination with relatively low sedimentation rates at the Galicia Margin no tectonic deformation is recorded in synsedimentary fashion since the Eocene. Thus the topography is considered to be unchanging. On the other hand, in the Angola working area, high sedimentation rates and ongoing active salt-tectonism lead to a setting in which displacement and sedimentary filling act on the same timescales. Thus growth faults influenced by contour currents induce extremely complex sedimentation pattern, in which it is difficult to extract paleoceanographic information. However, comparison of these two representative regional examples for interaction with a static and dynamic topography reveals that the separated mounded drifts build in both, only the dynamic topography induces further variation in the temporal evolution of the deposit.

Our comprehension of the interaction of the hydrodynamic regime with the adjacent topography is constantly improving by means of hydrodynamic models. Also, despite the fact most examples are very complex, the understanding of the impact of the interaction products on the sediment depositional pattern has advanced during the past decades. However, site-specific hydrodynamic models have been proven to be suitable to unravel even very complex interaction processes (e.g. Hanebuth et al., 2015 and Zhang et al., 2016). An important task for future research is to compare the very specific models and conceptual models, which often only apply one interaction mechanism. Such a comparison would make it possible to rank processes by their impact on the sedimentary archive, so that on the one hand the work intensive process of site-specific modelling would not always be necessary and, furthermore,

the record of ancient contourites might be interpreted although some input parameters for a model are not known.

Furthermore, the data in this thesis have proven to be capable to resolve temporal variation of deposits on sub-myr timescales, with high-resolution data such as the available Parasound Echosounder data, variations on shorter timescales is accessible. Especially when it comes to resolve rapidly changing processes or even single mass transport events these data hold a huge potential which should be exploited in the future.

Acknowledgments

First of all, I would like to thank Volkhard Spieß for giving me the opportunity to carry out this work and beyond that, providing numerous opportunities for me to broaden my horizon. Special thanks goes to him and to Tilmann Schwenk, without whose day to day patient advice and support on any arising issue, this work would not have been possible.
I furthermore would like to thank David Van Rooij for agreeing to review this thesis and for enthusiastic discussions in Nagoya, Capetown and Bremen.
More special thanks goes to my thesis committee, Till Hanebuth, Javier Hernández-Molina and Hendrik Lantzsch for stimulating discussions, valuable input, constant interest in my work and open ears at any time.
Many thanks goes also to Tim Daskevic, who supported this project as a student assistant.The work in Bremen would not be the same without the members of the MTU working group (including the ones who left us already to work somewhere else): Hanno Keil, Luisa Palamenghi, Noémi Fekete, Benedikt Weiss, Lena Steinmann, Aisgo Oguro, Carlos Ramos, Florian Meier, Helga Reinermann, Anna Reusch, Asli Özmaral, Zsuzsanna Tóth, Fenna Bergmann, Nora Schulze and Stefan Wenau, thank you all for scientific and technic help on numerous occasions, coffee breaks, streamer repair sessions, the occasional beer and so on…. all this has made my PhD time a lasting experience.
And although they are included in the already mentioned or following groups of people I would like to especially thank Lena, Julia and Julian, who were present and calmed my nerves throughout the final phase.
More thanks goes to all my friends within and without of FB5, thank you for being supportive and understanding of my work but also for keeping an eye out that I do get an occasional beer or a few days of holidays.
Last and most importantly I want to greatly thank my Family, especially my parents, my sister with her small family and Julian, for giving me the confidence that there are always open ears and arms waiting for me.

List of Figures

List of Tables

References

Ala, M.A., Selley, R.C., 1997. Chapter 8 The West African Coastal Basins. Sedimentary Basins of the World 3, 173-186.

Baringer, M.O.N., Price, J.F., 1997. Mixing and Spreading of the Mediterranean Outflow. Journal of Physical Oceanography 27, 1654-1677.

Batteen, M. L., Martinho, A. S., Miller, H. A., and McClean, J. L., 2007, A process-oriented modelling study of the coastal Canary and Iberian Current system: Ocean Modelling, v. 18, no. 1, p. 1-36.

Bell, D. B., Jung, S. J. A., Kroon, D., Hodell, D. A., Lourens, L. J., and Raymo, M. E., 2015, Atlantic Deep-water Response to the Early Pliocene Shoaling of the Central American Seaway: Scientific Reports, v. 5, p. 12252.

Bender, V. B., Hanebuth, T. J. J., Mena, A., Baumann, K.-H., Francés, G., and von Dobeneck, T., 2012, Control of sediment supply, palaeoceanography and morphology on late Quaternary sediment dynamics at the Galician continental slope: Geo-Marine Letters, v. 32, no. 4, p. 313-335.

Boillot, G., Auxietre, J.-L., Dunand, J.-P., Dupeuble, P.-A., and Mauffret, A., 1979, The Northwestern Iberian Margin: A Cretaceous Passive Margin Deformed During Eocene, Deep Drilling Results in the Atlantic Ocean: Continental Margins and Paleoenvironment, American Geophysical Union, p. 138-153.

Boyer, D. L., and Zhang, X., 1990, Motion of Oscillatory Currents Past Isolated Topography: Journal of Physical Oceanography, v. 20, no. 9, p. 1425-1448.

Brune, S., Heine, C., Clift, P. D., and Pérez-Gussinyé, M., 2017, Rifted margin architecture and crustal rheology: Reviewing Iberia-Newfoundland, Central South Atlantic, and South China Sea: Marine and Petroleum Geology, v. 79, p. 257-281.

Ceramicola, S., Rebesco, M., De Batist, M., Khlystov, O., 2001. Seismic evidence of small-scale lacustrine drifts in Lake Baikal (Russia). Marine Geophysical Researches 22, 445-464.

Cramez, C., Jackson, M.P.A., 2000. Superposed deformation straddling the continental-oceanic transition in deep-water Angola. Marine and Petroleum Geology 17, 1095-1109.

Davies, R., Cartwright, J., Pike, J., and Line, C., 2001, Early Oligocene initiation of North Atlantic Deep Water formation: Nature, v. 410, no. 6831, p. 917-920.

De Mol, B., Van Rensbergen, P., Pillen, S., Van Herreweghe, K., Van Rooij, D., McDonnell, A., Huvenne, V., Ivanov, M., Swennen, R., Henriet, J.P., 2002. Large deep-water coral banks in the Porcupine Basin, southwest of Ireland. Marine Geology 188, 193-231.

Dias, J. M. A., Gonzalez, R., Garcia, C., and Diaz-del-Rio, V., 2002a, Sediment distribution patterns on the Galicia-Minho continental shelf: Progress in Oceanography, v. 52, no. 2–4, p. 215-231.

Dias, J. M. A., Jouanneau, J. M., Gonzalez, R., Araújo, M. F., Drago, T., Garcia, C., Oliveira, A., Rodrigues, A., Vitorino, J., and Weber, O., 2002b, Present day sedimentary processes on the northern Iberian shelf: Progress in Oceanography, v. 52, no. 2–4, p. 249-259.

Duque-Caro, H., 1990, Neogene stratigraphy, paleoceanography and paleobiogeography in northwest South America and the evolution of the Panama seaway: Palaeogeography, Palaeoclimatology, Palaeoecology, v. 77, no. 3, p. 203-234.

Duval, B., Cramez, C., Jackson, M.P.A., 1992. Raft tectonics in the Kwanza Basin, Angola. Marine and Petroleum Geology 9, 389-404.

Ercilla, G., García-Gil, S., Estrada, F., Gràcia, E., Vizcaino, A., Váquez, J. T., Díaz, S., Vilas, F., Casas, D., Alonso, B., Dañobeitia, J., and Farran, M., 2008, High-resolution seismic stratigraphy of the Galicia Bank Region and neighbouring abyssal plains (NW Iberian continental margin): Marine Geology, v. 249, no. 1–2, p. 108-127.

Falcini, F., Martorelli, E., Chiocci, F.L., Salusti, E., 2016. A general theory for the effect of local topographic unevenness on contourite deposition around marine capes: An inverse problem applied to the Italian continental margin (Cape Suvero). Marine Geology 378, 74-80.

Faugères, J.-C., Stow, D. A. V., Imbert, P., and Viana, A., 1999, Seismic features diagnostic of contourite drifts: Marine Geology, v. 162, p. 38.

Faugères, J. C., and Stow, D. A. V., 2008, Chapter 14 Contourite Drifts: Nature, Evolution and Controls, *in* Rebesco, M., and Camerlenghi, A., eds., Developments in Sedimentology, Volume Volume 60, Elsevier, p. 257-288.

Fiúza, A. F. G., Hamann, M., Ambar, I., Díaz del Río, G., Gonzaléz, N., and Cabanas, J. M., 1998, Water masses and their circulation off western Iberia during May 1993: Deep Sea Research Part I: Oceanographic Research Papers, v. 45, no. 7, p. 1127-1160.

Fort, X., Brun, J.-P., Chauvel, F., 2004. Salt tectonics on the Angolan margin, synsedimentary deformation processes. AAPG Bulletin 88, 1523-1544.

García, M., Hernández-Molina, F.J., Llave, E., Stow, D.A.V., León, R., Fernández-Puga, M.C., Diaz del Río, V., Somoza, L., 2009. Contourite erosive features caused by the Mediterranean Outflow Water in the Gulf of Cadiz: Quaternary tectonic and oceanographic implications. Marine Geology 257, 24-40.

Gordon, A.L., Bosley, K.T., 1991. Cyclonic gyre in the tropical South Atlantic. Deep Sea Research Part A. Oceanographic Research Papers 38, S323-S343.

Groupe Galice, 1979. The continental margin off Galicia and Portugal: acoustical stratigraphy, dredge stratigraphy and structural evolution. In: J.C. Sibuet, W.B.F. Ryan et al., Init. DSDP, 47 (2):663-662.

Guiraud, R., Maurin, J.-C., 1992. Early Cretaceous rifts of Western and Central Africa: an overview. Tectonophysics 213, 153-168.

Hanebuth TJJ, Alekseev W, Andrade Grande A, Baasch B, Baumann K-H, Behrens P, Bender VB, von Dobeneck T, dos S. Marques AI, Frederichs Th, Haberkorn J, Hangen J, Hilgenfeldt Chr, Just J, Kockisch B, Lantzsch H, Lenhart A, Lipke A, Lobo Sánchez FJ, Mena Rodríguez A, Müller H, Petrovic A, Rodríguez Germade I, Roud S, Schwab A, Schwenk T, Voigt I, Wenau S (2012). Cruise Report and Preliminary Results RV METEOR Cruise M84 / 4 GALIOMAR III, Vigo – Vigo (Spain), May 1 – 28, 2011. Berichte, Fachbereich Geowissenschaften, Universität Bremen, 283: 139 pp.

Hanebuth T, Bender V, Bujan S, Elvert M, Frederichs T, Kockisch B, Krastel-Gudegast S, Lantzsch H, Rodríguez AM, Schmidt F, Strozyk F, Wagner-Friedrichs M (2007). Report and First Results of the POSEIDON Cruise 342 GALIOMAR – Galician Ocean Margin Expedition, Vigo (Spain) – Lisboa (Portugal), Aug 19 – Sept 06, 2006. Berichte, Fachbereich Geowissenschaften, Universität Bremen, 255: 203 pp.

Hanebuth, T. J. J., Zhang, W., Hofmann, A. L., Löwemark, L. A., and Schwenk, T., 2015, Oceanic density fronts steering bottom-current induced sedimentation deduced from a 50 ka contourite-drift record and numerical modeling (off NW Spain): Quaternary Science Reviews, v. 112, p. 207-225.

Haug, G. H., and Tiedemann, R., 1998, Effect of the formation of the Isthmus of Panama on Atlantic Ocean thermohaline circulation: Nature, v. 393, no. 6686, p. 673-676.

Hebbeln, D., Samankassou, E., 2015. Where did ancient carbonate mounds grow — In bathyal depths or in shallow shelf waters? Earth-Science Reviews 145, 56-65.

Hebbeln, D., Van Rooij, D., Wienberg, C., 2016. Good neighbours shaped by vigorous currents: Cold-water coral mounds and contourites in the North Atlantic. Marine Geology 378, 171-185.

Hebbeln D, Wienberg C, Bender M, Bergmann F, Dehning K, Dullo C, Eichstädter R, Flöter S, Freiwald A, Gori A, Haberkern J, Hoffmann L, Mendes João F, Lavaleye M, Leymann T, Matsuyama K, Meyer-Schack B, Mienis F, Bernardo Moçambique I, Nowald N, Saco del Valle CO, Ramos Cordova C, Saturov D, Seiter C, Titschack J, Vittori V, Wefing A, Wilsenack M, Wintersteller P (2017) Cruise Report and Preliminary Results RV METEOR Cruise M122 ANNA - Cold-Water Coral Ecosystems off Angola and Namibia. Cruise, Walvis Bay – Walvis Bay (Namibia), December 30, 2015 – January 31, 2016. Meteor-Berichte/Reports, M122, 66pp, DFG-Senatskomission für Ozeanographie. 2017 doi:10.2312/cr_m122.

Heezen, B.C., Hollister, C., 1964. Deep-sea current evidence from abyssal sediments. Marine Geology 1, 34.

Heezen, B.C., Hollister, C.D., Ruddiman, W.F., 1966. Shaping of the Continental Rise by Deep Geostrophic Contour Currents. Science 152, 502-508.

Hernández-Molina, F. J., Larter, R. D., Rebesco, M., and Maldonado, A., 2006, Miocene reversal of bottom water flow along the Pacific Margin of the Antarctic Peninsula: Stratigraphic evidence from a contourite sedimentary tail: Marine Geology, v. 228, no. 1–4, p. 93-116.

Hernández-Molina, F.J., Llave, E., Stow, D.A.V., 2008a. Chapter 19 Continental Slope Contourites, in: Rebesco, M., Camerlenghi, A. (Eds.), Developments in Sedimentology. Elsevier, pp. 379-408.

Hernández-Molina, F. J., Maldonado, A., and Stow, D. A. V., 2008b, Chapter 18 Abyssal Plain Contourites, *in* Rebesco, M., and Camerlenghi, A., eds., Developments in Sedimentology, Volume Volume 60, Elsevier, p. 345-378.

Hernández-Molina, F.J., Paterlini, M., Violante, R., Marshall, P., de Isasi, M., Somoza, L., Rebesco, M., 2009. Contourite depositional system on the Argentine Slope: An exceptional record of the influence of Antarctic water masses. Geology 37, 507-510.

Hernández-Molina, F. J., Serra, N., Stow, D. A. V., Llave, E., Ercilla, G., and Rooij, D., 2011, Along-slope oceanographic processes and sedimentary products around the Iberian margin: Geo-Marine Letters, v. 31, no. 5-6, p. 315-341.

Hernández-Molina, F. J., Stow, D. A. V., Alvarez-Zarikian, C. A., Acton, G., Bahr, A., Balestra, B., Ducassou, E., Flood, R., Flores, J.-A., Furota, S., Grunert, P., Hodell, D., Jimenez-Espejo, F., Kim, J. K., Krissek, L., Kuroda, J., Li, B., Llave, E., Lofi, J., Lourens, L., Miller, M., Nanayama, F., Nishida, N., Richter, C., Roque, C., Pereira, H., Sanchez Goñi, M. F., Sierro, F. J., Singh, A. D., Sloss, C., Takashimizu, Y., Tzanova, A., Voelker, A., Williams, T., and Xuan, C., 2014, Onset of Mediterranean outflow into the North Atlantic: Science, v. 344, no. 6189, p. 1244-1250.

Hernández-Molina, F. J., Wåhlin, A., Bruno, M., Ercilla, G., Llave, E., Serra, N., Rosón, G., Puig, P., Rebesco, M., Van Rooij, D., Roque, D., González-Pola, C., Sánchez, F., Gómez, M., Preu, B., Schwenk, T., Hanebuth, T. J. J., Sánchez Leal, R. F., García-Lafuente, J., Brackenridge, R. E., Juan, C., Stow, D. A. V., and Sánchez-González, J. M., 2016, Oceanographic processes and morphosedimentary products along the Iberian margins: A new multidisciplinary approach: Marine Geology, v. 378, p. 127-156.

Hohbein, M. W., Sexton, P. F., and Cartwright, J. A., 2012, Onset of North Atlantic Deep Water production coincident with inception of the Cenozoic global cooling trend: Geology, v. 40, no. 3, p. 255-258.

Hudec, M.R., Jackson, M.P.A., 2002. Structural segmentation, inversion, and salt tectonics on a passive margin: Evolution of the Inner Kwanza Basin, Angola. Geological Society of America Bulletin 114, 1222-1244.

Hudec, M.R., Jackson, M.P.A., 2004. Regional restoration across the Kwanza Basin, Angola: Salt tectonics triggered by repeated uplift of a metastable passive margin. AAPG Bulletin 88, 971-990.

Knutz, P. C., 2008, Chapter 24 Palaeoceanographic Significance of Contourite Drifts, *in* Rebesco, M., and Camerlenghi, A., eds., Developments in Sedimentology, Volume Volume 60, Elsevier, p. 511-535.

Kouwenhoven, T. J., and van der Zwaan, G. J., 2006, A reconstruction of late Miocene Mediterranean circulation patterns using benthic foraminifera: Palaeogeography, Palaeoclimatology, Palaeoecology, v. 238, no. 1–4, p. 373-385.

Kukla, P.A., Strozyk, F., Mohriak, W.U., 2017. South Atlantic salt basins – Witnesses of complex passive margin evolution. Gondwana Research.Lantzsch, H., Hanebuth, T. J. J., and Bender, V. B., 2009, Holocene evolution of mud depocentres on a high-energy, low-accumulation shelf (NW Iberia): Quaternary Research, v. 72, no. 3, p. 325-336.

Lantzsch, H., Hanebuth, T. J. J., Bender, V. B., and Krastel, S., 2009, Sedimentary architecture of a low-accumulation shelf since the Late Pleistocene (NW Iberia): Marine Geology, v. 259, no. 1–4, p. 47-58.

Lantzsch, H., Hanebuth, T. J. J., and Henrich, R., 2010, Sediment recycling and adjustment of deposition during deglacial drowning of a low-accumulation shelf (NW Iberia): Continental Shelf Research, v. 30, no. 15, p. 1665-1679.

Lantzsch, H., Hanebuth, T.J.J., Horry, J., Grave, M., Rebesco, M., Schwenk, T., 2017. Deglacial to Holocene history of ice-sheet retreat and bottom current strength on the western Barents Sea shelf. Quaternary Science Reviews 173, 40-57.

Lavier, L.L., Steckler, M.S., Brigaud, F., 2001. Climatic and tectonic control on the Cenozoic evolution of the West African margin. Marine Geology 178, 63-80.

Lee, H. J., Locat, J., Desgagnés, P., Parsons, J. D., McAdoo, B. G., Orange, D. L., Puig, P., Wong, F. L., Dartnell, P., and Boulanger, E., 2007, Submarine Mass Movements on Continental Margins, Continental Margin Sedimentation, Blackwell Publishing Ltd., p. 213-274.

Lee, H. J., Syvitski, J. P. M., Parker, G., Orange, D., Locat, J., Hutton, E. W. H., and Imran, J., 2002, Distinguishing sediment waves from slope failure deposits: field examples, including the 'Humboldt slide', and modelling results: Marine Geology, v. 192, no. 1–3, p. 79-104.

Lundin, E.R., 1992. Thin-skinned extensional tectonics on a salt detachment, northern Kwanza Basin, Angola. Marine and Petroleum Geology 9, 405-411.

Marton, G.L., Tari, G.C., Lehmann, C.T., 2000. Evolution of the Angolan Passive Margin, West Africa, With Emphasis on Post-Salt Structural Styles, Atlantic Rifts and Continental Margins. American Geophysical Union, pp. 129-149.

Martorelli, E., Falcini, F., Salusti, E., Chiocci, F.L., 2010. Analysis and modeling of contourite drifts and contour currents off promontories in the Italian Seas (Mediterranean Sea). Marine Geology 278, 19-30.

McCave, I. N., and Hall, I. R., 2002, Turbidity of waters over the Northwest Iberian continental margin: Progress in Oceanography, v. 52, no. 2-4, p. 299-313.

McGinnis, J.P., Driscoll, N.W., Karner, G.D., Brumbaugh, W.D., Cameron, N., 1993. Flexural response of passive margins to deep-sea erosion and slope retreat: Implications for relative sea-level change. Geology 21, 893-896.

Mohrholz, V., Schmidt, M., Lutjeharms, J.R.E., 2001. The hydrography and dynamics of the Angola-Benguela Frontal Zone and environment in April 1999 : BENEFIT Marine Science, pp. p.199-208.

Muñoz, A., Acosta, J., and Uchupi, E., 2003, Cenozoic tectonics on the Galicia margin, northwest Spain: Geo-Marine Letters, v. 23, no. 1, p. 72-80.

Murillas, J., Mougenot, D., Boulot, G., Comas, M. C., Banda, E., and Mauffret, A., 1990, Structure and evolution of the Galicia Interior Basin (Atlantic western Iberian continental margin): Tectonophysics, v. 184, no. 3–4, p. 297-319.

Newkirk, D. R., and Martin, E. E., 2009, Circulation through the Central American Seaway during the Miocene carbonate crash: Geology, v. 37, no. 1, p. 87-90.

Nielsen, T., Knutz, P.C., Kuijpers, A., 2008. Chapter 16 Seismic Expression of Contourite Depositional systems, in: Rebesco, M., Camerlenghi, A. (Eds.), Developments in Sedimentology. Elsevier, pp. 301-321.

Nisancioglu, K. H., Raymo, M. E., and Stone, P. H., 2003, Reorganization of Miocene deep water circulation in response to the shoaling of the Central American Seaway: Paleoceanography, v. 18, no. 1.

Oberle, F. K. J., Hanebuth, T. J. J., Baasch, B., and Schwenk, T., 2014a, Volumetric budget calculation of sediment and carbon storage and export for a late Holocene mid-shelf mudbelt system (NW Iberia): Continental Shelf Research, v. 76, no. 0, p. 12-24.

Oberle, F. K. J., Storlazzi, C. D., and Hanebuth, T. J. J., 2014b, Wave-driven sediment mobilization on a storm-controlled continental shelf (Northwest Iberia): Journal of Marine Systems, v. 139, no. 0, p. 362-372.

Oliveira, A., Vitorino, J., Rodrigues, A., Jouanneau, J., Dias, J., and Weber, O., 2002, Nepheloid layer dynamics in the northern Portuguese shelf: Progress in Oceanography, v. 52, no. 2-4, p. 195-213.

Pérez-Gussinyé, M., Ranero, C. R., Reston, T. J., and Sawyer, D., 2003, Mechanisms of extension at nonvolcanic margins: Evidence from the Galicia interior basin, west of Iberia: Journal of Geophysical Research: Solid Earth (1978–2012), v. 108, no. B5.

Pomar, L., Morsilli, M., Hallock, P., Bádenas, B., 2012. Internal waves, an under-explored source of turbulence events in the sedimentary record. Earth-Science Reviews 111, 56-81.Poore, H. R., Samworth, R., White, N. J., Jones, S. M., and McCave, I. N., 2006, Neogene overflow of Northern Component Water at the Greenland-Scotland Ridge: Geochemistry, Geophysics, Geosystems, v. 7, no. 6.

Poore, H.R., Samworth, R., White, N.J., Jones, S.M., McCave, I.N., 2006. Neogene overflow of Northern Component Water at the Greenland-Scotland Ridge. Geochemistry, Geophysics, Geosystems 7.

Preu, B., Schwenk, T., Hernández-Molina, F. J., Violante, R., Paterlini, M., Krastel, S., Tomasini, J., and Spieß, V., 2012, Sedimentary growth pattern on the northern Argentine slope: The impact of North Atlantic Deep Water on southern hemisphere slope architecture: Marine Geology, v. 329–331, no. 0, p. 113-125.

Preu, B., Hernández-Molina, F.J., Violante, R., Piola, A.R., Paterlini, C.M., Schwenk, T., Voigt, I., Krastel, S., Spiess, V., 2013. Morphosedimentary and hydrographic features of the

northern Argentine margin: The interplay between erosive, depositional and gravitational processes and its conceptual implications. Deep Sea Research Part I: Oceanographic Research Papers 75, 157-174.

Raymo, M. E., Hodell, D., and Jansen, E., 1992, Response of deep ocean circulation to initiation of northern hemisphere glaciation (3–2 MA): Paleoceanography, v. 7, no. 5, p. 645-672.

Rebesco, M., 2005. SEDIMENTARY ENVIRONMENTS | Contourites, in: Selley, R.C., Cocks, L.R.M., Plimer, I.R. (Eds.), Encyclopedia of Geology. Elsevier, Oxford, pp. 513-527.

Rebesco, M., Hernández-Molina, F. J., Van Rooij, D., and Wåhlin, A., 2014, Contourites and associated sediments controlled by deep-water circulation processes: State-of-the-art and future considerations: Marine Geology, v. 352, p. 111-154.

Rebesco, M., Özmaral, A., Urgeles, R., Accettella, D., Lucchi, R.G., Rüther, D., Winsborrow, M., Llopart, J., Caburlotto, A., Lantzsch, H., Hanebuth, T.J.J., 2016. Evolution of a high-latitude sediment drift inside a glacially-carved trough based on high-resolution seismic stratigraphy (Kveithola, NW Barents Sea). Quaternary Science Reviews 147, 178-193.

Rebesco, M., Stow, D., 2001. Seismic expression of contourites and related deposits: a preface. Marine Geophysical Researches 22, 303-308.

Roberts, D.G., Hogg, N.G., Bishop, D.G., Flewellen, C.G., 1974. Sediment distribution around moated seamounts in the Rockall Trough. Deep Sea Research and Oceanographic Abstracts 21, 175-184.

Robinson, S. A., and Vance, D., 2012, Widespread and synchronous change in deep-ocean circulation in the North and South Atlantic during the Late Cretaceous: Paleoceanography, v. 27, no. 1.

Rogerson, M., Rohling, E. J., Weaver, P. P. E., and Murray, J. W., 2005, Glacial to interglacial changes in the settling depth of the Mediterranean Outflow plume: Paleoceanography, v. 20, no. 3, p. PA3007.

Rögl, F., 1999, Mediterranean and Paratethys. Facts and hypotheses of an Oligocene to Miocene paleogeography (short overview): Geologica carpathica, v. 50, no. 4, p. 339-349.

Roth, P. H., 1986, Mesozoic palaeoceanography of the North Atlantic and Tethys Oceans: Geological Society, London, Special Publications, v. 21, no. 1, p. 299-320.

Rouby, D., Guillocheau, F., Robin, C., Bouroullec, R., Raillard, S., Castelltort, S., Nalpas, T., 2003. Rates of deformation of an extensional growth fault/raft system (offshore Congo, West African margin) from combined accommodation measurements and 3-D restoration. Basin Research 15, 183-200.

Schneider, R.R., Müller, P.J., Ruhland, G., 1995. Late Quaternary surface circulation in the east equatorial South Atlantic: Evidence from Alkenone sea surface temperatures. Paleoceanography 10, 197-219.

Schönfeld, J., and Zahn, R., 2000, Late Glacial to Holocene history of the Mediterranean Outflow. Evidence from benthic foraminiferal assemblages and stable isotopes at the Portuguese margin: Palaeogeography, Palaeoclimatology, Palaeoecology, v. 159, no. 1–2, p. 85-111.

Sclater, J.G., Christie, P.A.F., 1980. Continental stretching: An explanation of the Post-Mid-Cretaceous subsidence of the central North Sea Basin. Journal of Geophysical Research: Solid Earth (1978–2012) 85, 3711-3739.

Shipboard Scientific Party, 1998a. Site 1078. *In* Wefer, G., Berger, W.H., Richter, C., et al., *Proc. ODP, Init. Repts.,* 175: College Station, TX (Ocean Drilling Program), 143–176. doi:10.2973/odp.proc.ir.175.106.1998

Shipboard Scientific Party, 1998b. Site 1079. *In* Wefer, G., Berger, W.H., Richter, C., et al., *Proc. ODP, Init. Repts.,* 175: College Station, TX (Ocean Drilling Program), 177–199. doi:10.2973/odp.proc.ir.175.107.1998

Soares, D. M., Alves, T. M., and Terrinha, P., 2014, Contourite drifts on early passive margins as an indicator of established lithospheric breakup: Earth and Planetary Science Letters, v. 401, no. 0, p. 116-131.

Spathopoulos, F., 1996. An insight on salt tectonics in the Angola Basin, South Atlantic. Geological Society, London, Special Publications 100, 153-174.

Stille, P., Steinmann, M., and Riggs, S. R., 1996, Nd isotope evidence for the evolution of the paleocurrents in the Atlantic and Tethys Oceans during the past 180 Ma: Earth and Planetary Science Letters, v. 144, no. 1, p. 9-19.

Stoker, M.S., 1998. Sediment-drift development on the continental margin off NW Britain. Geological Society, London, Special Publications 129, 229-254.

Stow, D.A.V., 2001. Deep- sea sediment drifts. 1st edition of Encyclopedia of Ocean Sciences 2, 10.

Stow, D.A.V., Faugères, J.C., 2008. Chapter 13 Contourite Facies and the Facies Model, in: Rebesco, M., Camerlenghi, A. (Eds.), Developments in Sedimentology. Elsevier, pp. 223-256.

Stow, D. A. V., Faugères, J.-C., Howe, J. A., Pudsey, C. J., and Viana, A. R., 2002, Bottom currents, contourites and deep-sea sediment drifts: current state-of-the-art: Geological Society, London, Memoirs, v. 22, no. 1, p. 7-20.

Stow, D. A. V., Hernández-Molina, F. J., Alvarez-Zarikian, C., & Scientists, E. I. O. D. P. . (2013). Proceedings IODP, 339. Integrated Ocean Drilling Program Management International, Inc.. DOI: 10.2204/iodp.proc.339.2013

Stow, D. A. V., Hernandez-Molina, F. J., Llave, E., Sayago-Gil, M., Diaz del Rio, V., and Branson, A., 2009, Bedform-velocity matrix: The estimation of bottom current velocity from bedform observations: Geology, v. 37, no. 4, p. 327-330.

Stow, D. A. V., Hunter, S., Wilkinson, D., and Hernández-Molina, F. J., 2008, Chapter 09 The nature of contourite deposition: Developements in Sedimentology, v. 60, p. 14.

Stramma, L., England, M., 1999. On the water masses and mean circulation of the South Atlantic Ocean. Journal of Geophysical Research: Oceans (1978–2012) 104, 20863-20883.

Stramma, L., Schott, F., 1999. The mean flow field of the tropical Atlantic Ocean. Deep Sea Research Part II: Topical Studies in Oceanography 46, 279-303.

Sutra, E., and Manatschal, G., 2012, How does the continental crust thin in a hyperextended rifted margin? Insights from the Iberia margin: Geology, v. 40, no. 2, p. 139-142.

Thomas, D. J., Bralower, T. J., and Jones, C. E., 2003, Neodymium isotopic reconstruction of late Paleocene–early Eocene thermohaline circulation: Earth and Planetary Science Letters, v. 209, no. 3–4, p. 309-322.

Turnewitsch, R., Falahat, S., Nycander, J., Dale, A., Scott, R. B., and Furnival, D., 2013, Deep-sea fluid and sediment dynamics—Influence of hill- to seamount-scale seafloor topography: Earth-Science Reviews, v. 127, p. 203-241

Van Rooij, D., De Mol, B., Huvenne, V., Ivanov, M., Henriet, J.P., 2003. Seismic evidence of current-controlled sedimentation in the Belgica mound province, upper Porcupine slope, southwest of Ireland. Marine Geology 195, 31-53.

Van Rooij, D., Iglesias, J., Hernández-Molina, F. J., Ercilla, G., Gomez-Ballesteros, M., Casas, D., Llave, E., De Hauwere, A., Garcia-Gil, S., Acosta, J., and Henriet, J. P., 2010, The Le Danois Contourite Depositional System: Interactions between the Mediterranean Outflow Water and the upper Cantabrian slope (North Iberian margin): Marine Geology, v. 274, no. 1-4, p. 1-20.

Vandorpe, T., Martins, I., Vitorino, J., Hebbeln, D., García, M., and Van Rooij, D., 2016, Bottom currents and their influence on the sedimentation pattern in the El Arraiche mud volcano province, southern Gulf of Cadiz: Marine Geology, v. 378, p. 114-126.

Vandorpe, T., Van Rooij, D., and de Haas, H., 2014, Stratigraphy and paleoceanography of a topography-controlled contourite drift in the Pen Duick area, southern Gulf of Cádiz: Marine Geology, v. 349, no. 0, p. 136-151.

Varela, R. A., Rosón, G., Herrera, J. L., Torres-López, S., and Fernández-Romero, A., 2005, A general view of the hydrographic and dynamical patterns of the Rías Baixas adjacent sea area: Journal of Marine Systems, v. 54, no. 1–4, p. 97-113.

Via, R. K., and Thomas, D. J., 2006, Evolution of Atlantic thermohaline circulation: Early Oligocene onset of deep-water production in the North Atlantic: Geology, v. 34, no. 6, p. 441-444.

Vitorino, J., Oliveira, A., Jouanneau, J. M., and Drago, T., 2002, Winter dynamics on the northern Portuguese shelf. Part 2: bottom boundary layers and sediment dispersal: Progress in Oceanography, v. 52, no. 2–4, p. 155-170.

Woodruff, F., and Savin, S. M., 1989, Miocene deepwater oceanography: Paleoceanography, v. 4, no. 1, p. 87-140.

Wright, J. D., Miller, K. G., and Fairbanks, R. G., 1992, Early and Middle Miocene stable isotopes: Implications for Deepwater circulation and climate: Paleoceanography, v. 7, no. 3, p. 357-389.

Wynn, R. B., and Stow, D. A. V., 2002, Classification and characterisation of deep-water sediment waves: Marine Geology, v. 192, no. 1–3, p. 7-22.

Yilmaz, Ö., 2001, Seismic Data Analysis – Processing, Inversion and Interpretation of Seismic Data. Society of Exploration Geophysicists, Tulsa. 2027 pp.

Zachos, J., Pagani, M., Sloan, L., Thomas, E., Billups, K., 2001. Trends, Rhythms, and Aberrations in Global Climate 65 Ma to Present. Science 292, 686-693.

Zhang W, Cui Y, Santos A, Hanebuth TJJ (2016a) Storm-driven bottom sediment transport on a high-energy narrow shelf (NW Iberia) and development of mud depocenters. Journal of Geophysical Research – Oceans 121(8), 5751-5772.

Zhang W, Hanebuth TJJ, Stöber U (2016b) Short-term sediment dynamics on a meso-scale contourite drift (off NW Iberia): impacts of multi-scale oceanographic processes deduced from the analysis of mooring data and numerical modelling. In: Van Rooij D, Campbell C, Rueggeberg A, Wåhlin A (eds) “The contourite log-book: significance for palaeoceanography, ecosystems and slope instability”. Marine Geology 378, 81-100.